Integrated Geosteering Workflow for Optimal Well Trajectory

by

© Zhongqi Wang

A thesis submitted to the
school of Graduate Studies
in Partial fulfillment of the
requirements for the degree of
Master of Science

Department of Earth Science
Memorial University of Newfoundland
Mar 2017

St.John's Newfoundland Canada

Abstract

The enormous upfront expense of developing heterogeneous reservoirs and the desire to increase ultimate recovery has spurred oil companies to develop and use innovative reservoir characterization techniques. Geostatistics is a technique using a branch of statistics focusing on spatial datasets and was developed originally to predict probability distributions of ore grades for mining operations. Geostatistically derived reservoir modeling is perhaps the most successful means of improving performance predictions in heterogeneous reservoirs. A reliable geostatistical model can be used to guide the drilling path at field scale and make a more scientific field development plan.

The objective of this study is to optimize production performance by combined geostatistical algorithms, Logging While Drilling techniques and reservoir simulation methods. Formation petrol-physics models are built with Kriging and Sequential Gaussian simulation methods and then updated with real time Logging While Drilling data to guide the drilling process and finally compare the model difference with production indices.

The data used in this study is from E-Segment Norne Field located in the Norwegian Sea. 2-D and 3-D porosity & permeability geostatistical models and a simple reservoir simulation model are built to describe the formation porosity and permeability regional distribution. A new well trajectory is designed based on updated models. The results demonstrate that new well trajectories significantly improve the production performance with the updated models, which reflects the importance of geostatistics in treatment of reservoir heterogeneity.

Acknowledgments

I would like to gratefully acknowledge the contributions of many people and groups during the last two years. Without the support of them, this thesis would not have been possible. First and foremost, I wish to express my thanks to my supervisors Dr. Thormod Johansen and Dr. Lesley James for giving me the chance to work on this research. Thank you so much for all your guidance, enthusiasm, and support that helped me to complete the work, not only in academics but also in life. This is one of the most wonderful experiences in my life.

Secondly, I would like to thank all the students and research staffs in Hibernia EOR research group. I really learned a lot from the group meetings and presentations. People were doing different research in the group but there were some similarities that linked us together. The discussions between us always sparked my inspiration and sometimes greatly promoted my research.

I would like to take this opportunity to acknowledge the following groups and companies for their financial support, the Hibernia Management and Development Corporation (HMDC) and Memorial University of Newfoundland. I would also like to thank Chevron Canada Limited for giving me the Chevron Canada Rising Star Awards, which is truly an honor for me.

Finally, I will like to thank my parents and my girlfriend. No matter how much I failed, I always know that you would treat me like a winner. Thanks for being so supportive.

Contents

List of Figures

Nomenclature

a = variogram range (m)

C, c = covariance

C_0 = variogram sill

C_1 = variogram sill contribution for a variogram in combination model

E = expected value

g = gravity constent (m/s^2)

k = permeability (Darcy)

$\vec{L}$ = lag distance (m)

m = mean value

M_{Ea} = exponential variogram model with range a

M_{Ga} = Gaussian variogram model with range a

M_{Sa} = spherical variogram model with range a

n = number of variable pairs

p = pressure (bar)

v = Darcy velocity (m/s)

s^2 = variance

sm^3 /day = standard cubic meter per day

X, x = random variable

$X(\vec{u_i})$ = sample data

$X^*(\overrightarrow{u_0})$ = parameter estimate

Y, y = random variable

Greek Symbols

α = angle (degree)

γ = variogram

λ = kriging weight

ρ = density (kg/m^3)

ϕ = porosity

σ = standard deviation

θ = direction of maximum continuity

Subscripts

i, j = variable counters

1, 2 = unique random variable identifier

o, w = oil, water

Abbreviations

LWD = Logging While Drilling

MWD = Measure While Drilling

SPE = Society of Petroleum Engineers

TI = Training-image

CDF = Cumulative Distribution Fuction

1. Introduction

A detailed and reliable geological model can be used to guide the well drilling paths and make a more scientific field development plan. Geostatistics is a branch of statistics focusing on spatial or spatiotemporal datasets and was developed originally to predict probability distributions of ore grades for mining operations (Daine, 1951). It is currently widely applied in diverse disciplines including petroleum geology, hydrogeology, hydrology, meteorology, oceanography, geochemistry, geography, forestry, environmental control, landscape ecology, soil science, and agriculture. For geologists, geostatistics can be used as a tool to not only analyze data but also to interpret the geological variation. A tool can never replace data, but obviously it can help to build possible geological descriptions based on the statistical variation of the formation properties.

The data generated in geostatistics can be correlated spatially and temporally. The key point of geostatistics is to manage the spatial relationship and balance the weight between the local mean and the global mean. Through some stationarity assumption, the objective function most often optimized in geostatistical estimation is the estimation

variance, also called the Kriging variance. Also, some conditional simulation techniques like Gaussian simulation and P-field simulation are also applied in petroleum industry (Chambers et al., 2000). In general, the power of conditional simulation technique is derived from its ability to condition, with as much information as possible, and at the same time minimizes the computation that is required to simulate attribute values. Geostatistical Modeling can be divided as several steps included variogram modeling, kriging estimation or multi-point simulation process. Visually, a geostatistical model can give geologists some valuable images (equal-probability realizations) which in turn reflect the subsurface petrophysics and formation information.

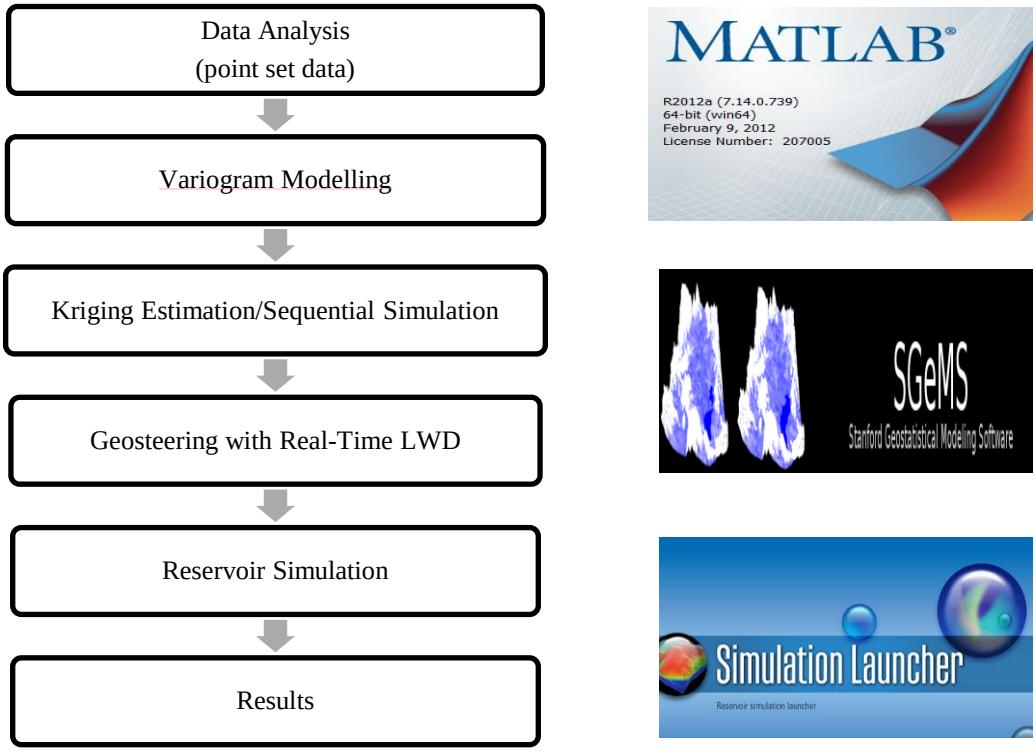

Figure 1.1 General Workflow with Toolbox

The general workflow is shown in Figure 1.1. This research integrated several toolbox and open-source applications. MATLAB, one of high-performance language toolbox for technical computing is used in the data analysis and variogram modelling process (Kroese, 2014). Kriging estimation and real-time geosteering with real-time LWD is

completed in the SGeMS, an open platform application developed at Stanford University (Remy, 2011). Eclipse 100 black oil simulator developed by Schlumberger is used in this research to simulate reservoir production performance with different geostatistical realizations (Liu et al., 2012). It is necessary to mention that the simulator can be easily replaced by any commercial reservoir simulation software or customized simulators since the data file generated in this workflow is mainly in ASCII, a common and flexible format.

The first step to build a variogram model is to obtain logging data from existing wells and check if the dataset needs transformation. Then, the data spatial relationship will be calculated. The spatial relationship of data is then represented by some parameters such as lag distance, tolerance and directions of continuity. Different experimental models must be selected and matched to the estimation by varying the parameters of the model discussed above. If the data distribution fits the selected model, the variogram modelling process is completed.

Either Kriging method or a multi-point simulation method such as Gaussian sequential estimation can be applied to build a porosity distribution model. With a certain variogram, thousands of realizations can be generated with equal probability.

After a porosity distribution map has been built, a reservoir flow simulator will be used to establish the fluid flow model in the near wellbore region for different geostatistical realizations. Dynamic information such as flow rate and water saturation will be calculated depending on available data. This step will focus on comparing different realizations and selecting the optimal geostatistical model and methodology by cross validation. In practice, a commercial platform is used, such as Schlumberger Eclipse, which normally requires long running time and complicated parameter input. Therefore, a relatively simple simulator must be used to upgrade the geological model during well drilling and guide the well trajectory.

1.1 Basic Concepts

1.1.1 Spatial Relationships

The major objective of geostatistical modelling is to determine the spatial relationship. The basic assumption of data sets in the working area is that two samples located geographically close to each other are more alike than values measured farther apart. In other words, a spatial relationship between data in the data set is assumed to be determined by spatial relative distance. In the case of reservoir spatial data, the estimated value calculated based on spatial relationship can be significantly different from the real value. There are many reasons that cause this situation. The first one is the existence of local variability. A heterogeneous reservoir always contains a number of different lithofacies and geological bodies, each of which shows its own characteristics. The simplest correlation between data sampled at different locations is caused by the spatial continuity of the underlying geological phenomenon. These scenarios must be understood and considered. Therefore, a reliable geological continuity model needs to be first and foremost quantified before taking geostatistics into application.

1.1.2 Statistical Concepts

Geostatistics is a form of statistics that takes advantage of the spatial continuity of a geological data set. In other words, geostatistics is the application of statistical concepts into the geology field. As in the theory of measuring data relationships, variance and covariance are the basis of geostatistics studies (Kelkar et al., 2002).

The variance represents the spread of the data and how widely the data are distributed. The square root of variance, which is called the standard deviation, is also widely used in statistics estimation. Mathematically, *variance* is defined as:

$$s^2 = \frac{\sum_{i=1}^{n} x_i^2 - n\bar{x}^2}{n-1}, \tag{1.1}$$

where s is standard deviation, $\bar{x}$ is sample mean and n is the total number of samples (Kelkar et al., 2002).

The covariance can be used as one of the functions that relates two variables located a certain distance and direction apart. *Covariance* is defined as

$$C\left[x(\vec{u}), x(\vec{u}+\vec{L})\right] = \frac{1}{n}\sum_{i=1}^{n} x(\vec{u}_i)x(\vec{u}_i+\vec{L}) - \frac{1}{n}\sum_{i=1}^{n} x(\vec{u}_i)\frac{1}{n}\sum_{i=1}^{n} x(\vec{u}_i+\vec{L}), \tag{1.2}$$

where *n* is the total number of sample points at vector distance $\vec{L}$ and $x(\overrightarrow{u_l})$, $x\left(\overrightarrow{u_l}+\vec{L}\right)$ are the values of the variable at locations $\overrightarrow{u_l}$ and $\overrightarrow{u_l}+\vec{L}$ (Kelkar et al., 2002).

The correlation coefficient can also be used to describe the spatial relationship. Mathematically, it can be presented as

$$r\left(\vec{L}\right) = \frac{C(\vec{L})}{\sigma_{\vec{u}}\sigma_{\vec{u}+\vec{L}}}, \tag{1.3}$$

where $r(\vec{L})$ is the correlation coefficient at *lag distance* $\vec{L}$, $C(\vec{L})$ is the covariance and $\sigma_{\vec{u}}$ and $\sigma_{\vec{u}+\vec{L}}$ are standard deviations for the data located at $\vec{u}$, $\vec{u}+\vec{L}$, respectively (Kelkar et al., 2002).

1.1.3 Variogram

The *variogram* is the most commonly used geostatistical technique for describing the spatial relationship between geological properties. Kelkar (2002) defined it as

$$\gamma(\vec{L}) = \frac{1}{2}V\left[x(\vec{u}) - x(\vec{u}+\vec{L})\right], \tag{1.4}$$

where V is the variance. It shows that with two given locations, $\vec{u}$ and $\vec{u}+\vec{L}$, inside the field of a regionalized variable $X(u)$, the variogram is half the variance of the difference between a sampled value and the estimated value with $\vec{L}$ distance away. A variogram can also be written in the following form

$$\gamma(\vec{L}) = \frac{1}{2n(\vec{L})}\sum_{i=1}^{n(\vec{L})}[x(\vec{u_i}) - x(\vec{u_i}+\vec{L})]^2, \tag{1.5}$$

where $n(\vec{L})$ is the number of pairs at lag distance $\vec{L}$, while $x(\vec{u}_i)$ and $x(\vec{u}_i+\vec{L})$ are the data values for the i^{th} pair located $\vec{L}$ lag distance apart.

Normally, a variogram model is selected from commonly used models: Gaussian, exponential, spherical, and combination models. The selection of variogram models is based on the original data trend. In most cases, experimental data will fit one of these variogram models. If the variogram model fits experimental model, the variogram model is applied to the Kriging estimation process. Variogram models with sill are applied in this research since porosity and permeability are used as target geological properties.

The four most commonly used variogram models with sills are shown below.

Spherical Model:

The spherical model is one of the most commonly used models to estimate the variogram with a sill. It is effective for models which increase rapidly in a certain range and have the highest slope at the origin. The structure of spherical model is shown in Figure 1.2. Mathematically, it can be written as

$$M_{Sa}(\vec{L}) = C_0\left[\frac{3}{2}\left(\frac{L}{a}\right) - \frac{1}{2}\left(\frac{L}{a}\right)^3\right] \; L \le a, \tag{1.6}$$

$$M_{Sa}(\vec{L}) = C_0 \quad L \ge a, \tag{1.7}$$

where M_{sa} is the spherical model with a distance of $\vec{L}$, a is range and C_0 is sill value.

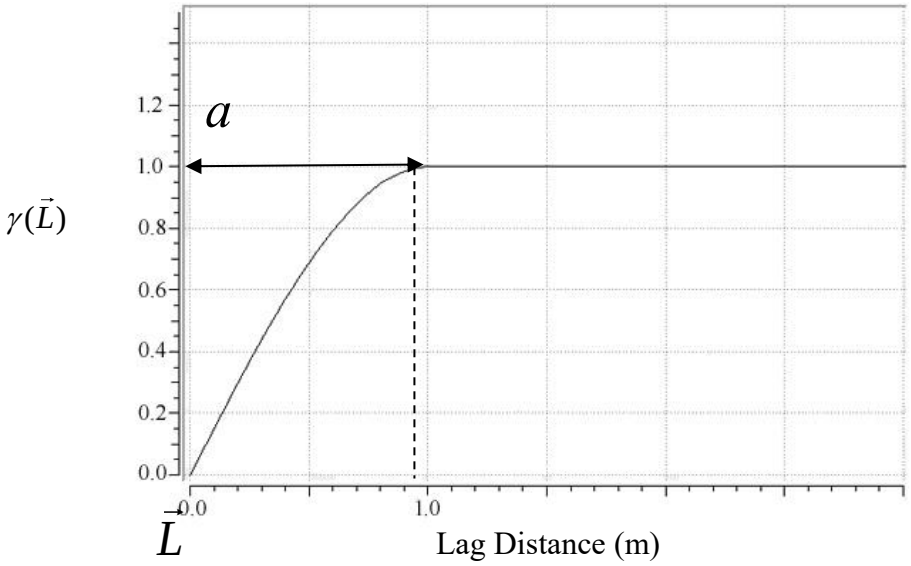

Figure 1.2 Spherical Variogram Model (Kelkar et al., 2002)

Exponential Model:

The feature of this model is that the variogram reaches the sill value only asymptotically. Therefore, the range a is normally defined as the lag distance where the variogram reaches approximately 95% of the sill value. As presented in Figure 1.2, the slope of the origin for the exponential model is smaller than that of the spherical model at the same range showing a higher gradual change in the variogram estimation. Mathematically the exponential model can be written as

$$M_{Ea}(\vec{L}) = C_0 \left[1 - exp\left(\frac{-3L}{a}\right) \right] L \geq 0 \qquad (1.8)$$

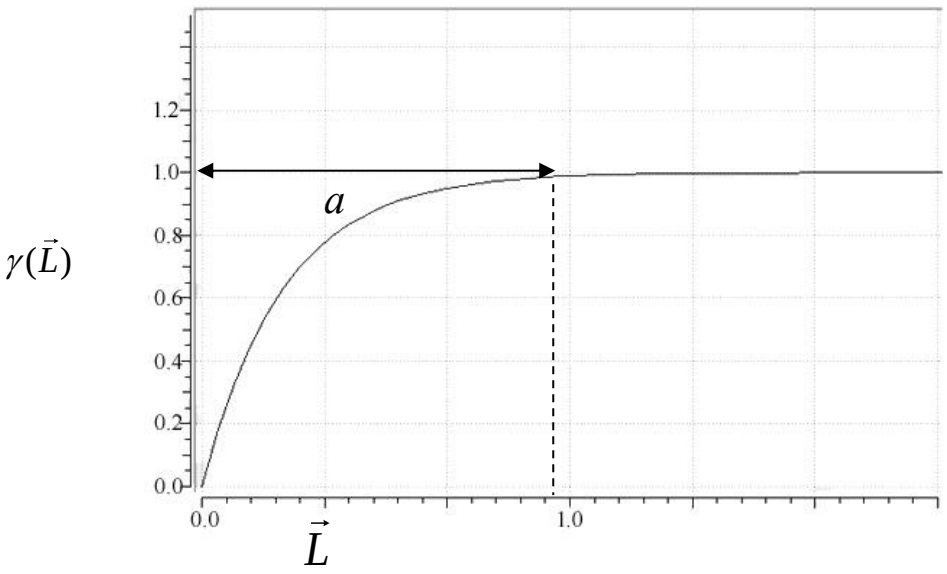

Figure 1.3 Exponential Variogram Model (Kelkar et al., 2002)

Gaussian Model:

The variogram equation for the Gaussian Model can be written as Equation 1.9. Figure 1.4 illustrates that the slope at the origin is approximately zero which means an extremely smooth variation in variables as a function of distance. Although the variogram changes very gradually at the origin, it increases rapidly when the variogram is closer to reaching a sill value. Mathematically, it can be written as

$$M_{Ga}(\vec{L}) = C_0 \left[1 - exp\left(\frac{-3L^2}{a^2}\right) \right] \quad L \geq 0 \,. \tag{1.9}$$

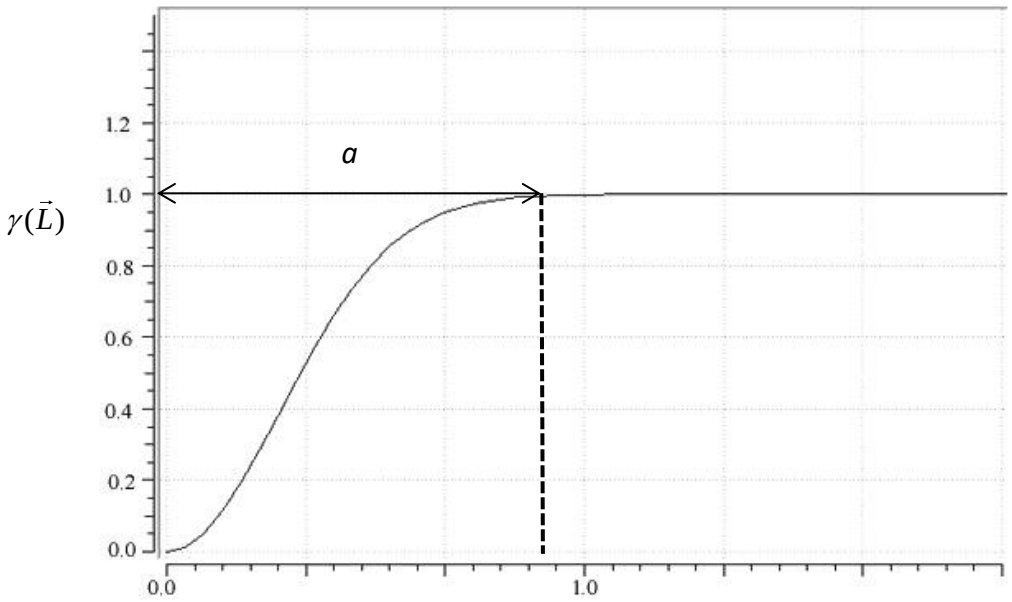

Figure 1.4 Gaussian Variogram Model (Kelkar et al., 2002)

Combination Model:

Some datasets may require a linear combination of these models using the three models mentioned above. Mathematically, it can be written as

$$\gamma(\vec{L}) = C_0 + C_1 M_{Sa}(\vec{L}) + C_2 M_{Ea}(\vec{L}) \ , \tag{1.10}$$

$$C_0 + C_1 + C_2 = 1 \ . \tag{1.11}$$

This equation represents a linear combination of three models: Nugget-effect model C_0, Gaussian model $C_1$and Exponential model C_2. Theoretically, this model can combine as many models as needed. The combination of four models are rarely used in real estimation processes. In this research, maximum 3 different models are combined.

1.1.4 Kriging methods

Geostatistical estimation techniques can be generally divided into conventional

estimation techniques and conditional simulation techniques. The Kriging technique is one of the conventional estimation techniques which was developed by Dannie Krige and first applied in South African gold mine industry (Agterberg, 2004). In geostatistical modelling, the Kriging method is used to describe the correlation between a set of samples based on a variogram model. The Kriging method is widely used in surface geography, hydrogeology, the mineral deposit and petroleum exploration and production. Many variants of Kriging methods have been developed and they can all be described as Equation 1.12. These methods are developed based on the same principles of data correlation and redundancy. Moreover, the technique assumes that the value at the unsampled location is estimated by

$$x^*(\overrightarrow{u_0}) = \sum_{i=1}^{n} \varphi_i \, x(\overrightarrow{u_i}) \ , \tag{1.12}$$

where $x^*(\overrightarrow{u_0})$ is the estimated value at the unsampled location, $x(\overrightarrow{u_i})$ is the value at the neighboring location and φ_i is the weight assigned to the neighboring value. The calculation of φ_i is different based on different Kriging estimation methods (Kelkar et al., 2002).

The key point of the Kriging method is to calculate the weights assigned to the individual neighboring points. These weights depend on the spatial relationship between the unsampled location and the neighboring values. The sample points used in estimating values at unsampled location is called the *searching neighborhood*. Theoretically, all the available sample points within the search neighborhood should be used in the estimation since all Kriging procedures use a linear estimation technique. However, in real applications, a smaller neighborhood is more suitable for specific circumstances. Simple Kriging method is applied in this research.

1.1.5 Sequential Conditional Simulation

As for the Kriging methods, the critical point of sequential conditional simulation in estimating variables at unsampled locations is to minimize the error variance. However, the conditional simulation techniques aim at simulating real conditions in the reservoirs rather than estimating variables based on certain criteria. The main theory behind this simulation method is called Monte Carlo simulation which is defined as a broad class of algorithms that is using repeated random sampling to obtain numerical results (Ricardo, 1999).

Normally, the reservoir petrophysical information is gathered from well data. However, the true distribution of reservoir properties is never known in practice. In these cases, conditional simulation techniques show more flexibility compared to Kriging methods. The significant difference between Kriging methods and conditional simulation is the selection of a searching neighborhood and the sample data used in the calculation procedure. Similar to Kriging techniques, the sample spatial relationship in conditional simulation is also based on variogram analysis. However, unlike Kriging methods, which only consider the original data from the dataset to generate the realization maps, conditional simulation methods use both original data and the previously estimated value for simulation. The original data is normally used as hard data and the previously estimated values are used as soft data. When a value at an unsampled location has been estimated by using Kriging methods, it will not reproduce the extreme values in the dataset. However, a lot of cases show that extreme values do represent important information in reservoir simulation therefore cannot be ignored.

1.1.6 Reservoir Characterization

Reservoir characterization can be defined as a large amount of procedures to describe detailed reservoir properties by using all available data from a broad spectrum of sources. The description can be qualitative or quantitative and the data can be static or dynamic. These types of data contain 2-D, 3-D or 4-D seismic data, core and log data, production data, well-test data, outcrop analogs, etc. Ideally, all the data from different sources and scales will be integrated to the final reservoir simulation model.

Generally, the higher quality data used, the more accurate the reservoir characterization will be. However, in practice, for various reasons such as time limited or different goals, not all data will be used. The data interpretation could be either qualitative or quantitative. In the geological analysis of a basin, some information such as sedimentary history and depositional environment is from the geologist's prior experience. This information may not be accurate, but nevertheless it can provide a valuable constraint to describe the reservoir properties. From basin exploration to reservoir production, data is collected step by step. In other words, data may not be available at the same time. First, geological information is provided by seismic surveys and outcrops. After the exploration and delineation wells have been drilled, the well logs, core information and also well test information is collected and analyzed. Once production starts, more and more dynamic data will be available during the reservoir development. The understanding of the basin is always based on the amount of available data. Obviously, with limited amount of data, the reservoir characterization has more uncertainty (Henning, 1998).

Furthermore, data is available at different scales. Since data is collected from different sources and techniques, sometimes they cannot be properly correlated. For example, core analysis is always done in laboratory and in most scenarios, are in macro-scale so

that information like porosity and permeability obtained from cores always show high resolution. However, porosity data collected by seismic surveys may have a resolution of 15 m. Thus, for cases like this, when information from different sources are used, the difference in scale must be considered in the analysis.

1.1.7 Darcy's Law

Darcy's Law is one of the most important laws in reservoir engineering which describes fluid flow through a porous medium. Darcy's Law is established based on the results of experiments (Darcy, 1856). As shown in Figure 1.5, a fluid is injected with a constant rate. Then, it travels through a rock core and exits at the same rate (steady state flow).

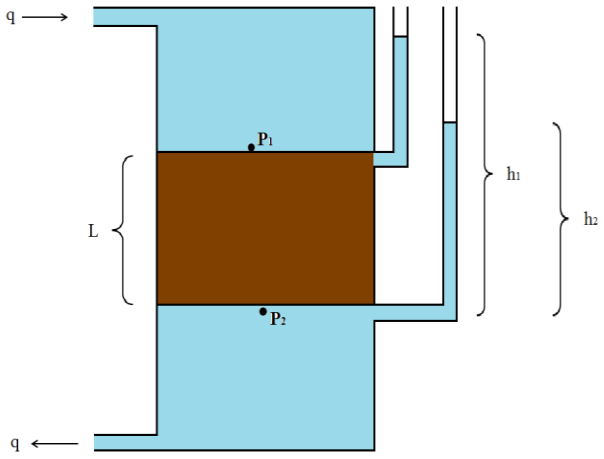

Figure 1.5 Experiment Process of Darcy's Law (Kelkar et al., 2002)

Mathematically, Darcy's Law can be written as

$$q = \frac{\kappa A}{L}(h_1 - h_2), \tag{1.13}$$

where q is the flow rate (m^3/s), L is the length of rock pack (m), A is the cross-section area (m^2), κ is constant of proportionality (m/s).

1.1.8 Porosity and Permeability

Porosity (∅):

Porosity is a fundamental rock property defined as the percentage of pore volume within a rock bulk volume. There are several reasons why a pore volume is formed from a geology point of view, such as the alteration of rock or structure activities in the deposition history. It is an important consideration of evaluating the volume of hydrocarbons contained in the formation. Porosity simulated in this study is based on sequential Gaussian simulation which is already introduced before. Mathematically, it can be calculated as

$$\phi = \frac{V_{pore}}{V_{bulk}}, \tag{1.14}$$

where V_{pore} is the pore volume excluding catenary and dead-end pores, V_{bulk} is the bulk volume.

Permeability (*K*):

Permeability is a concept typically used to measure the ability of a rock to transmit fluids. For different fluids and phases, measurements are different. Absolute permeability measures the single-phase fluid system while relative permeability measures a certain fluid through a rock within multi-phase systems. A general process of evaluating permeability of a core in the laboratory is applying a constant pressure gradient ΔP over the sample length and measuring the flow rate. Then, the Darcy's law which presented in Equation 4.2 is utilized to calculate the permeability of the sample.

Mathematically, absolute permeability for 1D horizontal flow can be calculated as

$$K = \frac{q}{A}\frac{\mu L}{\Delta p}. \tag{1.15}$$

However, if the formation contains more than one phase, different fluid fronts will move through the formation at different velocities. Relative permeability will be used to describe this phenomenon. In a two-phase reservoir with oil and water, the relative permeability can be presented as

$$k_{ro} = \frac{k_o}{K}\ , \tag{1.16}$$

$$k_{rw} = \frac{k_w}{K}\ , \tag{1.17}$$

where k_{ro}, k_{rw} are the relative permeability of oil and water, k_0, k_w are the oil and water permeability respectively and K is the absolute permeability.

Darcy's Law can be re-written as Equation 1.18 below. Note that the i refers to fluid phase (oil, water or gas)

$$q_i = \frac{Kk_{ri}(S_w)}{\mu_i}[\frac{\partial p_i}{\partial x} + \rho_i g \sin(\alpha)]. \tag{1.18}$$

$\frac{\partial p_i}{\partial x}$: the pressure gradient (Pa/m)

μ_i: fluid viscosity (Pa·s)

K: absolute permeability (mD)

k_{ri}: relative permeability

S_w: the water saturation

g: acceleration of gravity (m/s^2)

ρ: the density of fluid (kg/m^3)

a：the angle of flow inclination counterclockwise from the horizontal

1.1.9 Kozeny Equation

In practice, the porosity data is normally gathered from logging techniques or core analysis in laboratory. However, permeability is difficult to measure directly in situ. In this study, permeability is evaluated from porosity data based on porosity-permeability relationships such as the Kozeny Equation, which is presented as

$$K = const \cdot \frac{\phi D_p^{\,2}}{\tau} + a\,, \tag{1.19}$$

where K is the permeability, $const$ is the constant characteristic of a specific rock, τ is the tortuosity which is commonly used to measure the geometric complexity of a porous medium and D_p is the diameter of pore channels, a is a function of pore throat size and thereby obscures the physics of flow in porous media.

The permeability-porosity relationship varies with several features such as the type of rock and grain size. For an individual formation or rock, permeability-porosity relationship is commonly used in a linear relationship since the diameter of pore channel D_p and tortuosity τ are functions of rock. In Equation 1.19, all the other parameters are constant. Therefore, the relationship between permeability K and porosity ϕ is linear (Lucia, 1999). Figure 1.6 shows the permeability-porosity linear relationships for various rock types.

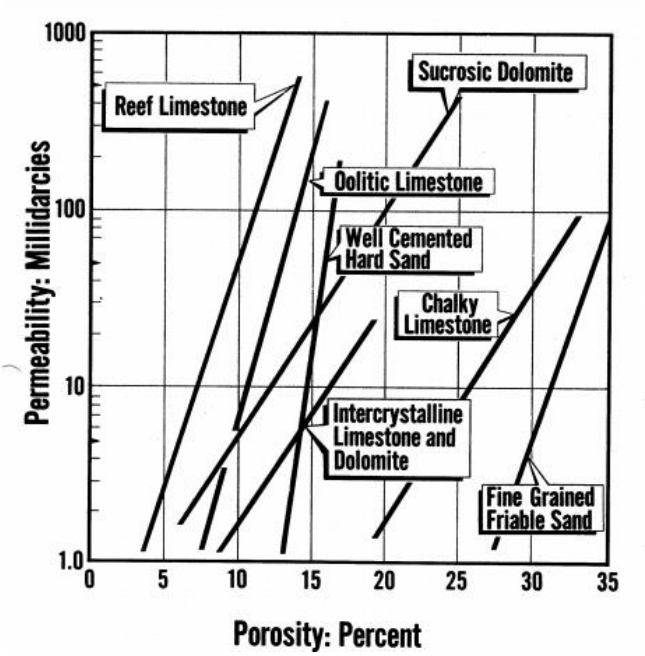

Figure 1.6 Permeability-Porosity relationships with various rock types (Lucia, 1999)

1.1.10 Logging Interpretation

Porosity logs measure the percentage of pore volume in a bulk volume of rock in a reservoir formation. The porosity can be obtained from several logging tools including density log, neutron log and sonic log. The first two measurements are based on nuclear response while sonic logs use acoustic measurements. For all these tools, the response is affected by the formation porosity, fluid properties and rock properties. In some cases, a combination of these measurement techniques will give a more accurate estimated result.

Density Log:

Density logs have been applied in petroleum exploration since 1950s. The basic theory is based on the principle of gamma ray absorption by Compton scattering. When gamma rays are emitted into the formation rock, Compton scattering reduces the energy of the

gamma rays. The photo-electric absorption will happen when the energy of the gamma rays decreases to a certain level, normally 0.5 MeV. The log tool records the flux of the gamma rays back from formation rock and the amount of attenuation reflects the density of electrons in the formation rock.

Density logging assumes that the measured bulk density only depends on matrix density and fluid density. These values are collected along the wellbore. This method is one of the most reliable porosity logging for sandstone reservoir and limestone reservoir since mineral density is well known (Toby, 2005).

A simple density log tool consists of a radioactive source and two detectors (one short range detector and one long range detector). Generally, a formation with a high bulk density reflects a high density of electrons. The electrons can significantly attenuate the gamma rays. Therefore, a low gamma ray count rate will be detected at the detectors. In a formation with low bulk density, the density of electrons is low. The electrons attenuate the gamma rays less than the high bulk density formation. Therefore, a high gamma ray count rate will be detected at the detectors.

The density porosity is calculated as

$$\phi_{density} = \frac{\rho_{matrix} - \rho_{bulk}}{\rho_{matrix} - \rho_{fluid}} \quad , \tag{1.20}$$

where ρ_{matrix} is the matrix density, for sandstone ρ_{matrix} = 2.65 g/cm^3, ρ_{bulk} is the formation bulk density and ρ_{fluid} is the density of formation fluid (oil, gas, water) respectively. In this equation, the bulk density is detected from log tools. Both fluid density and matrix density are known. Therefore, the density porosity can be calculated.

Neutron Log:

Neutron logs measure the hydrogen contents in the subsurface formation. This tool

emits high-energy fast neutrons from electronic or chemical sources. Neutrons collide with nuclei in the formation and the neutrons lose energy. A gamma ray will be emitted with enough collisions. In reservoir rocks, materials with large hydrogen content will slow down neutrons. The hydrogen is always correlated with fluids such as oil or water that fill the pore volume. Therefore, neutron logs can measure the porosity by measuring hydrogen (Glanville, 1970).

Sonic Log:

Sonic porosity is computed by comparing the time of sound passing through the formation. With different rock and fluid types, the travel time of sound is different. The interval transit time Δt of a sound travelling through the formation along the axis of the borehole is measured by recording the acoustic pulse from the transmitter to receivers. Sound travels more slowly though fluid-filled rocks than through rock matrix. Therefore, Δt_{log} reflects to porosity (Glanville, 1970). A commonly used equation is shown as

$$\phi_s = \frac{\Delta t_{\log} - \Delta t_{matrix}}{\Delta t_{fluid} - \Delta t_{matrix}} \quad , \tag{1.21}$$

where $\Delta t_{\log}$ is the acoustic transit time, Δt_{fluid} is the acoustic transit time of interstitial fluids and Δt_{matrix} is the acoustic transit time of the rock matrix, for sandstone Δt_{matrix} =51 (μs/ft).

1.2 Logging While Drilling Techniques (LWD)& Geosteering

The term logging while drilling (LWD) is sometimes used interchangeably with measurements while drilling (MWD), but there are some differences between them. LWD is commonly used for obtaining information about rock properties (porosity,

resistivity, etc.) while MWD is used for obtaining information about the progress of the drilling operation (rate of penetration, weight on bit, wellbore trajectory, etc.). LWD today often refers to geosteering measurements made to help deciding on adjustments to the wellbore trajectory (Scherbatskoy, 1982)

In addition to obvious economic benefits, there are some advantages to use LWD techniques: While drilling directional wells, LWD data is used in real time to determine the trajectory and lithology. Secondly, LWD can measure conventional logging items without wire line. The slower speed reduces the statistical error of radioactive logging and improves the vertical resolution of the instrument. Finally, LWD data is collected immediately after the formation is drilled. Therefore, the formation has not been affected or only slightly influenced by the drilling mud invasion; hence, logging response characteristics potentially better reflect the original formation.

Alberto et al. (2002) presented a new technology of drilling horizontal wells in thin oil columns and updated 3D geological model while drilling. This research used depth markers observed in several offset vertical wells to determine the uncertainty of the depth of the target layer in the geological model. LWD logs and resistivity images from downhole MWD and LWD tools are integrated into the predrilled geological model to update entire geological model. However, this research focused on updating the geological model to better simulate the target formation depth and didn't consider the formation petrophysical properties update.

Schlumberger developed an advanced geosteering techniques to update geological models with LWD tool responses ahead of the drill bit in real time (Schlumberger, 2007). This application is very powerful and capable of integrating all the relevant data from almost all the sources including seismic survey, well logs, core in a single application and quickly update their models. This application can also identify fault patterns, real-time monitoring and adjust the well trajectory to meet all the targets. However, this

application is integrated in the Petrel platform and users must follow all the instructions to import all the data and operate step by step since the core code is secured. Petrel is a nice software if you have all the data in one package and same data format. Otherwise, the result can be unreliable and need a long time to get.

SES is a 3D technical geosteering drilling software developed by Stoner Engineering Company. This software integrated the 3DStratBlock technical geosteering method with relative Stratigraphic Depth (RSD) signal mapping, Technical Hole Deviation (THD) calculations, traditional 3D/2D well planning and patented Fuzzy Logic Control technology. Meanwhile, it can use LWD data in the advanced visual geosteering interpretation tools (SES, 2015). One of the advantage of this software is the general 3D well planning without THD and grid data integration is free. However, with constant add on and updates, it is very clunky.

As one of the world's largest oil field service companies, Halliburton provided a series of services including drilling engineering solutions, geosteering services, LWD services, drilling optimization and logging techniques. Some software applications have been developed to support these services in real-time operations. MaxDrill Drilling Efficiency software is developed to calculate the efficiency of the drill bit in real time in relation to formation type and rock properties and guide the adjustment of drilling parameters, expected rate of penetration and projected bit wear. StrataSteer software integrates digital 3D geological models, directional well plans and real-time LWD sensor data into a dynamic and intuitive geosteering application. Daily production rate of many wells increased 10 percent in past operations. Halliburton has the world's top technology in LWD sensors especially with the largest and most robust high pressure, high temperature environment (Kumang, 2012). Unlike how Petrel integrated all the applications in a single platform, Halliburton software packages are separated into several different applications and are mainly used to support their services.

Since all the software packages discussed above are commercial software and code is secured, the core algorithms are unknown and different packages have different advantages and disadvantages. However, the general workflow is roughly the same. Data from seismic survey in the working area and data from well logs in nearby wells are used to build a basic geological model to describe the formation structure. Petrophysical properties are then filled into each grid block of the geological model by using geostatistical techniques. In the process of drilling, the base geological model is kept updated with real-time LWD data collected from down hole. Updated geological model is then used to guide the well trajectory and increase reservoir production. The comparison of the different software is shown in Table 1.1.

However, the integrated geosteering workflow developed in this research is quite different compared with the commercial software discussed above. First, the workflow is developed to be easily integrated using existing commercial software or custom code. It is totally free and easy to adjust. Second, in some cases, some important features may be lost during the model updating process from geological model to reservoir simulation due to the simplification of grid blocks. In this research, the data input is point-set porosity data with coordinates. The original data set is always applied as hard data and assigned a high weight. The results are more reliable. Third, the geostatistical model is updated directly with LWD data. The missing variables may increase the risk and uncertainty but this application is better for fast paced drilling in grain-dominated sandstone formations.

Table 1-1 Comparison of Different Packages

	Petrel	SES	Halliburton Packages	This research
Integrated and interchangeable platform	×	×	×	✓
Easily load/transfer data to other O&G apps	×	×	×	✓
Interpolate survey for coordinates at any Depth	✓	✓	✓	✓
Advanced Well logging techniques	✓	✓	✓	×
Vagriogram Modeling	✓	✓	✓	✓
Kriging Estimation	✓	✓	✓	✓
Geostatistical Model Updating	✓	×	✓	✓
Reservoir Simulation	✓	×	×	✓

1.3 Background Geostatistical Problems

The use of geostatistics to address problems in the exploration and production segments of the petroleum industry is steadily growing and showing a huge advantage of integrating data from different scales.

From basin exploration to reservoir production, models play a very important role in understanding and predicting a reservoir's geological and geophysical information and production performance. Seismic data can give a very coarse understanding of the extent of the reservoir. Well logs give a detailed petrophysical reflection. However, data is still limited in a huge 3D field. The estimation of formation petrophysical properties is always one of the key goals of reservoir characterization. Active geostatistical research programs (SGeMs by University of Stanford, GSLIB by Statios) are often found imbedded in engineering programs. Although geology is recognized as an

important and necessary component of geostatistical research, it is often the weakest academic link among different fields (Lake, 1986).

A challenge is that data input in this research is limited. Here, in this thesis, all data used in the case studies are collected from the Norne Field and mainly from exploration well reports. The lack of seismic and production data adds a lot of uncertainty while predicting reservoir behavior.

1.4 Objective and Motivation

The objective of this research is to develop a workflow of updating well trajectory with LWD data based on geostatistical model. The well trajectory design depends on the formation porosity distribution map. Therefore, a key point in the process is to map the reservoir porosity distribution.

In this research, the reservoir is divided into different grid blocks and geostatistical techniques are applied using available well log data to estimate the porosity value in each grid block, thereby creating a geostatistical model. Ignoring all the unnecessary features, the formation porosity distribution is assumed directly acquired from this geostatistical model. LWD techniques are applied in this thesis to collect well log data while drilling. These log data are used as hard data and integrated into the base model to update the local porosity distribution of the target reservoir formation. The updated model can better guide well trajectory and optimize production performance.

Most commercial platforms can apply LWD techniques to optimize drilling practices. However, these platforms require all the necessary program features input. This has advantages and disadvantages. The large amount of parameter input makes it more reliable but sometimes it may not meet specific goals and at the same time, it slows down the processing speed.

The goal of this research is to build an open platform integrated geosteering model which combines the necessary parameters in geostatistical techniques, LWD techniques and reservoir simulation methods. The base geological model is built from the generated geostatistical model and LWD data is directly applied on the geostatistical model to update the porosity distribution map. The integrated system is easy to adjust to reach specific goals. Meanwhile this application can be validated by production simulation results.

Compared with current research outcomes, this application is quite novel and time efficient. The details are described in Chapter 2. In most cases, updating the geological model with LWD data requires longer processing time. In this research, the local porosity distribution is updated rapidly with a point-set spatial relationship instead of recalculating the global porosity distribution. Once these log responses are received from down hole, the method is applied to update the porosity distribution in the well bore region. Although the accuracy is decreased with distance from the well bore, the updated porosity distribution can better guide the drilling trajectory and then optimize production performance. The reservoir simulation results also show advantages in production due to this real-time geosteering.

1.5 Thesis Outline

Chapter 1 is a basic introduction chapter that presents basic concepts, background geostatistical problems, the motivation and objective of this thesis. The main objective of this research is to develop an integrated geosteering workflow to optimize reservoir formation production. Existing commercial software is used and some applications are developed.

Chapter 2 reviews relevant research in applying geostatistical concepts in formation petrophysical modelling and current model updating while drilling techniques.

Methodologies are described in Chapter 3. Data input for this research includes well operation, reservoir attributes, petrol physical information, all from a real oil field. There are two case studies applied in this thesis. The first case study represents a general process of geostatistical modelling and the effect of geostatistical realization outcomes at the reservoir simulation stage by comparing production performance. The Second case study builds the geostatistical models using the same process as used in case study one. However, the main purpose of this case study is to update geostatistical models with LWD data and guide well trajectory while drilling with the updated model. Then, the model will be compared by production performance and economic evaluation.

Chapter 4 presents the results of case study one and case study two. The data output and input between different software platforms is shown in this chapter as well. As different software needed different data formats, the data files must be converted between each step. The results of case study one shows that the geostatistical modelling outcomes can significantly affect the reservoir simulation results.

Finally, conclusions and recommendations of this thesis are presented in Chapter 5.

2. Literature Review

2.1 General Review

This research is interdisciplinary and the literature review is divided into four different sections: geostatistical methods, reservoir petrophysical characterization, LWD techniques and model updating techniques. However, there is already some research published with similar objectives to this research.

2.2 Kriging and Geostatistics

The application of geostatistics in petroleum geology started in the late 1980s. However, this concept has been used in the mining industry since early 1950s. The transition from the application of geostatistics from mining to reservoir analysis is indeed a difficult task due to a lack of data and deposit differences between hydrocarbon and solid minerals. Therefore, in the 1980s, a few research groups started to develop new methodologies to apply the geostatistical concepts to reservoir characterization. These groups include the Institute of French Petroleum (Macleod et al., 2005); several U.S.

schools led by Stanford University (Remy et al., 2011); and some Norwegian schools such as University of Oslo (Damslet, 1997). Geostatistics can integrate different data and stochastically define a reservoir. Some researchers explored the possibility to create numerical models with data from different sources. Philippe (1988) introduced an approach of using a Co-Kriging technique to map porosity with seismic data. As compared to the standard least-squares approach, Co-Kriging techniques show not only more precise porosity estimates, but also relative confidence margins on the estimated values. Chopra et al. (1990) collected data from about 50 wells and used them to evaluate properties among wells. Two methods are used in their research, the Kriging method and the two-point inverse distance weighted interpolation method. The properties estimation results indicate that the geostatistical techniques have more potential to capture spatial correlations compared to conventional techniques like inverse distance weighted methods. The Kriging estimation results are more reliable.

To integrate a large set of data input, geostatistics were applied in reservoir characterization, Geostatistical methods were first developed in the 1950s by Danie Krige and used in the mining industry in South Africa (Krige, 1951). In the fall of 1988, the Society of Petroleum Engineers (SPE) held a forum on reservoir characterization in Grindenwald, Switzerland to discuss the idea of using stochastic methods for reservoir characterization (Olea, 1991). This represented a milestone in geostatistics research. Lake and Carroll (1986) had previously described methods for applying the concepts of geostatistics to reservoir simulation. Currently, geostatistical models are widely used to interpolate between wells and reduce reservoir uncertainty.

Kriging techniques and other traditional mapping techniques based on weighted averages are still widely used. Geologists started to explore the application of geostatistics in stochastic reservoir characterization since late 1990. However, the regular or smooth models generated by standard mapping techniques were unable to

meet the requirement of reservoir heterogeneity and subsequent flow simulations. Haas et al. (1994) indicated that geostatistical techniques can be used, not only to estimate petrophysical properties, but also be used at the earlier seismic inversion process stage. This idea embedded stochastic simulations directly into the inversion process to build high-resolution 3D acoustic impedance realizations and helped to characterize internal geological structures. However, the application of geostatistics in the inversion process must be applied to carefully prepared data, while the model needs to be validated using seismic and logging data.

Caers et al. (2000) published a series of papers on multiple-point geostatistics. The traditional application of geostatistics in reservoir characterization was limited by the variogram which can only capture two-point statistics. However, multi-point geostatistics is an algorithm which can capture multiple-point statistics and consider spatial relationships between multiple spatial locations jointly. This method can greatly enhance the ability of capturing the geological continuity of a reservoir compared to traditional two-point algorithms.

Willcott (2005) wrote an inspirational interdisciplinary thesis to analyze risk based on 2-D geostatistics to reduce uncertainty and optimize well trajectory. Their research focused on operation risk evaluation during drilling, specifically in the near well bore region. Jackson (2013) presented how a geostatistical realization can be used to describe reservoir heterogeneity in simulation models and the resulting impact on the flow properties. In their research, GeoMark software is used to predict fluid properties such as GOR, bulk petroleum phase volumes, etc. to enhance resource exploitation efforts.

The training-image (TI) algorithm is one of the object-based geostatistics which has allowed the creation of stochastic models to better recognize geology. It has been growing rapidly over recent years (Lantuejoul, 2002). TI algorithms do not need to use conditional data, but only need to represent the geo-objects and spatial relationship

between the objects. Maharaja (2008) took the generalist approach in writing the TI Generator plugin to SGeMS for describing a viability model to load user-defined geometries.

2.3 Reservoir Heterogeneity

The simplest reservoir simulation model is a homogeneous cake with the same properties throughout. This kind of model only requires reservoir volume and basic petrophysical properties. However, reservoirs are heterogeneous and rock properties, fluid properties vary from place to place. In this research, the estimation of porosity distribution is part of the reservoir heterogeneity study. Researches characterizing reservoirs with different points of view and new techniques has developed rapidly in recent years.

Rosman et al. (1977) showed reservoir heterogeneity, described with sophisticated sedimentary and diagenetic processes that are probably modified by tectonic changes. Seismic surveys can provide the spatial structure at the field scale and image reservoir features. Some research focuses on high resolution seismic interpretation techniques. Chopra et al. (2007) applied seismic attributes for prospect identification with different interpretation approaches. Bonnell (2006) discussed a theoretical statistical analysis of simulated lithologic detail with cross-well synthetic seismic data. Three case studies were derived from different sources and statistical estimation methods to reflect reservoir heterogeneity. The results display a unique distribution of reservoir properties for each case study. Oliver et al. (2008) discussed the application of inverse theory in history matching with nonlinear developments and updating reservoir simulation models by sequentially assimilating data.

Dong et al. (2007) developed a new downhole fluid analysis tool to detect reservoir fluid property heterogeneity with improved compositional algorithms. It is difficult to integrate all the parameters in one application. In most cases, the number of parameters is limited to solve the forward problem. However, the objective of all the research is to better characterize the reservoir properties.

2.4 LWD Techniques

MWD and LWD techniques were originally used as enhancements to early wire line logging technology and can be traced back to late 1970s (Segesman, 1995), while uniform industry standards were established in the 1990s. A typical MWD system consists of a down hole sensor unit, a power source, a telemetry system, and equipment on the surface to receive, record and display data. Many international companies have developed their own MWD and LWD systems such as VISION and the SCOPE systems developed by Schlumberger, Geo-Pilot system developed by Halliburton and On Track system by Baker Hughes (Wang, 2001). Due to its advantages of low-cost and risk control, these techniques are now widely used for geosteering drilling and formation evaluation, especially for high angle or horizontal wells.

Computer power limits the applicability of these methods for performance predictions of large-scale projects. It may take months to simulate the flow performance with a high-resolution grid block model. This is a problem throughout the entire process of upscaling research. Different methods are applied to upscale various properties to reduce information loss. Morton (2010) described a high-resolution model for geological information with lumped average parameter estimation. Trina (2010) showed some very meticulous code to integrate a flow simulation model. Abdideh and Mahmoudi (2013) indicated a new method called Uniaxial Compressive Strength (UCS) prediction to optimize the geomechanically estimation.

2.5 Geostatistical Model Updating

In the life of a field development project, a number of different models will be built and a number of updating processes will be performed as well. This type of updating can improve the reservoir description accuracy and decrease reservoir uncertainty.

There are many ways to update a geostatistical model depending on the demands of the project. Henning (1998) suggested a model updating process of large structure updating in his doctoral thesis. HIs study used response-based methods instead of traditional model-based methods to break the limits of measurement tools. Three case studies were performed in the thesis with increasing complexity. The study presented a unique way of predicting properties with limited information. However, it was difficult to integrate data from different resources in a field, since the underlying algorithm is based on analytically-defined sensitivities and is not subject to numerical approximations. It differs from the common workflow in oil and gas companies.

Marshall et al. (2000) explored an updating process which combined real-time logging while drilling data into a seismic model at a “relevant time”. The drilling data travels from down-hole to ground and a relevant time was calculated based on the data transfer speed and drilling position. However, some limits exist due to the lack of well data. The model was built using seismic data only. As drilling progressed, the correlation between log and seismic data changed and the time to depth conversions needed to be re-calculated. Although this study applied a key marker (normally marks the top of target formation) to correlate the log response between the new model and the predrill model, it was not very accurate.

There is also research on integrating dynamic data to update geostatistical models. Wen et al. (2006) discussed the application of the Kalman Filter technique (EnKF). This technique was used to update permeability distribution maps to match real-time

multiphase production data and reduce reservoir uncertainty (Sorenson, 1966). Sarma (2006) explored a simplified reservoir management approach called Closed Loop Approach that combined efficient optimization and model updating mainly in the history matching stage. In this study, two-point geostatistical estimation was applied to estimate the unknown parameters in terms of a Karhunen-Loeve expansion (Sorenson, 1966).

The literature quoted in this chapter demonstrates that work has been done linking geostatistics, logging while drilling techniques and the model updating process. These research studies and technologies are all aimed at the same purpose, to better characterize the reservoir underground.

3. Methodology

The objective of this research is to develop a workflow for real-time geosteering by updating the geostatistical model with LWD data. The geosteering trajectories are compared using integrated reservoir simulation. Basic concepts are already introduced in Chapter One. Geostatistical concepts are used to build a geostatistical model with formation porosity and permeability data; LWD techniques are used as real-time data to update the geostatistical model; reservoir characterization concepts are used to simulate production rate and compare the influence of the geostatistical model on the reservoir production stage. This chapter presents geostatistical concepts applied in this research including data spatial relationships, variogram modeling, Kriging estimation methods and sequential conditional simulation methods.

There are two case studies applied in this research. Case study one explores the influence of geostatistical estimation results in production performance by creating different porosity distribution maps with Kriging estimation methods. These porosity distribution maps are imported into a reservoir simulator and compared by production

performance. Case study two focuses on updating local porosity and permeability distribution maps with LWD data. The variogram analysis in this case study is similar to case study one but uses sequential simulation methods to generate global porosity and permeability distribution maps due to the lack of data. LWD data are then integrated into the base geological model to get more reliable local property distributions. Both case studies use the Norne field data for which to test the geostatistical updating as well as the open platform integrated geosteering application created.

3.1 Norne Field Introduction

The Norne field is located 200 km offshore the west coast of Norway in the Norwegian Sea. Figure 3.1 shows the location of Norne Field and nearby fields. The water depth in this area is about 380 m. It was discovered in December 1991, development drilling started in August 1996, and oil production started in November 1997. Natural gas has also been produced from the Norne field since 2001. This field has been developed with a production and storage vessel and is operated by Statoil (NTNU, 2004).

3.1.1 Geological Background

As can be seen in Figure 3.2, the Norne Field can be divided into two separate oil compartments: the main structure which includes C, D and E segments, and the Northeast G segment. Approximately 98% of oil in place is situated in the main structure. The C, D and E segments are separated by regional faults. The total hydrocarbon column is 135 m thick mainly consisting of rocks of lower and middle Jurassic age and includes a 110 m oil column and a 25 m gas cap (Statoil, 2001).

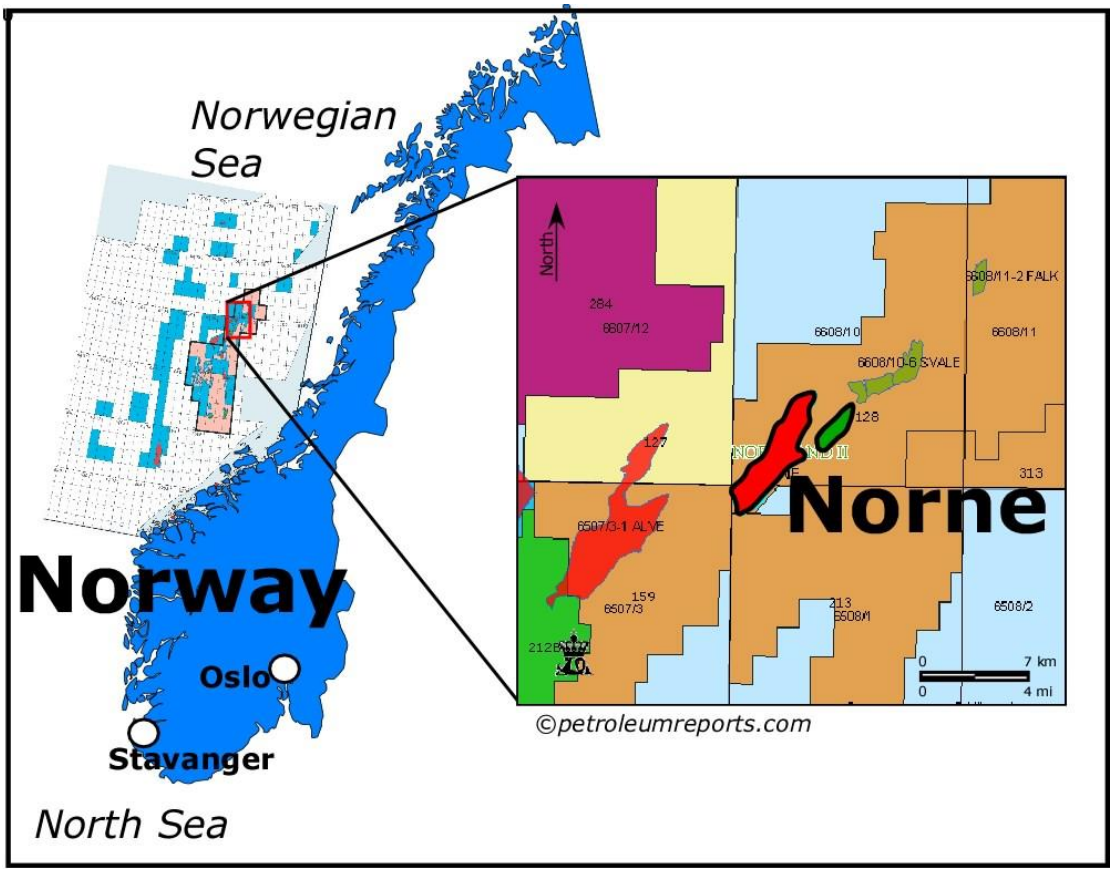

Figure 3.1 Norne Field Geographic Location (NTNU, 2004)

3.1.2 Structure and Petroleum System

Figure 3.3 shows the stratigraphy chart of Norne field. The source rocks are believed to be the Spekk formation in the upper Jurassic and there is formation of lower Jurassic age. The oil is mainly situated in the Ile and Tofte formations of middle to lower Jurassic age, and the gas cap is mainly situated in the Garn formation of middle Jurassic age. The Tilje formation of lower Jurassic age also contains some oil resources. The cap rock which seals the reservoir and keeps the hydrocarbon in place is the Melke Formation. Another main cap rock which separates the communication between the Garn and Ile formations are the Not formation. As displayed in Figure 3.3, from top to bottom, reservoir rock is dominated by fine grained channel sandstone and small amounts of

claystone and siltstone. Therefore, the reservoir is divided into four different formations: Garn, Ile, Tofte and Tilje.

Figure 3.2 Norne Field with all the Segments (NTNU, 2004)

The target segment in this case study is the E-segment in the main structure since the E-segment is relatively flat with no complex structures and has a number of wells that can be analyzed.

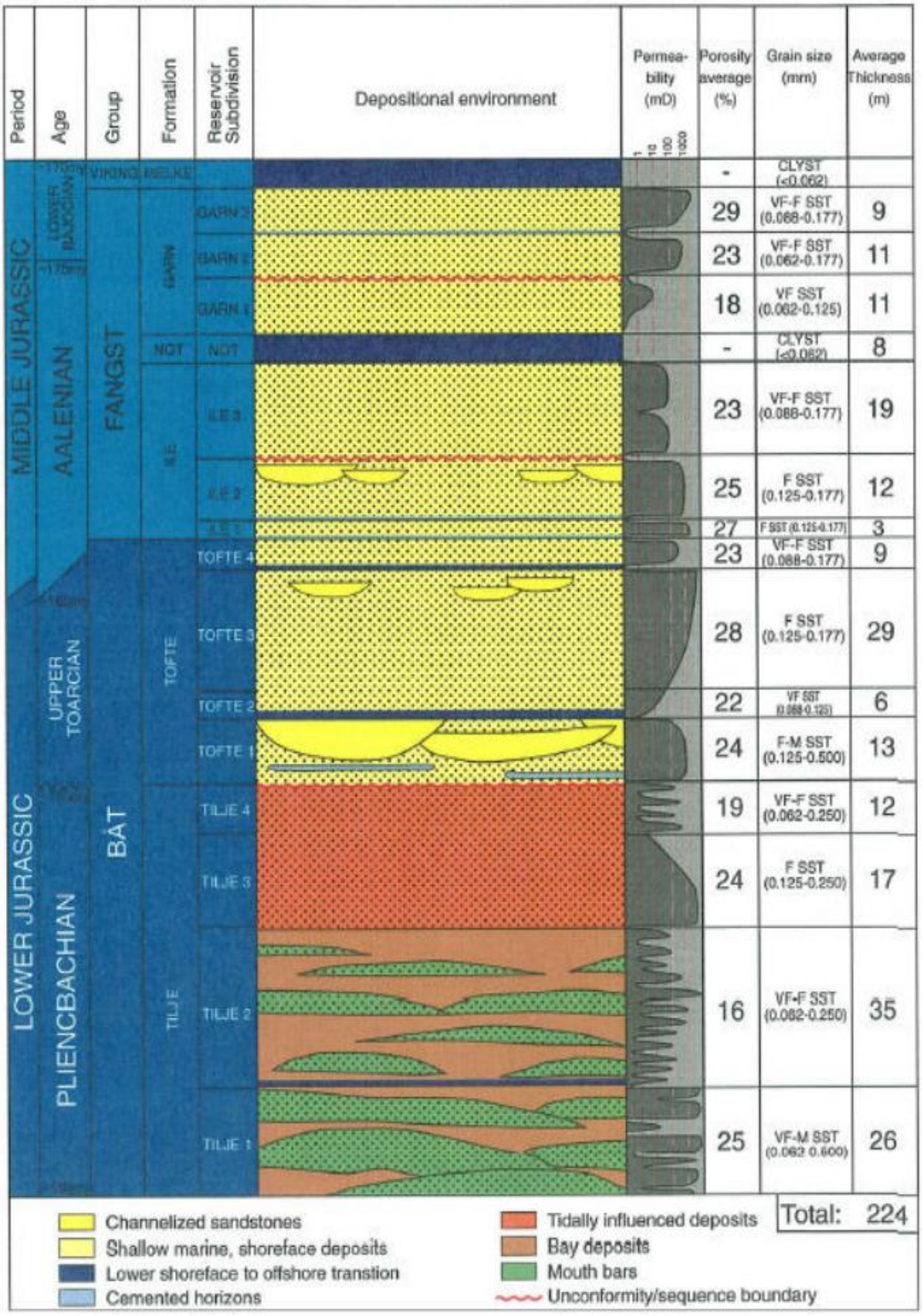

Figure 3.3 Norne Field Stratigraphy Chart (Statoil, 2001)

3.2 Case Study One: The Influence of Geostatistical Estimation Results on Production Performance

The workflow of case study one is shown in Figure 3.4. The first step is Data input and analysis. As introduced above, data input of this case study is the point-set porosity data with coordinates from Ile formation, E-Segment, Norne Field.

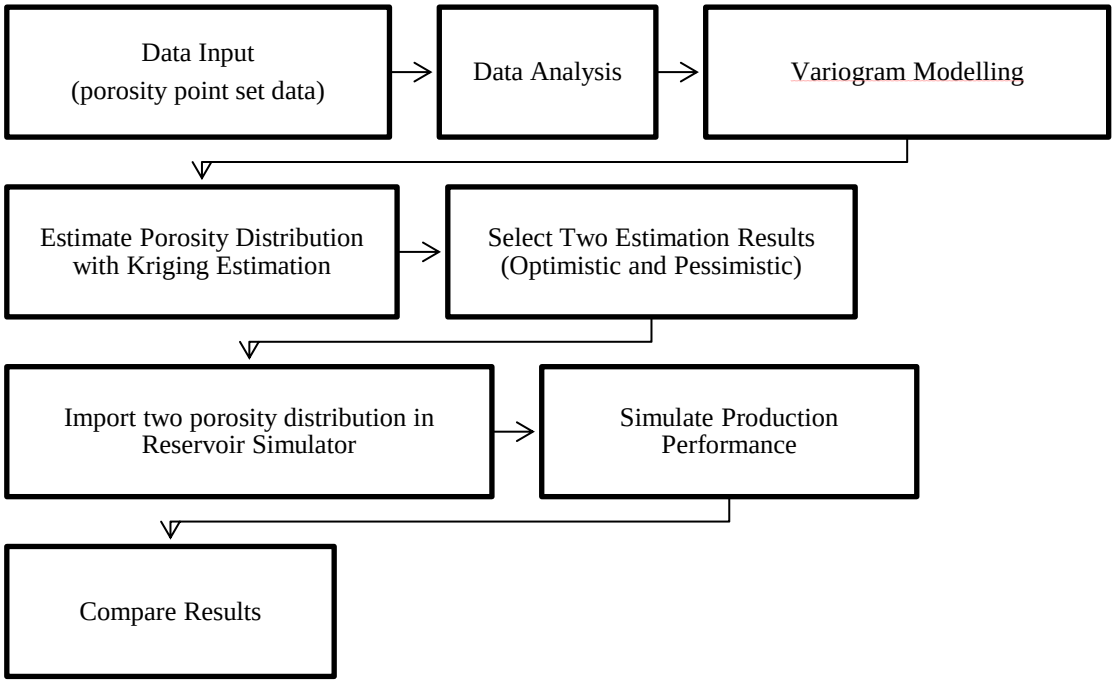

Figure 3.4 Case Study One Workflow

The second step is to analyze the data spatial relationship by building a variogram model. Variogram modelling includes: determining the major and minor directions; choosing parameters such as number of lags, angle and lag tolerance; plotting experimental variograms and choosing variogram model that fits the experimental variogram. Kriging techniques can then be used to estimate global porosity distribution. Due to the different visiting paths, thousands of distribution maps can be generated with same data input. Therefore, two estimation outcomes are selected, one is the most optimistic outcome with the highest porosity mean value and one is pessimistic outcome with the

lowest porosity mean value. The two estimation outcomes are imported into Eclipse to simulate production performance under the same reservoir conditions for comparison.

3.1.1 Data Analysis

Before a geostatistical analysis starts, it is necessary to first introduce the original dataset and data analysis process. As shown in Figure 3.5, a total of 540 sample points with porosity value are in the dataset. The detailed dataset is shown in Appendix A. The mean value of the dataset is approximately 0.2875 and the variance is very small. The histogram indicates that the target formation is a fine reservoir with a relatively high porosity distribution. The sample distribution is quite uniform so data pairs can be easily found within a certain search area. The upper right-hand side of the figure displays the summary data for the histogram as well as some of the univariate properties of the porosity dataset which are required by Kriging methods.

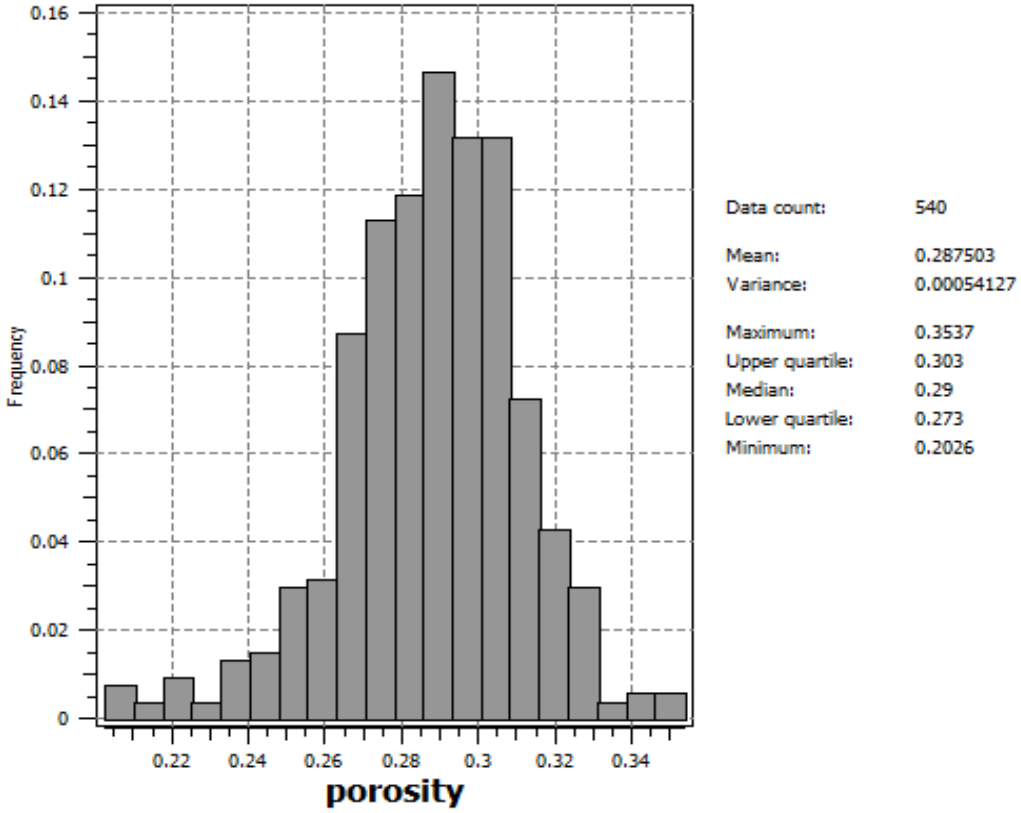

Figure 3.5 Histogram of the sample porosity

3.1.2 Variogram Modeling

Variogram modeling is the first step of estimating the porosity distribution in the field. Since the reservoir used in this study is heterogeneous in porosity, the variogram will vary in both distance and direction. Therefore, it is necessary to calculate the maximum continuity in different directions to explore which direction presents the most and least amount of continuity. In most cases, the least amount of continuity (which is also called the minor direction) is taken perpendicular to the direction of maximum continuity (Goovaerts, 1997). In this case, a number of variograms are calculated in different directions from 0^{o} to 180^{o}. Since the porosity samples in this case are in a point-set object, data do not strictly follow the regular spatial pattern. It is unlikely to find enough

pairs of data with a certain distance $\vec{L}$.

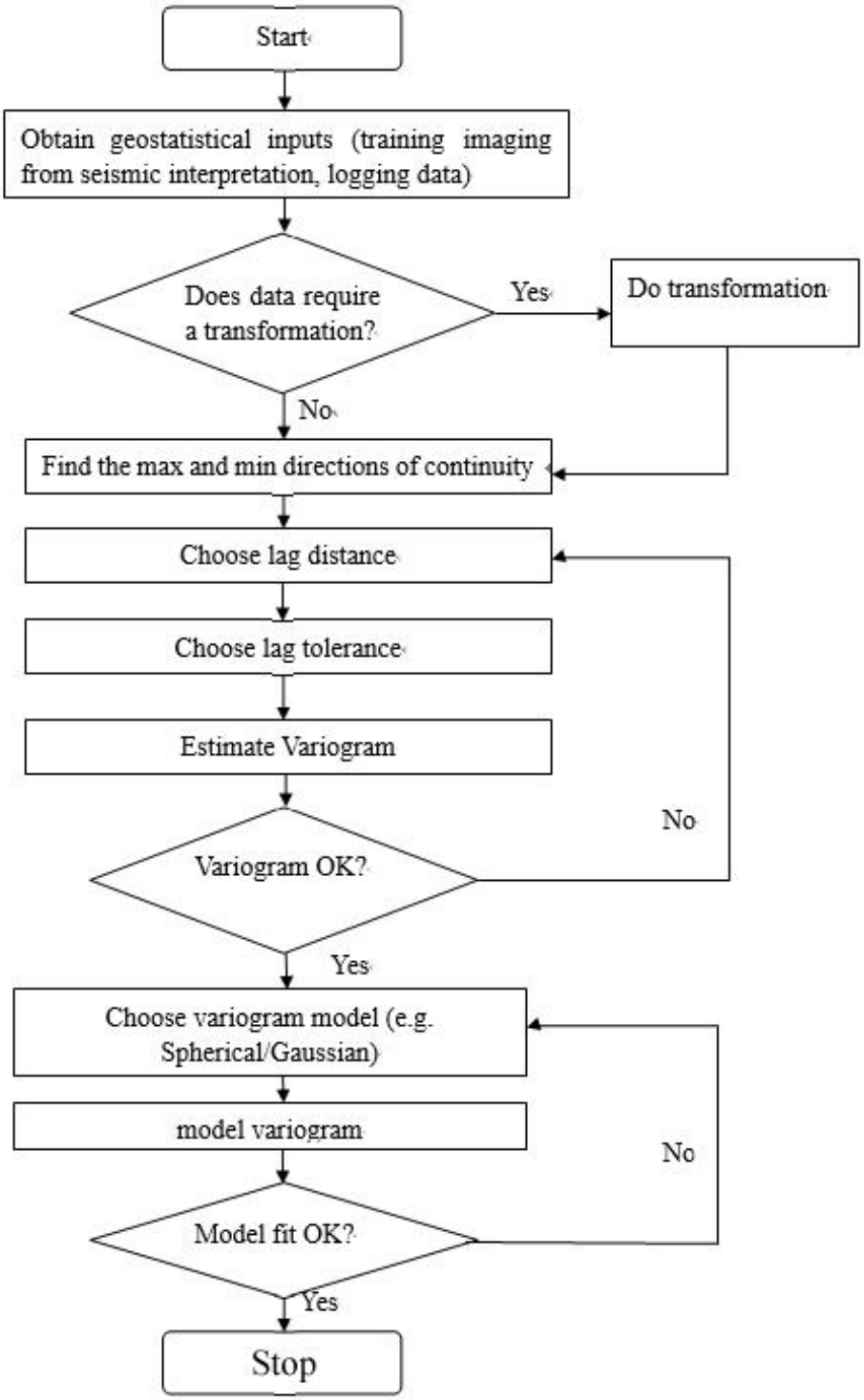

Figure 3.6 Variogram Methodology

Figure 3.6 presents the work flow of the variogram modelling. In order to keep the essential structure of the variogram model intact, some additional parameters are also considered in this case study.

Stationarity Requirement

Before analyzing the spatial relationships of data sets, some assumptions are required in this case study. The basic assumption, as mentioned before, is that all the data in the data sets have relationships between each other. It is inadequate to estimate porosity at a specific location based on the data from a different layer or geological body in the reservoir even though the spatial distance between them is close. Another important assumption is that any function is only related to the distance from the variable, not to the variable itself. This means that as long as the distance and direction between any two points are known, functions can be estimated between these two points. This is called first order of stationarity.

First order of stationarity can be written as

$$f[X(\vec{u})] = f\left[X\left(\vec{u} + \vec{L}\right)\right] , \tag{3.1}$$

where f [ ] is a function of a random variable X, where $\vec{u}$ and $\vec{u} + \vec{L}$ are defined as the two locations of the random variables. Therefore, if we use mathematical expectation as an example, this equation can be written as

$$E[X(\vec{u})] = E\left[X\left(\vec{u} + \vec{L}\right)\right] . \tag{3.2}$$

This equation states that the expected value of a random variable X at $\vec{u}$ is the same as the expected value of a random variable X at $\vec{L}$ distance away from the original location $\vec{u}$.

The second order of stationarity states that the covariance of different variables at the

same location should be equal to the global variance.

Second order of stationarity can be written as

$$C\left[X(\overrightarrow{u_1}), X\left(\overrightarrow{u_1}+\vec{L}\right)\right] = C\left[X(\overrightarrow{u_2}), X\left(\overrightarrow{u_2}+\vec{L}\right)\right]. \tag{3.3}$$

In applications, local means frequently differ significantly and the variables at the unsampled location is linearly related to the surrounding samples which can be expressed as

$$x^*\left(\vec{u}_0\right) = \sum_{i=1}^{n} \lambda_i x\left(\vec{u}_i\right), \tag{3.4}$$

where $x^*\left(\vec{u}_0\right)$ is the estimated value at the unsampled location $\vec{u}_0$, $x\left(\vec{u}_i\right)$ is the sample value at surrounding location $\vec{u}_i$, and λ_i is the weight assigned to sample $x\left(\vec{u}_i\right)$. In ordinary Kriging,

$$\sum_{i=1}^{n} \lambda_i = 1. \tag{3.5}$$

The second order of stationarity shows that any function of two random variables located $\vec{L}$ distance apart is independent of the locations. In other words, the spatial relationship between two variables is a function of distance and direction between two sample locations (Kelkar et al. 2002).

Lag Distance

The distance between two variable measurements is called the *lag distance*. As shown in previous equations, the strength of the relationship between a variable and its relative location is decided by the covariance between the variables and the lag distance instead of real locations of variables in the data set. The covariance is a function of the variable

at both locations, $\vec{u}$ and $\vec{u}+\vec{L}$.

$$C(\vec{L}) = C\left[x(\vec{u}), x(\vec{u}+\vec{L})\right]. \tag{3.6}$$

One of the most critical points of spatial relationship estimation is choosing the appropriate lag interval to determine the number of sample points in the search area. Too many sample points in the search area will cause long running times and data smearing while too few sample points will decrease the accuracy of the results. The optimization is based on experimentation and the source of the original data.

A simple example of lag distance calculation is discussed as an example. Table 3-1 represents some porosity data collected from Well E-2H at the Norne Field. There are 5 pairs of data with a vertical distance of 1 m. For a vertical distance of 2 m, there are 4 pairs. For a vertical distance of 3 m, there are 3 pairs. Recall that in Equation 3.6, *n* is the number of pairs. Increasing the number of pairs improves the strength of the spatial relationship. Generally, even for a small data set, at least seven to ten pairs of data are needed for a reliable estimation of the variogram with a certain lag distance.

Table 3-1 Lag distance example with Porosity data

Depth (m)	Porosity (%)
2585	0.14
2586	0.13
2587	0.10
2588	0.15
2589	0.18
2590	0.05

As can be seen in Figure 3.7, starting from the origin node, all nodes fall in the area with certain lag tolerance, angular tolerance, number of lags will be taken into consideration. The number of data pairs (between the node at origin and nodes in the certain area) can be determined (See example in Table 3.1).

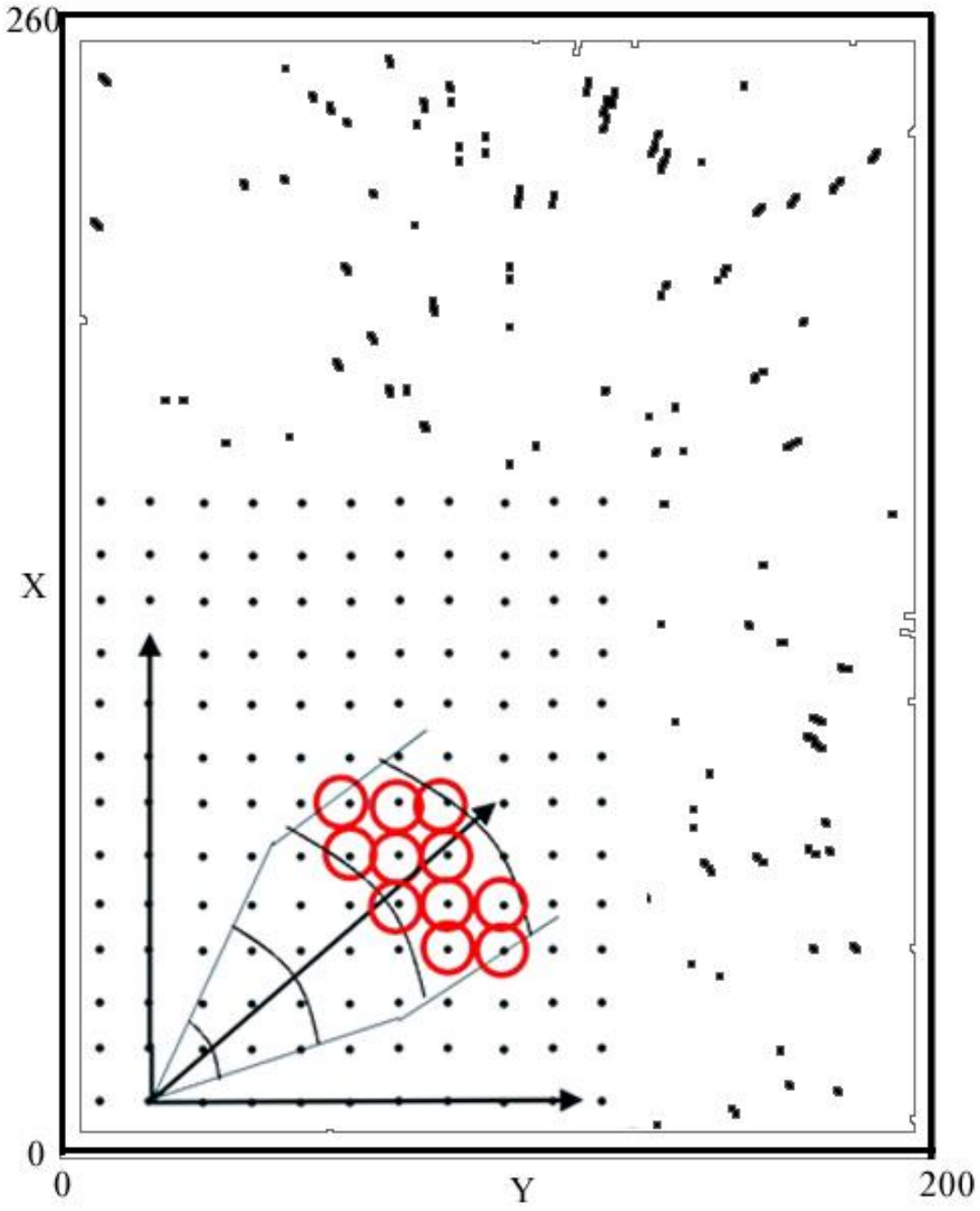

Figure 3.7 Variogram Calculation showing with node

The precise value of these parameters such as tolerance, number of lags cannot be simply calculated. The choice of these parameters depends on the variogram model results.

Since the target data set is from the heterogeneous and anisotropic reservoir formation, the anisotropic models are described in this section. The direction of most continuity can be found from existing exploration information from the working area. For example, for channel sandstone reservoirs, the porosity distribution in the direction of the channel shows better continuity than the direction across the channel (Clark, 2009).

The selection of major and minor directions, which show the maximum and minimum continuity, is one of the most important factors in anisotropy modeling. In this thesis, with a certain search neighborhood, variograms with different directions are estimated such as 0°, 22.5°, 45°, 67.5°, 90°, 112.5°, 135°, 157.5°, 180°. At each of these angles, an experimental variogram is plotted and the range is recorded. The direction with largest range (which reflects the data at this direction has maximum spatial continuity) is selected as the major direction.

Since both case studies in this research are in three dimensions, the approach to estimate anisotropy is to find ranges a_x, a_y, and a_z in the x, y, and z directions. Then, these variables are transformed from a three-dimensional lag vector $L= (L_x, L_y, L_z)$ into an equivalent isotropic lag using:

$$L = \sqrt{(\frac{L_x}{a_x})^2 + (\frac{L_y}{a_y})^2 + (\frac{L_z}{a_z})^2} \tag{3-1}$$

An anisotropic variogram is shown in Figure 3.8 with single layer porosity data input from Norne Field. With different azimuth at 0°, 45°and 90° directions, variograms show significant differences. Variograms at all the azimuths approach the same sill value of 0.0055. At azimuth of 90°, the variogram reaches the sill at 25 m distance which indicates that the geological continuity in this direction is quite good. At azimuth of 45°, all the points are approximately the same value. The structure may reach the sill at a very small range. The data in this direction show a very weak relationship. This may

due to the reduced number of data pairs used to estimate in this direction. At an azimuth of 0°, the variogram reaches the sill at 20 m distance. The spatial relationship of data in this direction is as good as that in azimuth of 90°. However, these directions are probably not the maximum or the minimum directions. Variograms can be estimated for any direction using the same principle.

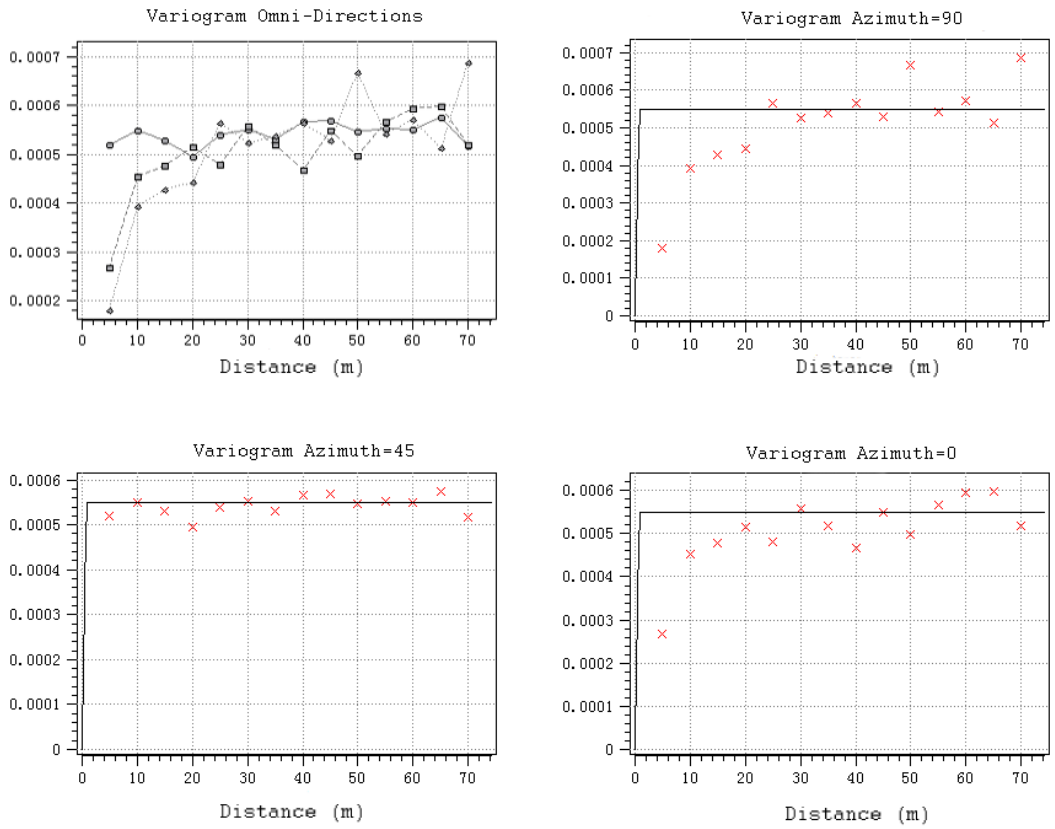

Figure 3.8 Variogram Models with Different Azimuth

3.1.3 Kriging Estimation

After the variogram model has been estimated, the next step is to estimate porosity values over the entire working area using the Simple Kriging estimation. The selection of using the Simple Kriging method is based on the original data spatial distribution in

the working area and the variogram model results. In this case study, the sample spatial distribution is quite uniform and variance is very small. The Simple Kriging (SK) procedure is the simplest but not necessarily the most practical. Mathematically, it can be written as

$$x^*(\vec{u}_0) = \lambda_0 + \sum_{i=1}^{n} \lambda_i x(\vec{u}_i), \tag{3.7}$$

where $x^*(\vec{u}_0)$ is the value at unsampled location, $x(\vec{u}_i)$ is the sample value at nearby locations $\vec{u}_i$, n is the total number of samples selected within a search neighborhood , λ_i is the weight assigned to each sample and λ_0 is a constant value.

The most critical point is to estimate the values of λ_i and λ_0. Recall that the stationarity requirement is

$$E[x^*(\vec{u}_0) - x(\vec{u}_0)] = 0 \ , \tag{3.8}$$

and

$$E[x(\vec{u}_i)] = E[x(\vec{u}_0)]. \tag{3.9}$$

Substituting Equation 3.8 and 3.9 into Equation 3.7, yields

$$\lambda_0 = m(1 - \sum_{i=1}^{n} \lambda_i), \tag{3.10}$$

where m is the global mean value of the dataset.

Furthermore, Simple Kriging estimation requires that the variance is minimized. Mathematically, this means that

$$V = s^2\left[x(\vec{u}_0) - x^*(\vec{u}_0)\right] \tag{3.11}$$

is minimized.

To satisfy these requirements, Equation 3.10 can be written as

$$\sum_{j=1}^{n}\lambda_j C(\vec{u_i},\vec{u_j}) = C(\vec{u_i},\vec{u_0}), \tag{3.12}$$

where $C(\vec{u}_i,\vec{u}_j)$ is the covariance value between points located at $\vec{u}_i$ and $\vec{u}_j$, and $C(\vec{u}_i,\vec{u}_0)$ is the covariance between sampled points located at $\vec{u}_i$ and the unsampled location $\vec{u}_0$.

In matrix form, Equation 3.12 can be written as

$$\begin{bmatrix} C(\vec{u_1},\vec{u_1}) & \cdots & C(\vec{u_1},\vec{u_n}) \\ \vdots & \ddots & \vdots \\ C(\vec{u_n},\vec{u_1}) & \cdots & C(\vec{u_n},\vec{u_n}) \end{bmatrix}\begin{bmatrix} \lambda_1 \\ \vdots \\ \lambda_n \end{bmatrix} = \begin{bmatrix} C(\vec{u_1},\vec{u_0}) \\ \vdots \\ C(\vec{u_n},\vec{u_0}) \end{bmatrix}. \tag{3.13}$$

To solve this equation, the relationship between the covariance and variogram also needs to be considered.

$$\gamma(\vec{L}) = C(0) - C(\vec{L}). \tag{3.14}$$

For a certain lag distance, $\gamma(\vec{L})$ can be calculated based on a certain variogram model. Furthermore, $C(0)$ is the sample variance which can be calculated based on the dataset. Therefore, $C(\vec{L})$ can be calculated based on Equation 3.13.

$$C(\vec{u}_i,\vec{u}_i) = C(0) \tag{3.15}$$

$$C(\vec{u}_i,\vec{u}_j) = C(0) - \gamma\left(\vec{L}\right) = C(\vec{L}) \tag{3.16}$$

Therefore, the only unknown parameter in Equation 3.13, λ_i, can be calculated by solving Equation 3.16. After λ_i is known, λ_0 can be calculated using Equation 3.10. The estimated value $x^*(\vec{u}_0)$ at unsampled locations is then solved using Equation 3.13.

The critical variable in this case study is porosity. In this case a 3D regular Cartesian grid is defined. The number of cells in the x, y, z directions are 100, 130, 10 respectively, where x, y represent the horizontal axes while z represents the vertical axis. The size of cells in the x, y, z directions are 2 m* 2 m*5 m. The geographical location of the origin of the grid is ignored since this is a theoretical case study and the real location of the working area will not affect the results. Based on the distribution of sample locations and the histogram of sample porosity, simple Kriging was chosen since the variogram model indicates that the spatial relationship of the data is quite close. The sample mean is used as the global mean.

Then, the following step is made to decide the size of the searching neighborhood. Data will be searched in an ellipse with a major radius of 24 m and a minor radius of 17 m. Four of the closest sample points were used to estimate the porosity at each grid block.

Recall Equation 3.13 and Equation 3.14:

$$\begin{bmatrix} C(\overrightarrow{u_1},\overrightarrow{u_1}) & \cdots & C(\overrightarrow{u_1},\overrightarrow{u_n}) \\ \vdots & \ddots & \vdots \\ C(\overrightarrow{u_n},\overrightarrow{u_1}) & \cdots & C(\overrightarrow{u_n},\overrightarrow{u_n}) \end{bmatrix} \begin{bmatrix} \lambda_1 \\ \vdots \\ \lambda_n \end{bmatrix} = \begin{bmatrix} C(\overrightarrow{u_1},\overrightarrow{u_0}) \\ \vdots \\ C(\overrightarrow{u_n},\overrightarrow{u_0}) \end{bmatrix} . \tag{3.13}$$

$$\gamma(\vec{L}) = C(0) - C(\vec{L}), \tag{3.14}$$

Every individual weight λ_i can be calculated such that

$$V[x(\vec{u}_i)] = V[x(\vec{u}_i + \vec{L})] = C(0), \tag{3.17}$$

The covariance for the left and right-hand sides of the matrix will first be calculated. Then the weighting parameters λ_i can be calculated by inverting the covariance matrix on the left-hand side of the Equation 3.13 and multiplying it by the covariance vector on the right side. The estimated porosity can be calculated by Equation 3.7. This procedure is repeated for each point until every grid block is visited by a path.

It is important to analyze the estimation results with different visiting paths. The chosen visiting path will significantly affect the result of the geostatistical realizations. Figure 3.9 displays the original porosity distribution in point set. The Kriging estimation utilizes a weighting system to compute the value of a variable. If the estimation starts from the relative higher value area (for example the left upper corner), each empty surrounding grid block will be assigned a higher value since the high value sample points (hard data) populate the area.

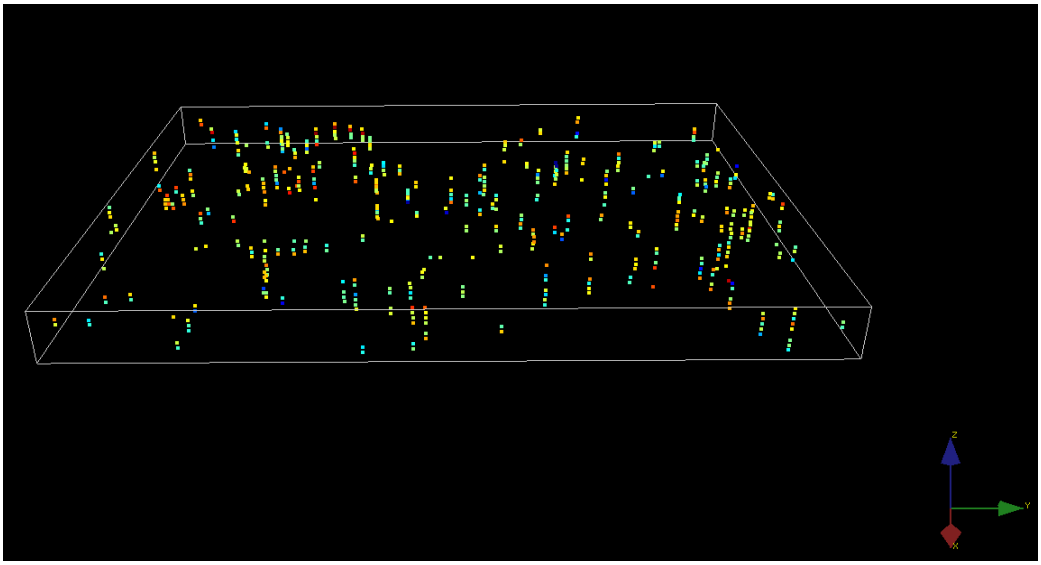

Figure 3.9 Porosity Distribution in Wire Frame

3.1.4 Reservoir Definition

The reservoir used in this case study is a hypothetical field with the length, width, height

as 260 m * 200 m * 50 m. Other factors such as fluid properties and rock properties are imported from the Norne Field data gathered from the Statoil Annual Report. The viscosity of oil is 0.3 centipoise (cP). The rock compressibility is set as $4.0*10^{-6}$ $Pa^{-1}$and oil compressibility is set as $1.65*10^{-5}$ Pa^{-1} (Statoil, 2004). However, some simplifying assumptions are made in this study since the high level of complexity of the initial problem is unnecessary in describing the methodology.

These assumptions are:

1. The reservoir permeability is assumed homogenous at 300 millidarcy (Ile formation average permeability) everywhere and in all directions.
2. The reservoir is assumed to be a single-phase reservoir and completely saturated with oil.
3. The oil is produced by depletion using a target rate and minimum bottom hole pressure.

The main variable of this study is therefore porosity. The sample points of porosity are collected throughout the reservoir and are imported from the Norne field well log report. The total number of sample points is 540. Figure 3.10 shows the sample distribution map generated in Petrel software and the specific data are given in Appendix B.

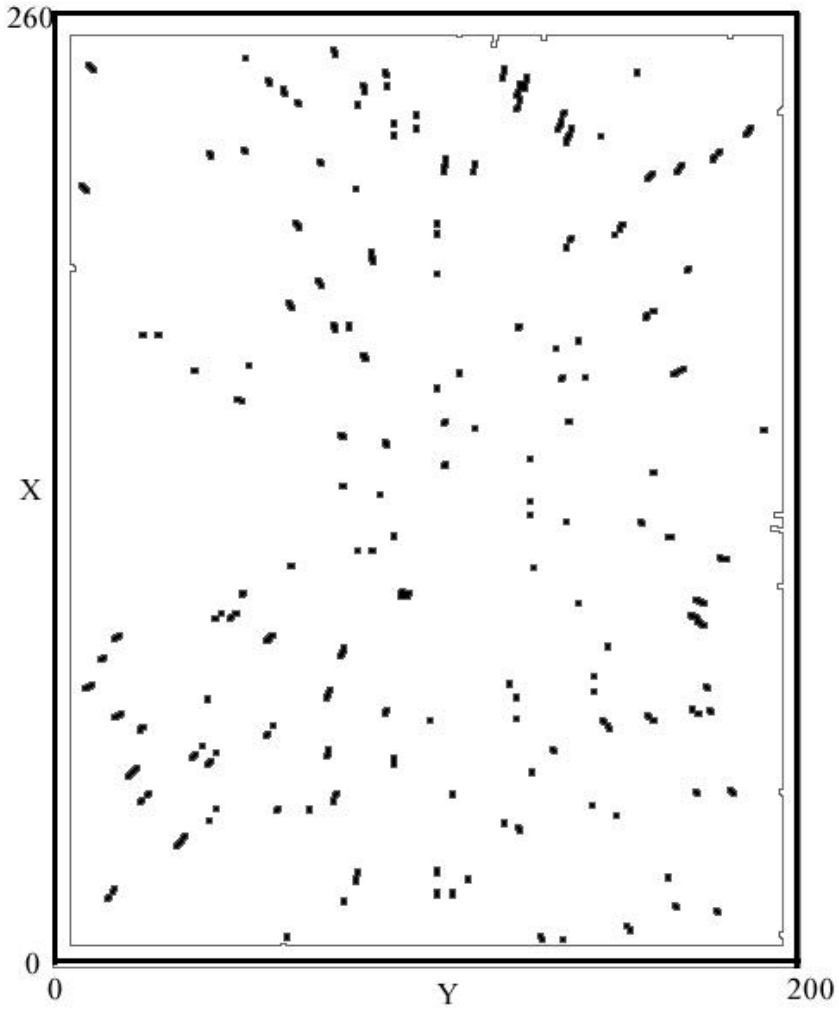

Figure 3.10 The distribution of porosity sample location in the field.

3.1.5 Reservoir Simulation

As introduced above, the reservoir is assumed to be completely saturated with oil. To simplify problems in this case study, there is only one production well in the center of the field and no injection wells. Figure 3.11 shows the location of the production well in the field. The well goes through all 10 layers. The production will be driven by pressure depletion. Meanwhile, to quantify the influence of porosity distribution on the production, other parameters are kept fixed during the production period. However, it is necessary to note that the Kozeny Equation can be used to obtain a permeability field

corresponding to the porosity field.

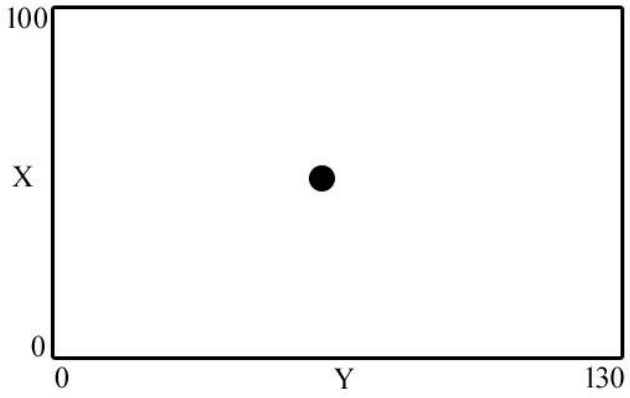

Figure 3.11 Well System Example

Since geostatistical realizations will vary depending on the visiting paths, production calculations were used in this case study to estimate the influence of different realizations on the production. As discussed before, the distribution of porosity will significantly influence the production performance in the field and can help guiding the choice of trajectory of production wells. The basic outline of using production calculation to estimate the influence of geostatistical realization involves the calculation of the change of bottom hole pressure, the daily oil production rate for the well and the fluid production rate and cumulative production.

3.3 Case Study Two: Integrated Geosteering Module

The work flow chart of case study two is shown in Figure 3.12. The details of the geostatistical modeling are discussed in Case study one and the geostatistical modeling work flow is shown in Figure 3.4. The most critical part of this case study is the model updating process. The local porosity value in each node is recalculated due to the new data integration and new data pairs appears. With the porosity distribution continually updating, the more reliable local porosity distribution map can better guide the well

trajectory, chasing high porosity distribution areas and optimizing production performance.

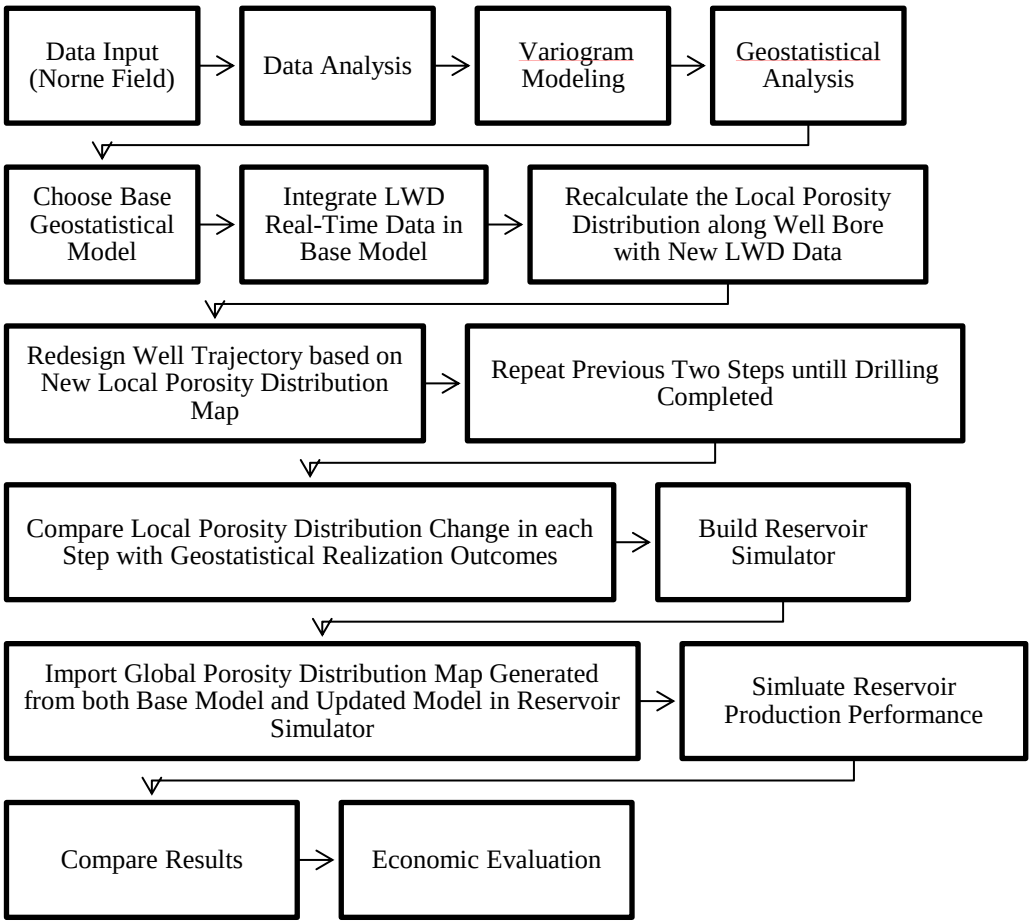

Figure 3.12 Case Study Two Work Flow

Data input for this case study includes well operation, reservoir attributes and petrophysical information from a real oil field. This case study builds geostatistical realizations using the same process as used in case study one. However, the main purpose of this case study is to update geostatistical realizations with LWD data and guide well trajectory while drilling with the updated model. Finally, base model and updated model will be compared using production performance and economic evaluation. Another problem that will be investigated as part of this case study is the data output and input between different software platforms. As different software need

different data formats, the data files must be converted between each step. Therefore, a clear organization of data processing from original geostatistical realization to flow simulation will be presented for this case study.

3.2.1 Data Analysis

The data input of this case study is well log data from 7 wells in E-Segment, Norne Field. This case study integrates several software and customized codes. Therefore, it is very important to unify the data format so that data can be transferred from one platform to another. An initial distribution of petrophysical properties will be used to generate the base geostatistical realization. This initial distribution must be completed with geostatistics or other estimation procedures. In this case study, the reservoir is initialized by actual field data from Norne field.

The data input in this case study is well log data and information from well geological and petrophysical reports. All data is given in field units while calculations in the reservoir simulation process is completed in SI units. Unit conversions are done during data analysis.

There is a total of eight wells drilled in E-segment, including five production wells and three injection wells. As presented before, four formations contain hydrocarbon resources. The Garn formation is mainly saturated with gas and Tofte, Tilje formation are mainly relatively tight sandstone with lower porosity. Therefore, the target formation in this case study is selected as Ile Formation in the E-Segment. Seven wells were drilled through the Ile formation and details are shown in Table 3.2. The Base model was built with six wells except the well E-2AH. Well E-2AH was used as the new logging while drilling source since there is no point comparing two models both built from simulated data. The model is updated with well E-2AH while drilling through

the target Ile formation.

Table 3-2 Wellbore Information in E-Segment

Well	Well Type	Content	Completion Depth (m)
E-1H	Production	Oil	4150.0
E-2AH	Production	Oil	4350.0
E-3H	Production	Oil	3775.2
E-4AH	Production	Oil	3010.0
F-1H	Injection	Water	3168.0
F-2H	Injection	Water	3048.0
F-3H	Injection	Water	3750.0

Some wireline logging and logging while drilling methods have also been used to measure porosity and permeability in the Ile formation. Wireline logging like density log was utilized during the whole drilling process, while LWD techniques were only used for formations with hydrocarbon potential since these techniques are more expensive compared with regular wireline logging.

Figure 3.13 shows locations of seven wells with the porosity data distribution along the well trajectories. All the wells are drilled from the same offshore platform at a water depth of 380 m. The porosity data is interpreted from density log and calculated by Equation 1.20:

$$\phi_{density} = \frac{\rho_{Matrix} - \rho_{Bulk}}{\rho_{Matrix} - \rho_{Fluid}}. \tag{1.20}$$

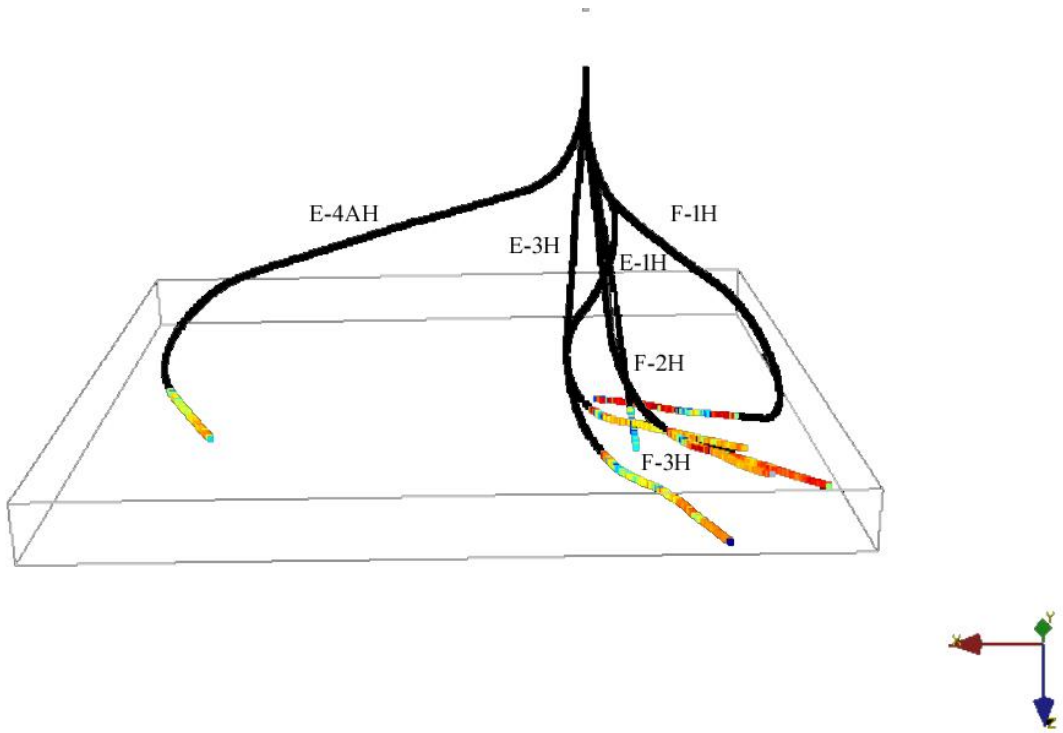

Figure 3.13 Well Location with Porosity Sample Points in the Ile Formation

3.2.2 Variogram Modeling

The process of variogram modeling is the same as case study one. Again, the data spatial correlation generated in the experimental variogram plot is the only way of choosing which variogram model to be used.

3.2.3 Sequential Conditional Simulation Methods

Sequential conditional simulation is applied in this case study since the original data input cannot generate enough data pairs for complete geostatistical estimation of all grid blocks. Using sequential conditional simulation instead of Kriging methods is because the precise local porosity distribution is more important than the global porosity distribution. Simulated Annealing is more suitable for estimating the global optimum in

a large search space while probability field simulation is normally applied for hard mineral resources since it can correct realization results with high nugget effect.

Sequential conditional simulation allows these extreme values to be possible simulation results. Conditional simulation techniques emphasize certain types of variables and minimize other variables of the reservoir. The distribution of properties might be well preserved by using conditional simulation but it cannot be the same. For example, some high permeability data in this case study exists between an injection well and a production well. Although it only exists in a small area, these high values will significantly influence the production performance such as injection fluid breakthrough and fluid production rate.

The realizations may vary depending on the different simulation methods and visit paths. In this case study, the simulation can be divided into 5 steps.

1. Transforming the raw dataset into a new domain

The first step is to check where the data have a Gaussian distribution so that a well-known transform of the data can be used. In this case study, a normal-score transform is performed from the original domain to a new domain. A Gaussian distribution is used because the data input is porosity and permeability data. It is easier to establish conditional distributions. The shape of all conditional distributions is Gaussian and the mean value and variance are given by the histogram chart.

Sequential conditional simulation can simulate both discrete and continuous variables. In this case study, all sample values are arranged in ascending order to build a cumulative distribution function (CDF) with Equation 3.45, which is

$$F(x) = \int_{-\infty}^{x} f(t)dt, \tag{3.18}$$

where *f(t)* is the probability density function.

2. Estimate the variograms in the transformed domain

The second step has already been presented. Variogram modelling and multi-point simulations are both completed in the new domain.

3. Define the visit path to visit all unsampled grid blocks

The third step is the most critical step in the simulation process. After the data are transformed into a new domain and variograms are estimated, a visit path is selected to make sure that every unsampled location is visited.

The random path selection is completed using a random number generator which is integrated into the program SGeMS (The Stanford Geostatistical Modeling Software). Figure 3.14 shows the process of visiting path generation. The generator assigns a unique number for each grid block. If the process starts from the node at the origin, the next visiting node can be any nodes close to the origin node. This creates a number of different visiting path. A new number will be assigned at the beginning of each new simulation process every time.

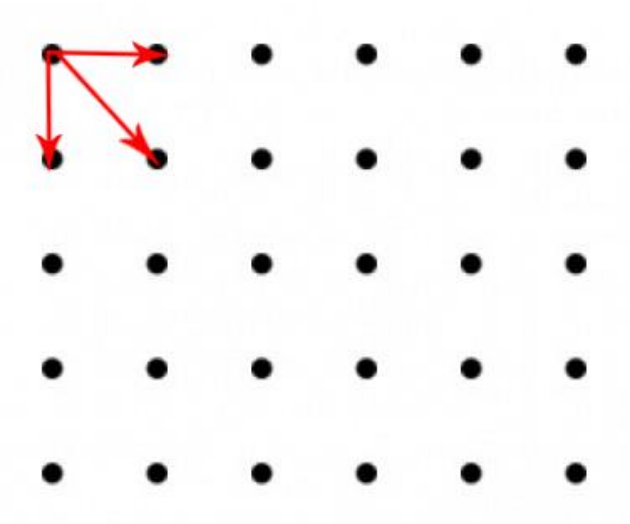

Figure 3.14 Visiting Path Process Example

Conditional simulation methods gather both original data and the estimated data in the

search neighborhood to generate values at unsampled locations. Therefore, the selection of the visit path will significantly affect the simulation outcomes. Moreover, thousands of different realizations could be generated based on the same original data set and each of them is equally possible. For example, if a visit path is started from a high value area, the simulated values will also be high, since the values after that are calculated based on the previous locations with high estimated values. This kind of bias can be avoided by randomly selecting the visit order and by controlling the maximum number of prior simulated values within the search neighborhood.

4. Estimate variables at unsampled grid blocks sequentially

The fourth step is to estimate variables in all grid blocks sequentially. Reservoir properties such as porosity and permeability are assigned to each grid block. The value for each unsampled grid block is calculated based on both the original data and the estimated values within the neighborhood until all grid blocks are populated. It is emphasized that the porosity distributions will be different due to different visiting paths.

5. Back-transforming the data into the original domain

After all the grid blocks are assigned, the fifth step is to back-transform the data into the original domain with the same principle as step one.

3.2.4 Reservoir Definition

Before simulation starts, the first step is to initialize some critical reservoir parameters such as fluid properties and reservoir temperature. It is necessary to note again at this point that the data source of this case study is based on actual field data from Norne Field. However, the complexity of the actual reservoir is not fully represented in this case study since the main goal of this research is to show the application of geostatistics in well trajectory optimization. There is no need to have unnecessary complexity.

A reservoir simulation model with a regular grid of 2000 m by 4000 m laterally and 50 m in depth is defined in Eclipse. The input file is in Appendix C. The original reservoir grid is more complex, but due to the constraints of the geostatistical simulator, it is simplified for time efficiency. The size of each grid is standardized as 10 m by 10 m by 5 m. Some critical reservoir attributes applied in the simulation are based on the geological report from Statoil and shown below (Statoil, 2004).

- Initial Pressure: 273 bar at 2638m TVD (Ile formation bottom)
- Reservoir Temperature: 98 ℃
- Oil Density: 859.5 Kg/m^3
- Rock Compressibility: 4×10^{-6} Pa^{-1}
- Water density: 1033 Kg/m^3
- Oil Compressibility: $1.65*10^{-5}$ Pa^{-1}

The variables of interest in this study are porosity and permeability. The porosity distribution in the reservoir is directly imported from the geostatistical realizations while the permeability distribution is calculated using the permeability porosity relationship in Figure 4.9. Therefore, the porosity is defined as the most sensitive parameter of this reservoir. Well trajectory is mainly designed based on the porosity distribution of the reservoir.

3.2.5 Model Updating

The first step of updating a geostatistical realization while drilling is to build a base realization that incorporates all the existing data. Building the base geostatistical realization is one of the most important steps of the whole workflow. It will be used not only to guide drilling operations but also as a reliable reference for the design of the

development plan in the future. Relative prediction and analysis such as log response of new wells and risk evaluations are also based on the specific scenarios (Pedersen 2005). In this case study, the base geostatistical realization is built by geostatistical techniques with well logging data.

A predrilling plan is designed to create the optimal well trajectory before actual drilling starts. In this research, well trajectory is designed using the porosity distribution map. The well is designed to drill through the high porosity area. Figure 3.15 is a 2D porosity distribution map of the Ile formation, Norne Field. As can be seen in the figure, there are two high porosity areas in this working field (shown as red color). The black line is the simulated well trajectory to go through the high porosity area to approach optimum production.

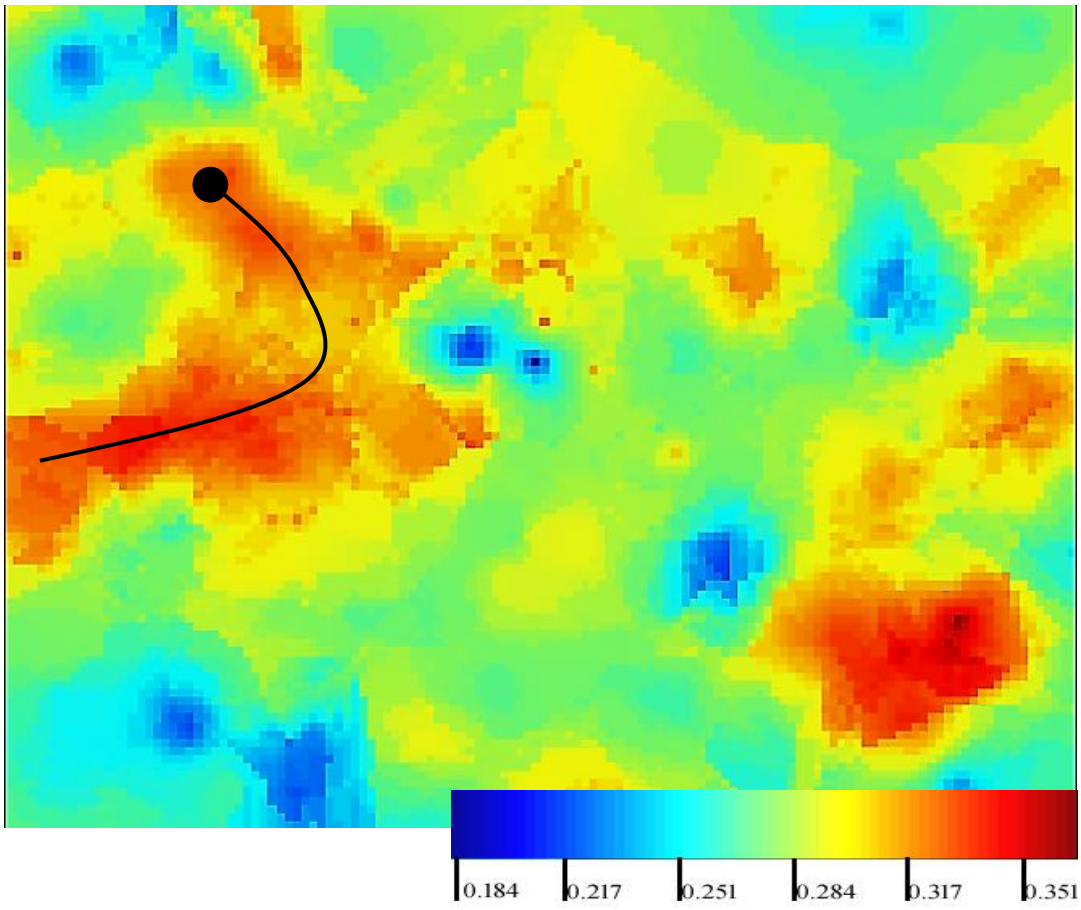

Figure 3.15 Well Trajectory Design Example

The third step is the real-time updating process. In this research, well E-2AH well log is applied as real-time well log data. Once new well log response integrated into base realization, the local porosity distribution can be re-calculated again by kriging estimation as new hard data appears in the search neighborhood. Ideally, geostatistical realizations can be updated every time a new log response is integrated. However, computing time is needed to update the model and generate the new distribution map. In this research, the model is designed to update every 50 m so that it has enough time to integrate new well log data and compute the kriging algorithm. In other words, the well trajectory is adjusted every 50 meters based on the updated local porosity distribution map. The length of the well trajectory is 400 meters. The model is updated a total of eight times in this process and the results and comparison are shown in Chapter 4.

In almost every drilling operation, the drilling response does not always follow the predrilling plan because of the existence of uncertainty. A fault or unexpected geological bodies like coal or calcite layers may be encountered while drilling. The updating process will improve the reservoir accuracy to optimize the production rate. Since there are no major faults or fractures in E-Segment, this case study focuses on the porosity updating.

4. Results and Discussions

4.1 Case Study One: The Influence of Geostatistical Estimation Results on Production Performance

This section presents an oil based reservoir production case study which shows how to employ geostatistics to estimate properties at point locations. These data are then used to estimate productivity in a field example. Since the data are available in different measuring units, all the calculations are converted to SI units. There are three main purposes of this study:

1. Estimate variogram with porosity data to explore the spatial relationship of porosity data.
2. Generate a regional porosity distribution map with the Kriging estimation method.
3. Compare the influence of geostatistical realizations by importing different

porosity distribution maps into the reservoir simulator. Production performance is used as index.

4.1.1 Variogram Model Results

As introduced in the methodology, with a certain tolerance and number of lags, a variogram model can be plotted. Different value of parameters is used to plot variogram models in this process. The first and most important step is to figure out the major and minor directions. As discussed in the Chapter 3, the direction with the most continuity reaches the experimental sill value at the largest lag distance. The variogram models with different directions from 0^o to 180^o are shown in Appendix B. After comparing variograms model in different directions, the direction at 135^o counter clockwise from positive x axis is chosen as the direction of maximum continuity, since this direction not only has more pairs of data, but also the maximum lag distances. The direction at 45^o is chosen as the minor direction since the minor direction is normally taken perpendicular to the direction of major direction. Besides the directions, the distance between every sample location in the dataset must be calculated. After multiple attempts, the final chosen configuration has an angular lag tolerance of 20 degrees, a number of lags of 45 m, a lag tolerance of 1 m, and search angles in the direction of maximum and minimum continuity.

Recalling Equation 3.7, which is used to calculate variograms, and searching the data methodically, the estimated variogram models at 135^o (maximum continuity) and 45^o (minimum continuity) are shown in Figure 4.1 and Figure 4.2 respectively.

As presented in Figure 4.1 and Figure 4.2, although there are still some fluctuations in the estimates, the essential structure is obvious. Both variograms increase with increasing distance, then reach the sill value at a certain lag distance. However, it can

also be noticed that some points near zero show anomaly high values in the 135° direction. This may be caused by a nugget effect. Given the existence of geometric anisotropy, the two variograms in different directions lead to the same sill of 0.00055 but over different ranges. However, the overall structure fits the trend and removes fluctuations in this case study.

Different models are selected based on the data distribution and trends, which are introduced in Chapter 3. In this case study, there is a variogram model for each direction. Based on the data distribution in Figure 4.1 and Figure 4.2, both models are models with a sill and nugget effect. As discussed in the methodology chapter, the selection of the model is not quantitative. As can be seen in Figure 4.1 and Figure 4.2, black points represent variogram values at different lag distances. Some of the variogram values near the origin show high values. This may be caused by the nugget effect. However, the general trend for the variogram increases rapidly from zero and slowly reaches the sill. The Gaussian model variogram increases slowly near the origin and then rapidly reaches the sills. Therefore, the spherical model is selected for both models since the porosity data trend for the experimental variogram best fits the spherical model. The structure of the four commonly used models is introduced in chapter one. Both variogram models have the same sill value but at different distances due to the existence of geometric anisotropy. The variogram models are shown with equations below;

For azimuth at 135 degrees (maximum continuity),

$$\gamma\left(\vec{L}\right) = 0.0001+0.00045\mathrm{M}_{S(25)}\left(\vec{L}\right). \tag{4.1}$$

For azimuth at 45 degrees (minimum continuity)

$$\gamma\left(\vec{L}\right) = 0.0001+0.00045\mathrm{M}_{S(17)}\left(\vec{L}\right), \tag{4.2}$$

where *S* indicates the spherical model and 17 is the range.

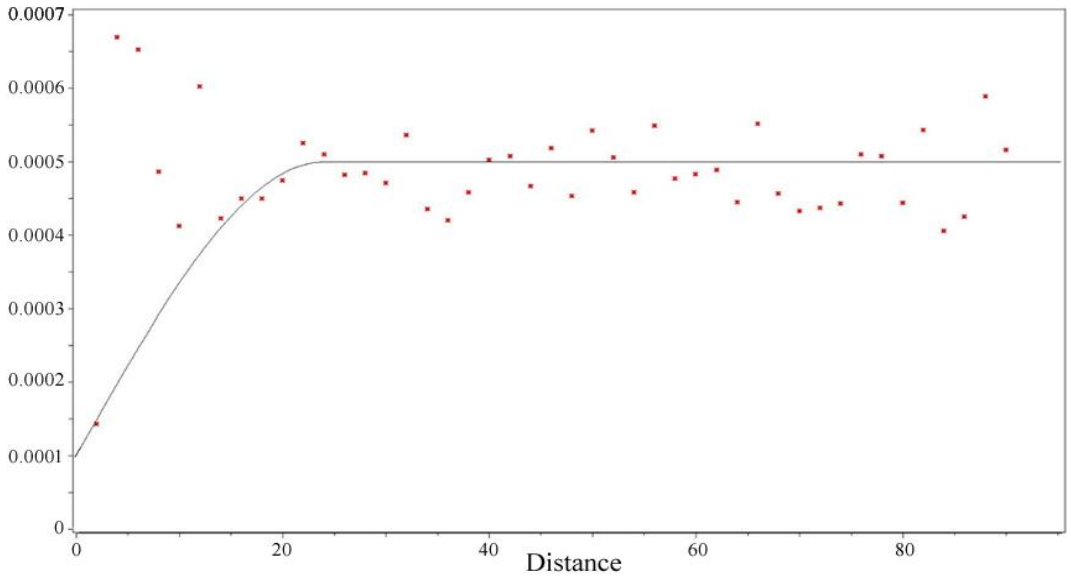

Figure 4.1 Estimated Variogram in the direction of 135 degrees (maximum continuity)

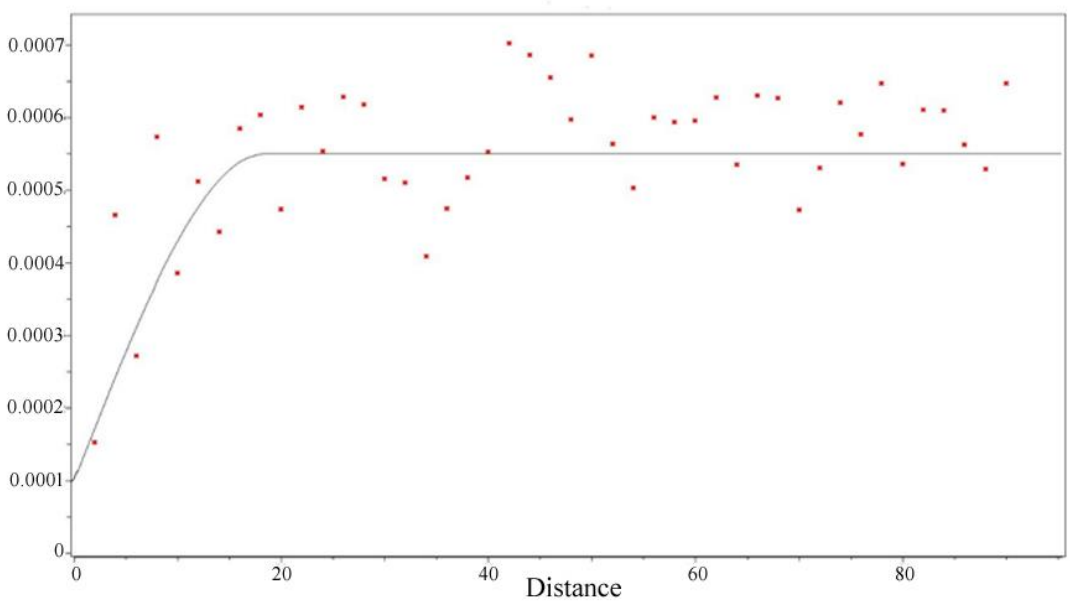

Figure 4.2 Estimated Variogram in the direction of 45 degrees (minimum continuity)

4.1.2 Kriging Estimation Results

The purpose of this case study is to evaluate the influence of geostatistical realizations on reservoir simulations by comparing the production rates. Therefore, two different 3D

geostatistical realizations are selected in this case study from 20 different realization outcomes (realization with the maximum global porosity mean and the minimum global porosity mean). The rest of the outcomes are shown in Appendix B. Results of Model Two are obtained using the optimistic porosity distribution outcomes with an average porosity of 0.324, while results of Model One are obtained using the pessimistic porosity distribution outcomes with an average porosity of 0.252. However, both are generated from the same porosity distribution input and the same Kriging estimation algorithm. Figure 4.3 and Figure 4.4 show all 10 layers of porosity distribution outcomes in two geostatistical models from the top to bottom layers in the target formation. Table 4-1 shows the porosity mean and variance comparison for both models in layers.

Table 4-1 Porosity Mean and Variance Comparison of Both models in layers

	Model One (Pessimistic)		Model Two (Optimistic)	
	Porosity Mean	Variance	Porosity Mean	Variance
Layer 1	0.239	0.00054	0.295	0.00077
Layer 2	0.241	0.00059	0.287	0.00075
Layer 3	0.241	0.00056	0.286	0.00075
Layer 4	0.238	0.00056	0.284	0.00070
Layer 5	0.237	0.00054	0.284	0.00074
Layer 6	0.243	0.00061	0.283	0.00072
Layer 7	0.242	0.00058	0.282	0.00066
Layer 8	0.242	0.00049	0.283	0.00065
Layer 9	0.240	0.00053	0.283	0.00067
Layer 10	0.238	0.00054	0.290	0.00067

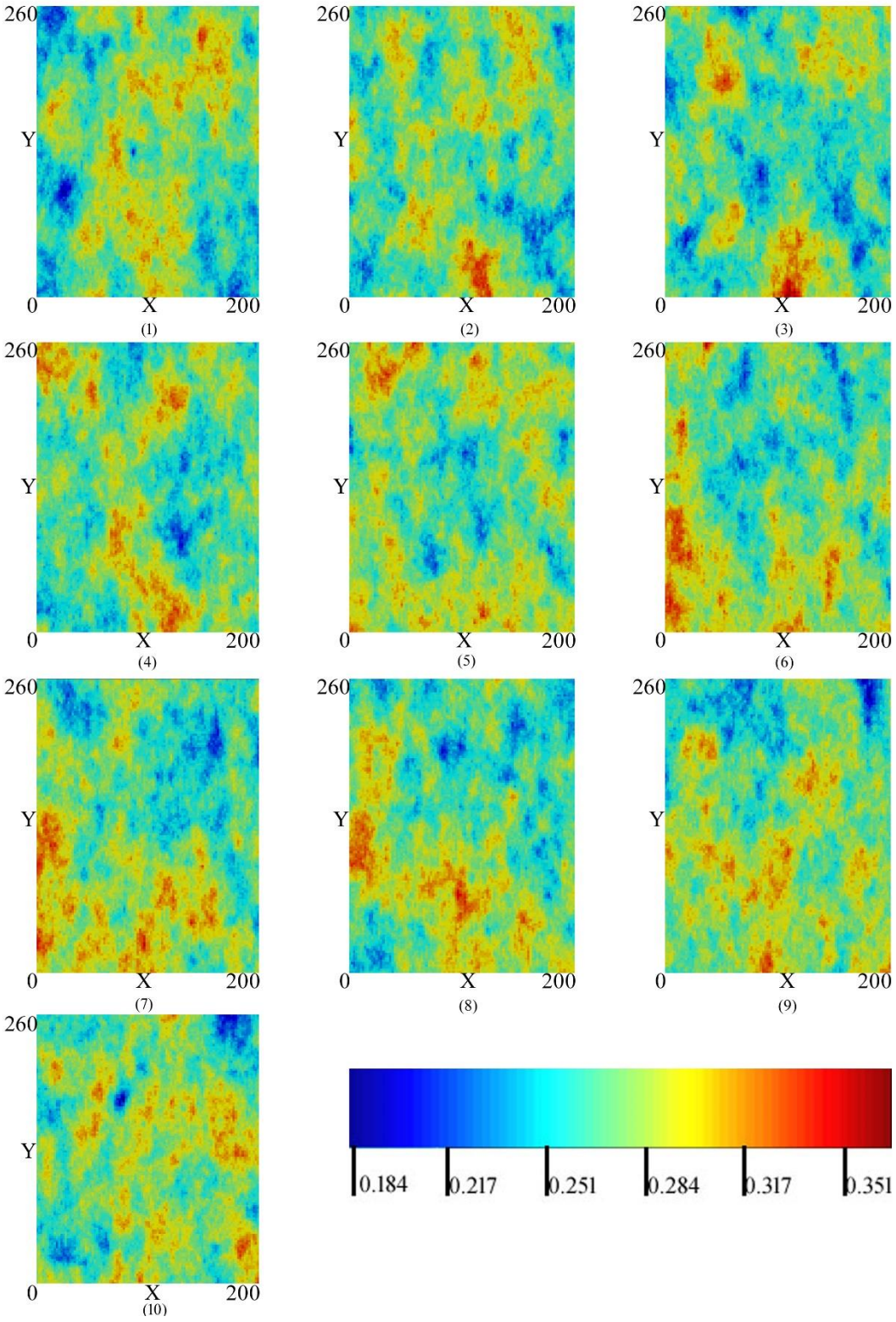

Figure 4.3 Model One: 2D Pessimistic Porosity Distribution Plot by Layers

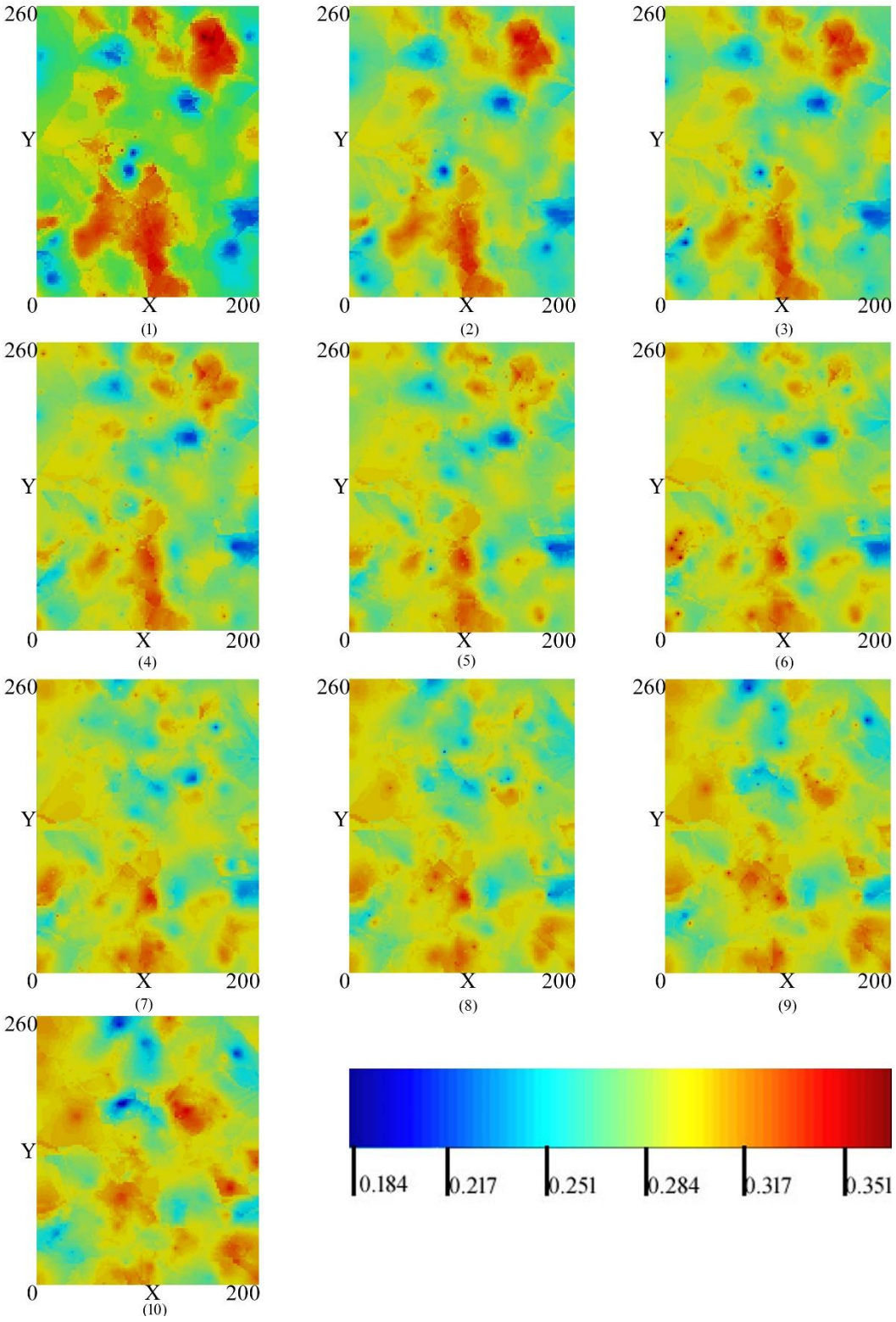

Figure 4.4 Model Two: 2D Optimistic Porosity Distribution Plot by Layers

As displayed in Figure 4.3 and Figure 4.4, similarities can be seen for different layers in the same model. The two models are shown to be visually appropriate based on sample data input. Although average porosity in the optimistic model is relatively high compare to that in pessimistic model, high porosity values appear around the same areas if we compare the same layer in the two models. For example, high porosity occurs at the right top and the left bottom area in the top layer. The color bar shows that the range of porosity varies from 0.284 to around 0.38.

4.1.3 Production Simulation Results

In this case study, the target formation is defined as a single-phase reservoir and saturated with oil initially. The simulation is completed in Schlumberger Eclipse 100 which is a comprehensive reservoir simulation package widely used in the petroleum industry to mathematically simulate reservoir performance. The estimated porosity geostatistical realizations are input into Eclipse100.

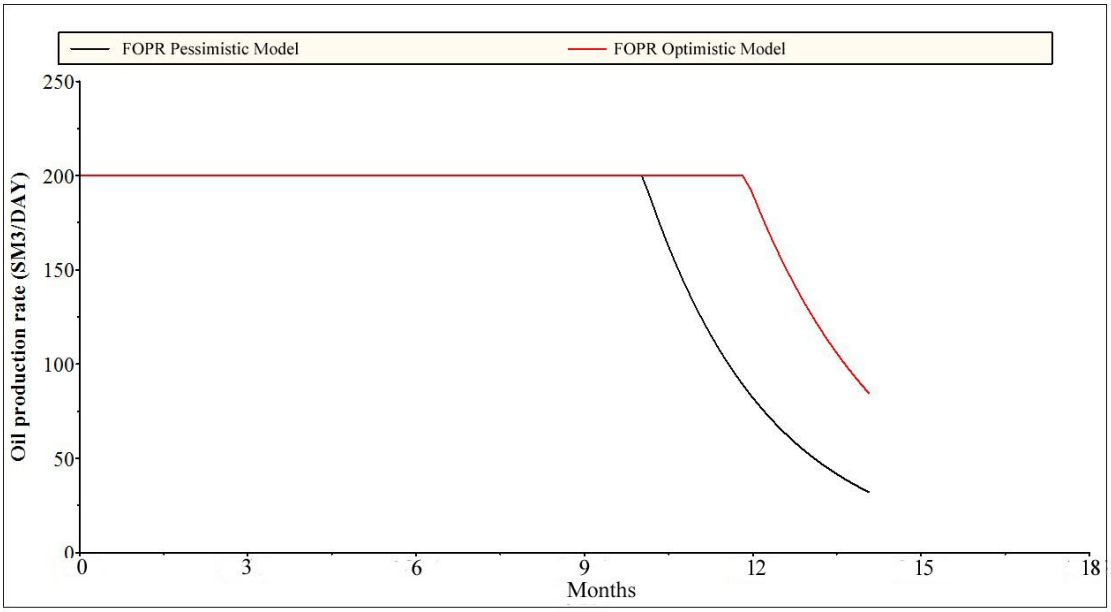

Figure 4.5 Daily Oil Production Rate for Pessimistic Model and Optimistic Model

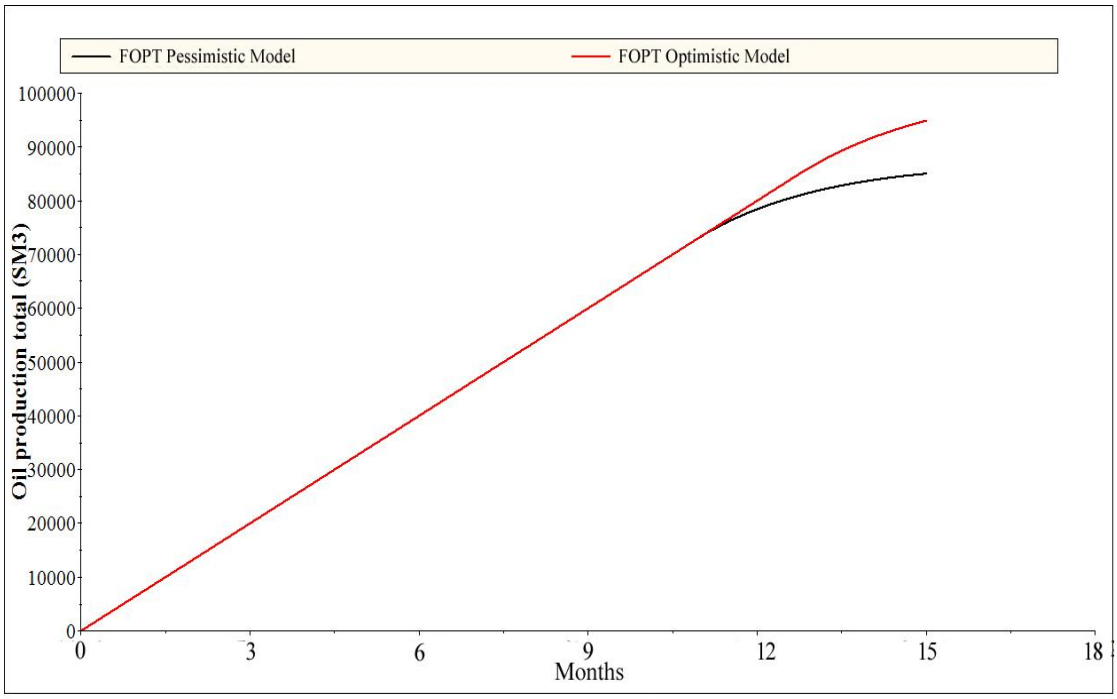

Figure 4.6 Total Oil Production for Pessimistic Model and Optimistic Model

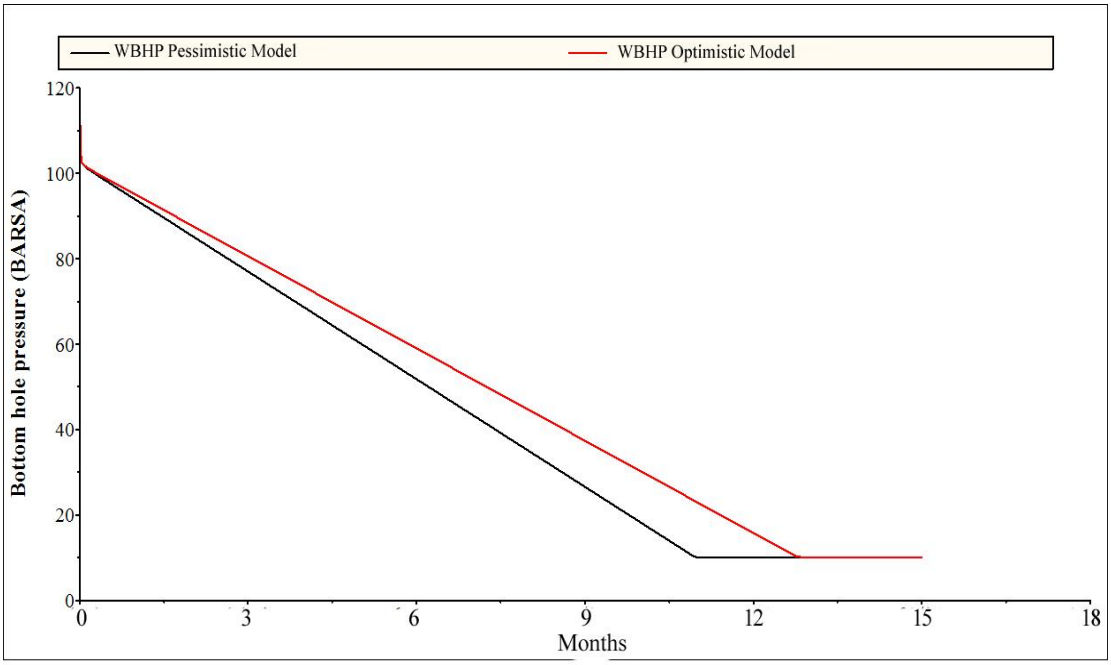

Figure 4.7 Bottom Hole Pressure of Production Well for Pessimistic Model and Optimistic Model

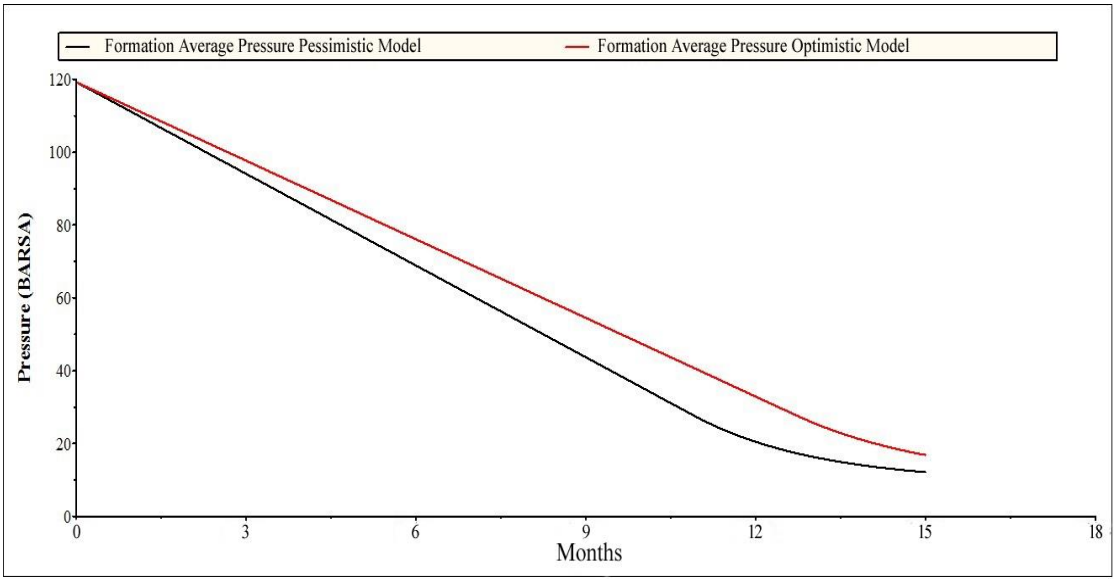

Figure 4.8 Formation Average Pressure for Pessimistic Model and Optimistic Model

As demonstrated in Figure 4.5, with a target production rate of 200 Sm^3/day, the optimistic model maintained the oil production rate of 200 Sm^3/day for 13 months. Then, the oil production rate starts to decrease due to the reservoir pressure drop. The pessimistic model produces oil with a target rate for 10 months and then production rate starts to decrease. In other words, the optimistic model maintained the production rate for three months longer than the pessimistic model. It is also shown in Figure 4.6 that the total production difference between two models is 10000 Sm^3, which is the approximately a 13% difference. The reason for the oil production rate drop is that the models reach a minimum allowed bottom hole pressure of 15 bar. Figure 4.7 shows the change of bottom hole pressure during the production period. The bottom hole pressure decreases from 105 bar to 15 bar and then remains constant once it reaches the minimum bottom hole pressure. The bottom hole pressure kept decreasing from the beginning of production since the production is only driven by natural reservoir pressure and no injection wells exist to slow down the pressure drop. Figure 4.8 indicates the change of formation average pressure over 15 months. Formation average pressure drops from 120 bar to approximately 20 bar for both the optimistic and the pessimistic model.

However, the optimistic model drops slower than the pessimistic model. The drop of average pressure also confirms the change in bottom hole pressure. The reservoir is too small to maintain the production rate.

4.1.4 Summary

The objective of case study one was to describe the general process of building a geostatistical model for porosity data. A methodology to quantify the influence of porosity distribution on the production simulation associated with a geological uncertainty is introduced. This case study built a base variogram estimation with point set porosity sample input and then two 3D porosity distribution maps were generated with a random number generator. Both models were built with ordinary Kriging estimation using the same base variogram estimation. The comparison was completed by evaluating the difference in daily production rate, total production and bottom hole pressure change. The results show a significant difference when simulating the reservoir performance with different geostatistical realizations. The further study of using the geostatistical estimation images and real time LWD data to predict porosity value and steering the drilling trajectory is demonstrated in the next case study.

4.2 Case Study Two: Integrated Geosteering Workflow

This section applies geostatistical methodology to manage uncertainty while drilling using real-time reservoir data. As discussed in case study one, although geostatistical estimation techniques can quantify uncertainty and reflect the properties of underground formations, these techniques do have some restrictions due to the pre-assumptions and lack of data. Therefore, different methods will be selected depending on the conditions of specific cases.

The objective of this case study is to explore a relatively high speed updating process for fields without complex structure, using software packages including customized code and open platform software. Compared to case study one, this case study analyzes the reservoir realizations more rigorously. More importantly, it presents a detailed and feasible procedure of using geostatistical realizations to steer the drilling process and optimize the well trajectory with respect to production performance. The realizations are updated with LWD data throughout the drilling process. Results are compared in three cases. In case one, reservoir is produced over a 50 m length of perforate well in pool one with the original porosity distribution. In case two, reservoir is produced over a 50 m length of perforate well in pool one with the updated porosity distribution. In case three, the reservoir is produced over a 50 m length of perforate well in pool two, an additional pool resolved from the updated porosity distribution. The comparison is mainly between case one and case two since the main purpose is to illustrate the advantage of the integrated geosteering workflow in this study. The data from the Norne Field is used in this case study, since this field has well drilling reports, detailed geological information, log data, and production data. These data sources make it possible to build the customized geological model and reservoir simulation model. Comparisons can be made since the reservoir is assessed as fully characterized and reservoir simulation results reflect actual production performance. Economically, updating the well trajectory with LWD real time data impacts operating and capital costs.

Sample permeability was calculated from a correlation of porosity and permeability using the Kozeny Equation:

$$k = \alpha \frac{\phi r^2}{\tau} \tag{4.7}$$

The porosity permeability relationship in the Ile formation is generated in Excel and is shown in Figure 4.9. Porosity and permeability values are interpreted from well logs

and gathered from well reports. As displayed in this figure, the scatter plot creates a cloud of data and the relationship is quantified by using a line of best fit through the data cloud. As discussed in section 1.1.9, the porosity and permeability relationship based on the Kozeny Equation is applied as a linear relationship. Meanwhile, the plot can also be used to validate the original data and help to understand the results later.

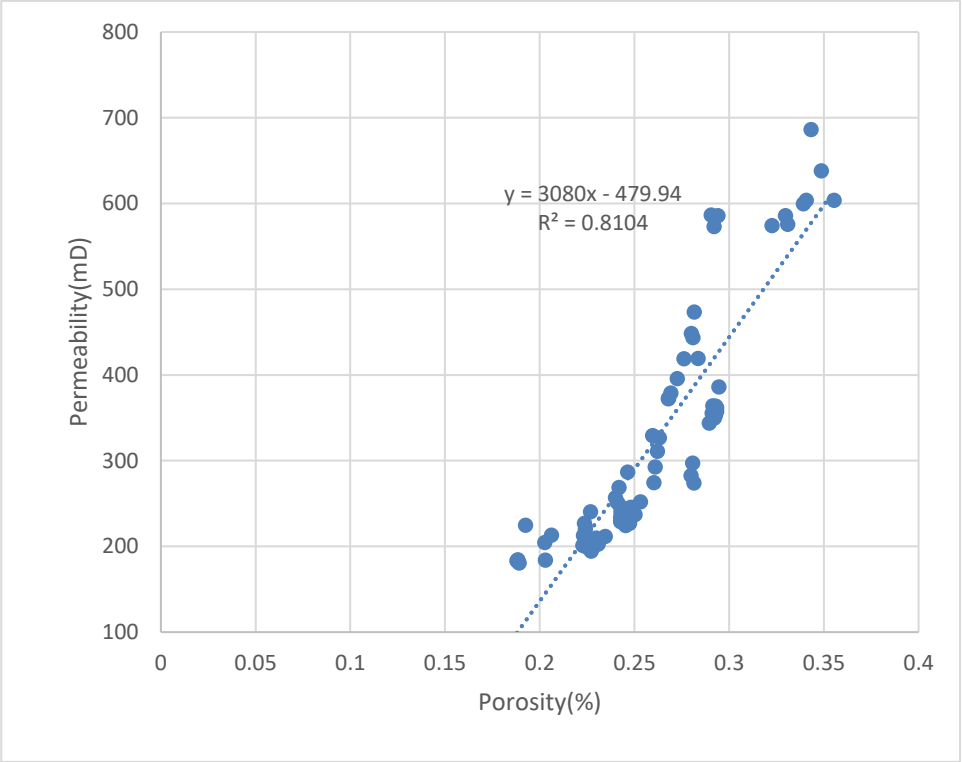

Figure 4.9 Porosity-Permeability Relationship in the Ile Formation

The distribution of the source data is one of the main factors in designing an initial well trajectory in a drilling project. The porosity and permeability distributions are shown in the histogram chart in Figure 4.10 and Figure 4.11. The histograms reflect the probability frequency and cumulative distribution of porosity and permeability values. The plots indicate that the porosity values are mainly around 0.2 to 0.3 while the permeability values are mainly around 100 to 10000 mD.

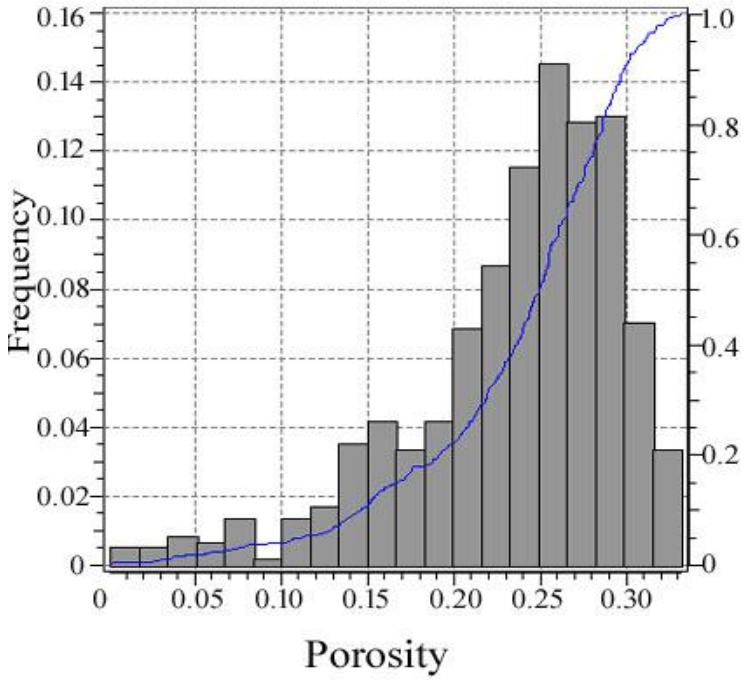

Data count: 7966

Mean: 0.239

Variance: 0.004

Maximum:0.38

Median: 0.258

Minimum: 0

Figure 4.10 Sample Porosity Histogram and Cumulative Probability Distribution

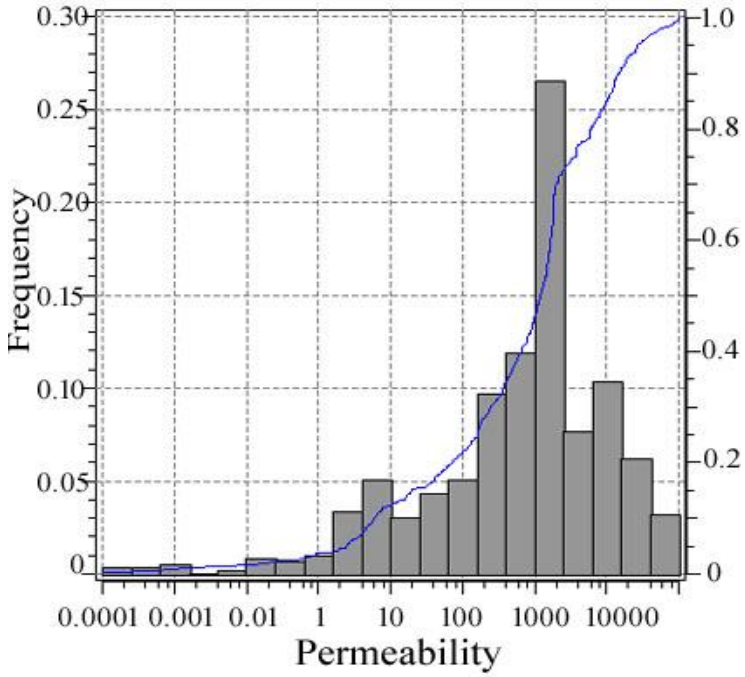

Data count: 7966

Mean: 1458

Variance: 22150.4

Maximum:97570.24

Median: 1175

Minimum: 0

Figure 4.11 Permeability Histogram and Cumulative Probability Distribution (mD)

4.2.1 Variogram Modelling Results

The variogram modelling result is shown below in Figure 4.12. The red dots are the variogram values for different lag distances and the black line is the variogram model. The selection process was discussed in Section 4.1.1. The Gaussian model appears to most closely match the porosity data trend in Figure 4.12 which the data increase slow at origin and then increase fast after. The porosity variogram is estimated with the spherical model and permeability is calculated based on Kozeny Equation with porosity-permeability relationship. The geostatistical realization outcomes based on this variogram model may have high uncertainty. That is one of the reasons that the permeability distribution map is calculated using the porosity-permeability relationship instead of using permeability directly interpreted from the well log. Mathematically, the porosity variogram model can be written as

$$\gamma(L) = 0.0028 + 0.004\left[1 - exp\left(\frac{-3L}{12}\right)\right] \quad . \tag{4.3}$$

In summary, the parameters chosen for the variogram estimation of porosity are shown in Table 4-2. The details of parameters selection are the same as for case study one discussed in section 4.1.1.

Table 4-2 Parameters for Variogram Estimation

	Lag Distance (m)	Lag Tolerance (m)	Angular Tolerance	Direction of Maximum Continuity	Direction of Minimum Continuity
Porosity	5	1	10°	75°	115°

Compared with the estimation in case study one, this case study used sequential Gaussian simulation (SGS) instead of Ordinary Kriging estimation. The reason for using the sequential Gaussian simulation method are that there are only limited wells

drilled in the working area and well log data (hard data) distribution is uneven. The Kriging estimation method cannot gather enough data pairs in the search neighborhood to complete the estimation. The sequential Gaussian simulation method can utilize all available information as well as previously estimated values to determine the value of a variable at an unsampled location. This part is completed using the SGeMS software, an open platform software developed by Stanford University.

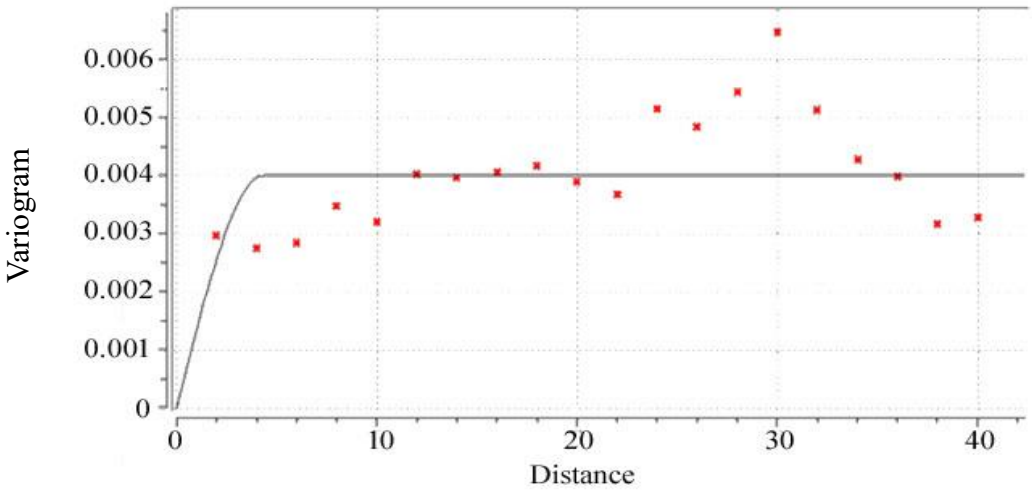

Figure 4.12 Porosity Spherical Variogram Model

4.2.2 Sequential Simulation Results

As introduced above, due to the random visiting path algorithm, a number of geostatistical outcomes are generated based on the same initial dataset. All geostatistical realizations are equally possible from a statistical point of view. A reliable realization outcome is not randomly selected. In practice, the first step is to generate as many geostatistical realizations as possible depending on the time available. Generally, the more realizations that are generated, the more accurate a reservoir characterization can be achieved. Then, these realizations are compared based on geological information and

geophysical data. Geological information background may help for selecting geological body attributes as well. Combining all the information, a reliable realization outcome is generated and utilized in the following analyses.

The target petrophysical property is porosity. The rock in Ile formation is mainly a channel sandstone. Sandstone deposits in channels normally have relatively high porosity, while sandstone in a side bar normally shows relatively low porosity, since it contains flood plain mudstone.

In this case study, all the realization outcomes will be shown in 2D plots since they can show more details of data distribution compared with 3D plots. There is a total of 100 realizations generated with the same data input. The log data are shown in Appendix A. Figure 4.13 shows some realization outcomes in 2D plots generated using the sequential Gaussian simulation method. Based on the porosity data gathered from the well E-2AH, realization (1) appears to most closely match the data since the area where the E-2AH well trajectory was drilled through the Ile formation shows a high porosity distribution. Combined with the log data from the E-2AH well log report, the realization outcome (1) in Figure 4.13 is applied as the base realization and used in the updating process.

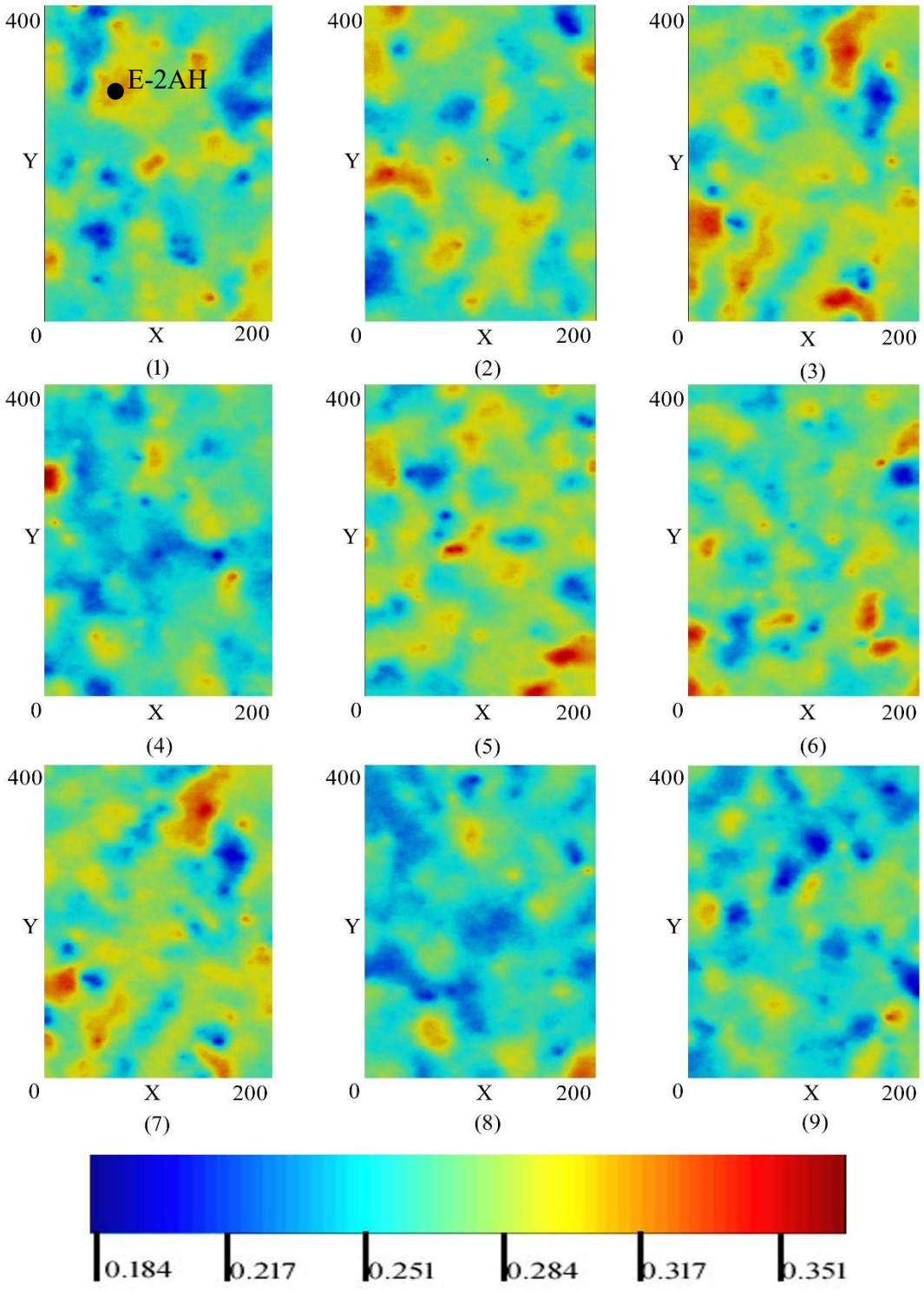

Figure 4.13 Geostatistical Realization Samples in 2D Plot (Layer 1-9)

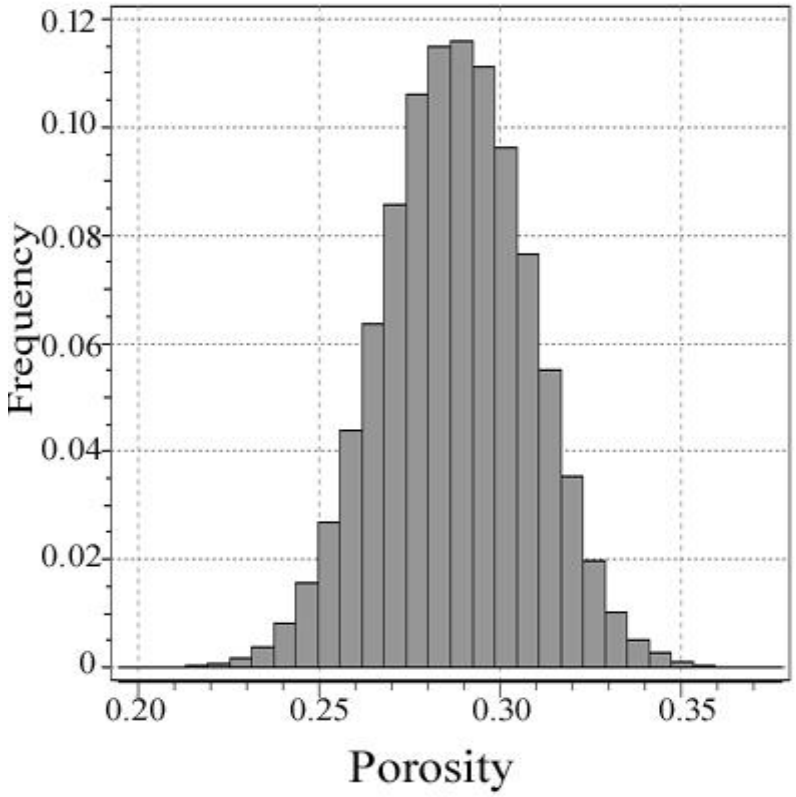

Figure 4.14 Histogram of Porosity in Base Realization

The histogram of the porosity distribution for this realization outcome is shown in Figure 4.14. The porosity is normalized very well. The maximum porosity value is around 0.38 while the mean porosity value is around 0.29.

4.2.3 Model Updating Results

As introduced before, logging data from horizontal well E-2AH is assumed to be the logging while drilling data source and utilized in the real-time updating process. Before the actual drilling process starts, a predrilling plan is made based on the original porosity distribution. Figure 4.15 shows the well location and original well trajectory design with original porosity distribution from the geostatistical simulator. The well trajectory is shown as the black dash line in the horizontal direction. As can be seen in the figure, the well trajectory is designed to go through the high porosity area in order to approach

the optimal production performance.

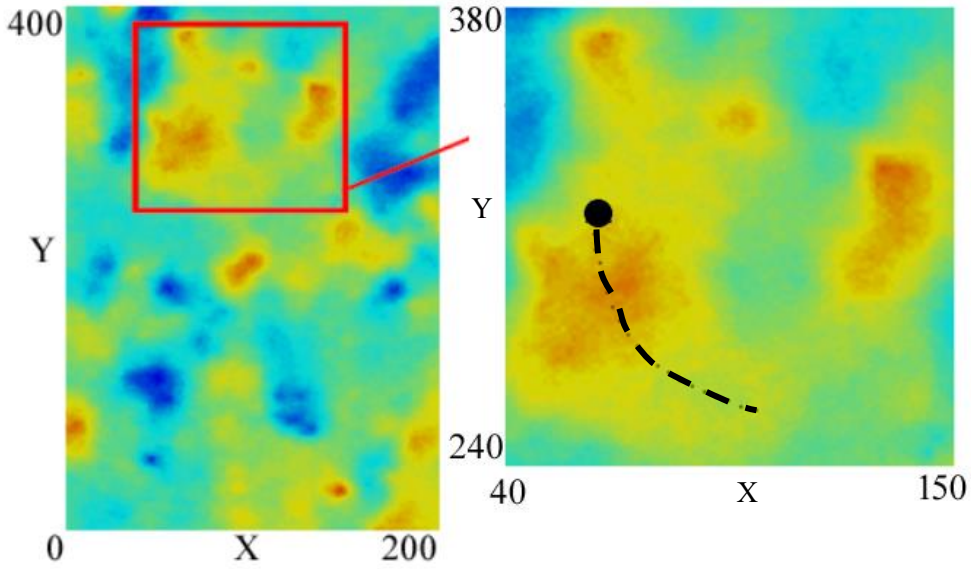

Figure 4.15 Well Trajectory Design with Original Porosity Distribution in Pool 1

Once the predrill plan is established, drilling starts. Since the structure is not the key component in this case study, the depth of the top of the Ile formation is assumed to be the same as that of the base model. After the bore hole reaches the Ile formation, the logging data starts to be collected and the real time updating process starts. The total length in the horizontal direction is 400 meters and the realization is updated every 50 meters which allows sufficient time for the logging interpretation process. The realization is updated 8 times during the drilling process and all stages are shown in Figure 4.16. The first figure is the start point when the new well is drilled and the real-time LWD data start to be integrated. Comparing the layer 1 in Figure 4.13 and the first figure in Figure 4.16, the porosity in the near well region decreases from 0.31 to 0.29 (color from light red to yellow) which indicates that the porosity is not as good as expected from the original porosity distribution.

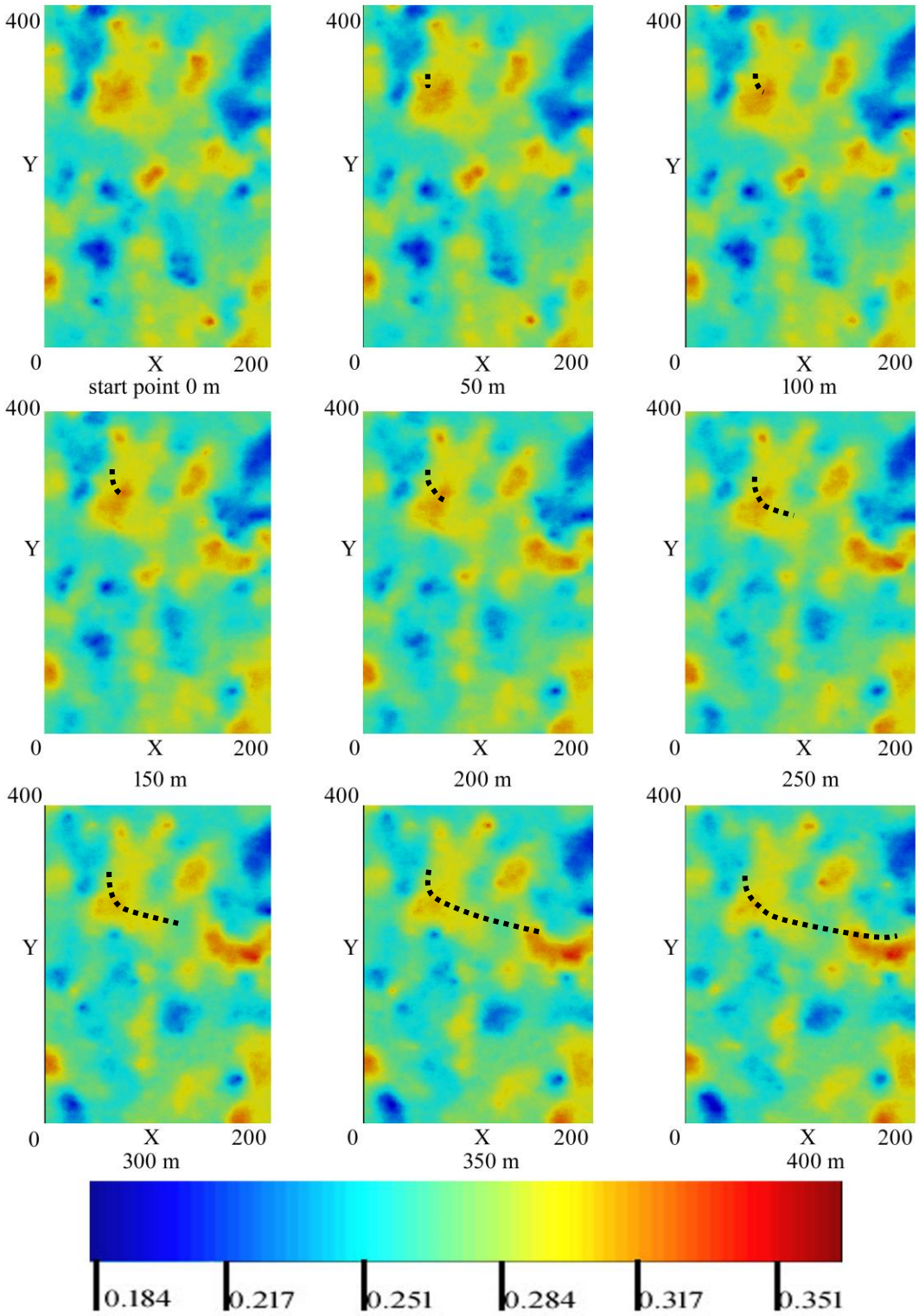

Figure 4.16 2D Geostatistical Realization Change During Updating Process

In Figure 4.16, the first realization at the top left is the base realization. To the right are updated realization outcomes from first to last update stage numbered from (1) to (8). From this figure both similarities and differences can be seen. Porosity distributions in all realizations are changing regularly and new information is shown as the drilling process proceeds.

The porosity at each stage is shown in Appendix D in the histogram. Figure 4.17 and Figure 4.18 present the global mean and variance of porosity in all grid blocks during the updating process. As can be seen in Figure 4.17, the global mean at the start point (base realization) is 0.2877 and then drops to around 0.2874 at stage 1. From stage 1 to 8, the global mean of porosity keeps increasing. The drop of mean value from base realization to step 1 reflects that the porosity in the base realization is over estimated. Therefore, after well E-2AH drilled in the Ile formation and real-time log data were gathered, the updated results show that the porosity is not as good as expected. However, with each update from stage 1 to stage 8, a prospective new area appears, which shows a high porosity distribution that affects the mean value of porosity for the whole working area. However, the size of the new-found area is quite small compared to the whole working area, therefore, the global mean only changes from 0.2874 to 0.2888. The trend confirms the realizations outcomes in Figure 4.17.

The variance change during the realization updates appears in Figure 4.18. The variance has minor fluctuations during the realization update process but roughly remains constant and small. This result shows that the global porosity distribution has no major changes with the real-time data input into the realizations.

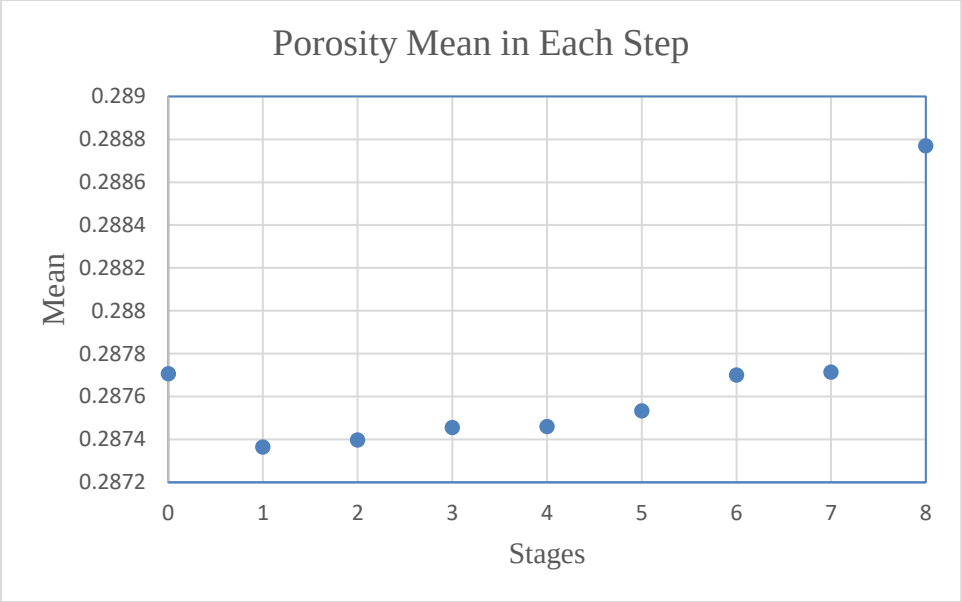

Figure 4.17 Porosity Mean for Each Step during the Updating Process

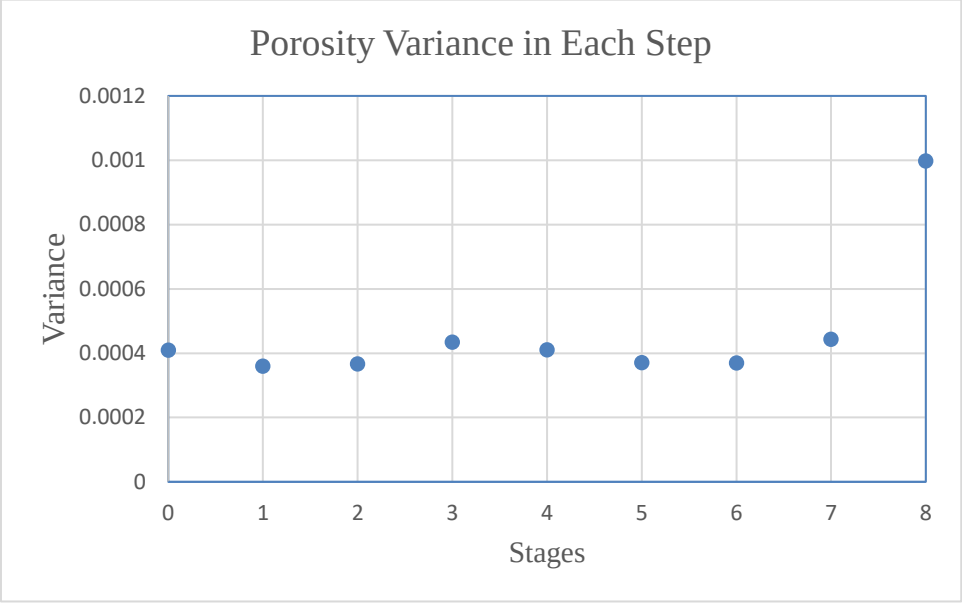

Figure 4.18 Porosity Variance for Each Step during the Updating Process

Figure 4.19 shows the new well trajectory based on the updated realization. As can be seen in the figure, a new high porosity population area is shown in the middle right area with updating. The base well trajectory is shown as the dash line and a new well trajectory is shown as the solid line. This new-found area may contain hydrocarbon resources with high economic value. In order to approach optimal production

performance, the well trajectory is adjusted and extended to the new drilling target.

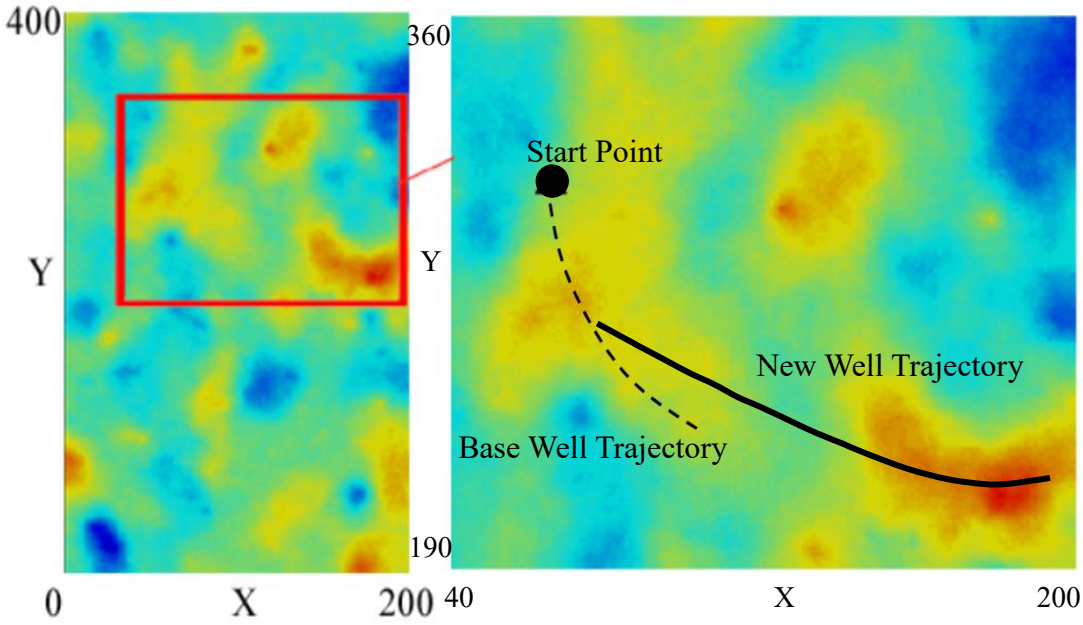

Figure 4.19 New Well Trajectory with Updated Realization

4.2.4 Reservoir Simulation Results

The two geostatistical realizations are imported into Eclipse 100 to simulate production performance. Realization one is the base realization indicated in Figure 4.13. Realization two is the new geostatistical realization after 8 times updates as indicated in Figure 4.16. Production was predicted for both the base realization and the updated realization. In both cases 50 m of the horizontal well was perforated in order to compare results. In this case study, water is injected into the reservoir at the same rate in both base and updated cases for pressure maintenance. The details are introduced in section 3.2.4. The code is shown in Appendix C.

The reservoir is simulated in three cases. In case one, the reservoir is produced over a 50 m length of perforate well in pool one with the original porosity distribution. In case two, the reservoir is produced over a 50 m length of perforate well in pool one with the

updated porosity distribution. In case three, the reservoir is produced over a 50 m length of perforate well in pool two, an additional pool resolved from the updated porosity distribution. The comparison is mainly between case one and case two since the main purpose is to illustrate the advantage of integrated geosteering workflow in this study.

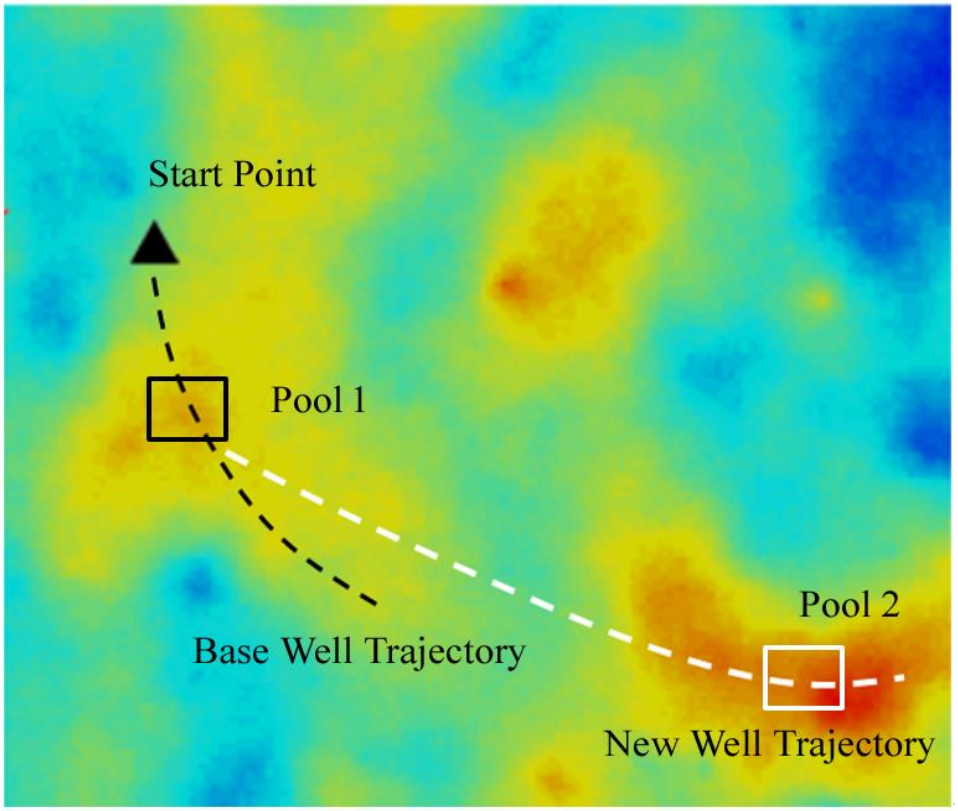

Figure 4.20 Three Cases: Perforated Interval

Figure 4.20 shows the perforated interval for the three cases. Both case one and case two are produced at pool 1 since this area shows relative high porosity. However, the new-found area in the updated realization indicates that pool 2 has high porosity distribution as well. Case three involves the new well trajectory designed to go through this area. Therefore, a separate simulation is also made in this area to explore the production potential. The reservoir simulation for the three cases are all produced for the same amount of time, simulated with the same production time, 1000 days.

Figure 4.21 to Figure 4.24 represent some simulated production results for the two

realizations. The red curve represents the updated realization while the black curve represents the base realization. As can be seen in Figure 4.21, the updated realization maintained the preset daily production of 150 m^3/day for 920 days. However, the predicted production starts to drop after 780 days. With the water injected in the reservoir, as can be seen Figure 4.22, water breakthrough happened approximately 150 days later in the updated realization compared to the base realization. The time of water breakthrough marks the point in time that a molecule of water travels the entire distance of the reservoir between the production well and the injection well. After 1000 days' production, the cumulative production in pool 1 of the updated realization and the base realization are approximately 150,000 Sm^3 and 140,000 Sm^3, respectively. The difference is 7%. The results are presented in Figure 4.23. The difference is not as much as expected since the porosity distribution in the pool1 shown in Figure 4.23 is not as good as estimated in the base realization, even if the well trajectory is adjusted to optimize production performance.

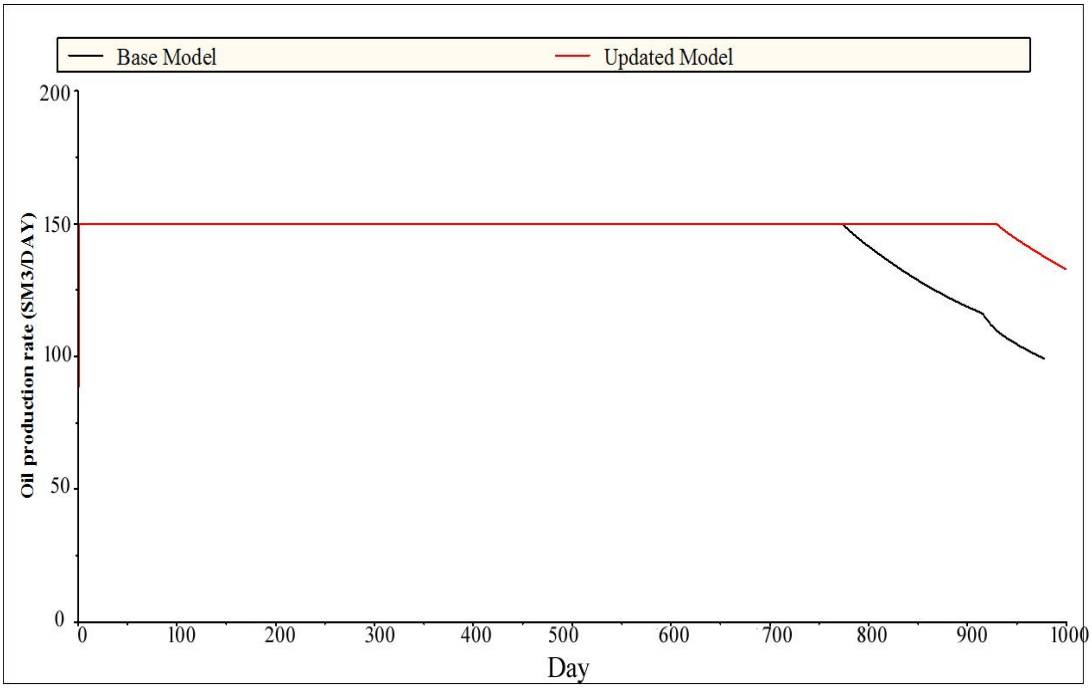

Figure 4.21 Daily Production Rate in Pool 1

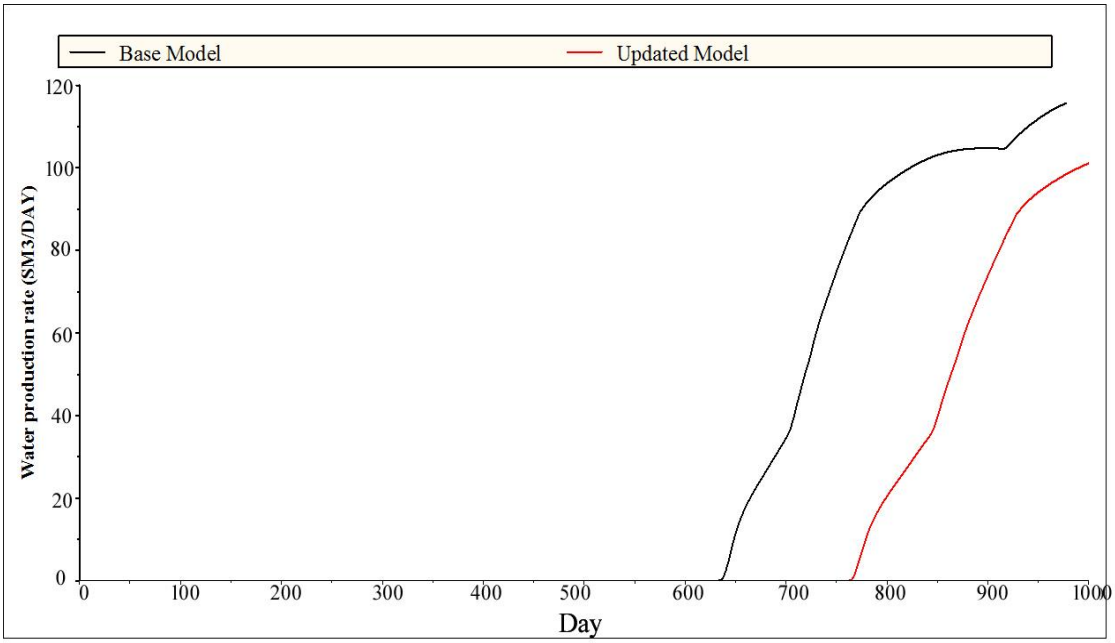

Figure 4.22 Water Production Rate in Pool 1

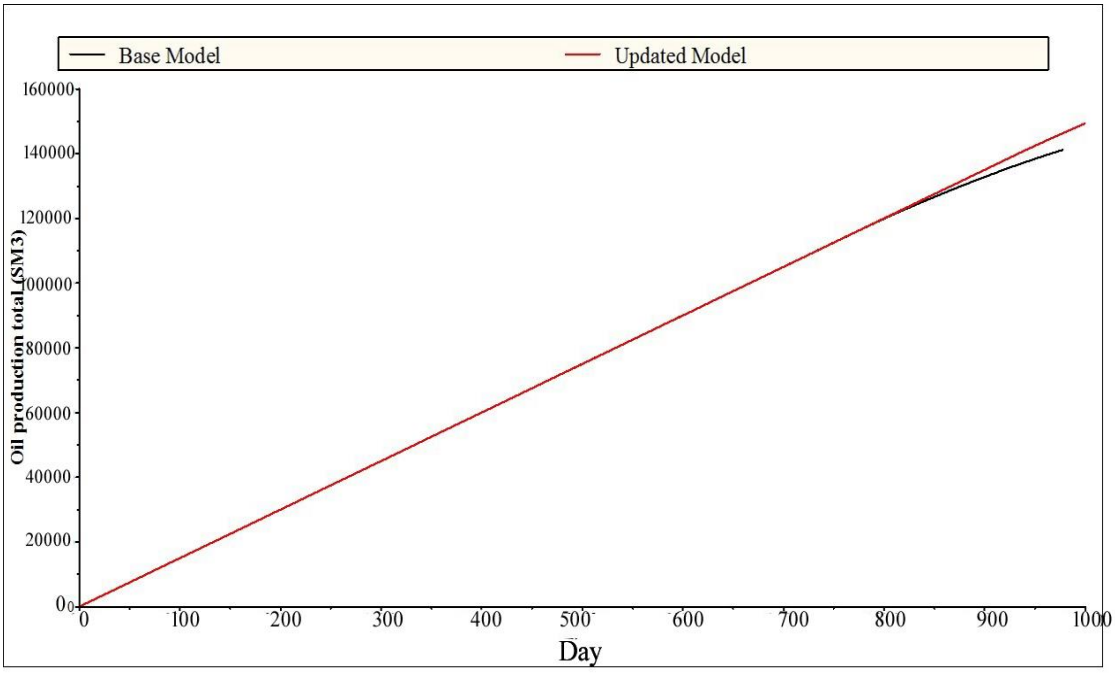

Figure 4.23 Cumulative Predicted Oil Production in Pool 1

In order to show the influence of well trajectory adjustment, the production performance in the new target area (white pool) is presented separately. The total production from the new target area (pool 2) is presented in Figure 4.24. The cumulative production is

approximately 180,000 Sm^3. The results show that the new area has even better production potential. The predicted cumulative production for 1000 days is 180,000 Sm^3 compared with 150,000 Sm^3 in pool 1. Therefore, combining the two pools, the cumulative production amount can be doubled if both are produced.

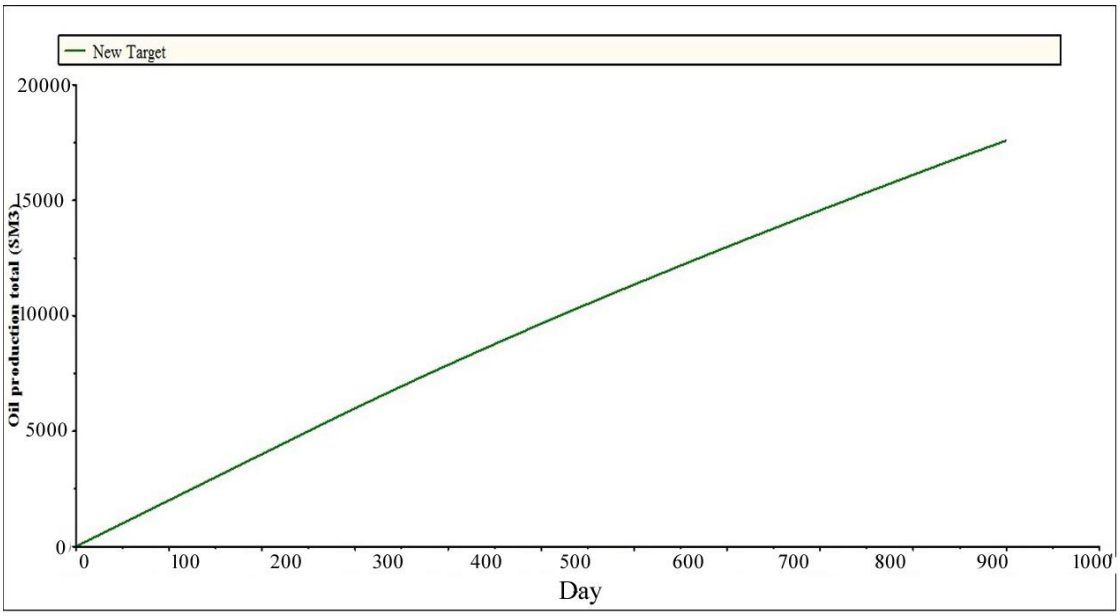

Figure 4.24 Total Oil Production in New Target (Pool2)

4.2.4 Economic Evaluation

Economics drive development in the petroleum industry. Almost all the decisions are made based on the economic evaluation and all the techniques are aimed to reduce costs and maximize the profit. Net Present Value (NPV) is the most important index used to determine the value of an investment using an effective interest rate. It is defined as the difference between the present value of cash inflows and cash outflows. Generally, a positive NPV represents that the project is a profitable one while a negative NPV means in a net loss (Ross, 1955).

Figure 4.25 is the cash flow profile for a hypothetical field development. As can be seen in the figure, ground construction started a few years before production. The emergence

of gross revenues marks the start of production. After this, capital costs still exist and operating costs such as tax, royalties start to appear. The Net Present Value Profit is calculated as

$$\text{Profit } (NPV) = \sum_{i=1}^{N_2} a_i (1+\frac{p}{100})^{-i} - \sum_{i=1}^{N_1} c_i (1+\frac{p}{100})^{i}, \quad (4.4)$$

where $c_i = Gross\ revenue - Opex - Tax - Royalties$ in year 'i' after production starts, a_i is the expenses in year 'i' before production starts and p is the effective interest rate (Khudiri, 2008).

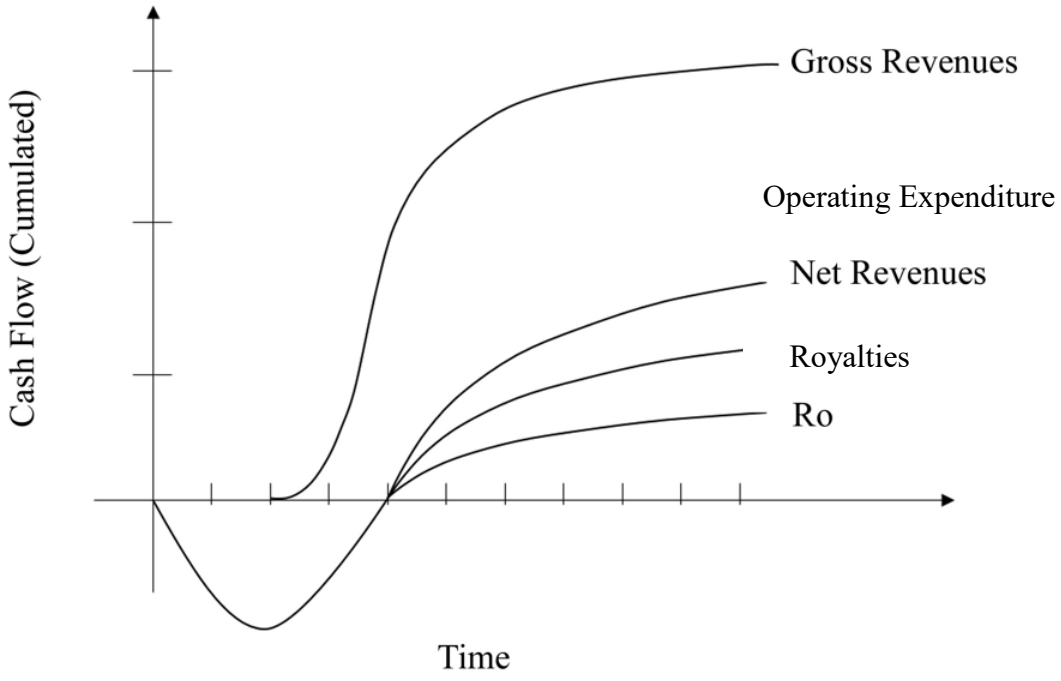

Figure 4.25 Cash Flow Profiles (Khudiri, 2008)

Due to limited data, the economic evaluation is discussed with some assumptions. The oil price is set as \$50/bbl and effective interest rate is set as 5%. In this case study, the well path in the updated realization has longer a length in horizontal direction. Therefore, the capital cost and operation cost will be higher compared with the base realization.

However, it is difficult to find the actual operating costs. The capital cost and operation cost are assumed to be the same in the two realizations.

Profit (NPV) is calculated with Equation 4.4. The result of profit difference between the two realizations is approximately $54,099,000. In other words, the updated realization estimates $54.1 million more profit compared with the base realization. The total production amount of the updated realization is much higher. The results also demonstrate that the oil produced from the new discovered drilling target brings huge revenues. All in all, the updated realization presents huge economic advantages.

4.2.5 Summary

The second case study presents an example of an integrated geosteering workflow and how it can be used to optimize well trajectory based on updating a geostatistical realization with real time data. Production performance and economic estimation are compared for the base geostatistical realization and the updated realization during drilling which includes the production from another potential pool (pool 2).

Geostatistics are used to build equally possible realizations of porosity distribution in the target reservoir formation. The spatial relationship of porosity is estimated using variogram realization and then simulated using sequential Gaussian simulation techniques. The spatial relationship of permeability is estimated using the porosity permeability relationship calculated by the Kozeny equation.

A base realization is selected among 100 of realizations based on the geological analysis. Moreover, a predrill well trajectory is designed based on the predrilling realization. The realization is then updated 8 times with simulated logging while drilling data, while the porosity distribution is updated with logging information.

The two realizations are compared with production performance in the reservoir

simulator. One is the base realization with the original well trajectory, while the other is the updated realization with the new well trajectory. The results demonstrate that the updated realization shows longer constant production rate and later water breakthrough time compared with the base realization.

5. Conclusions and Recommendations

The objective of this research is to develop an open-source integrated geosteering workflow which combines geostatistics, reservoir engineering and logging while drilling concepts together to optimize the well trajectory during the drilling process. Each of these theories is not new in practice. Some companies developed their own applications to solve similar problems such as Petrel platform developed by Schlumberger, SES application developed by Stoner Engineering and Strata Steer developed by Halliburton. Most of these commercial applications are discommodious and requires a large amount of data input to solve problems even for simple cases. Meanwhile, few studies directly apply logging while drilling techniques on geostatistical realizations. Compared with complex commercial software, customized code and systems can better meet specific goals. Based on all the discussion in previous chapters, some conclusions and accomplishments can be summarized here.

Firstly, porosity is one of the major parameters in reservoir characterization. A detailed and reliable porosity distribution map guides the design of an optimal well trajectory. This research demonstrates basic concepts of geostatistics and highlights a general

workflow of building a geostatistical realization from variogram analysis to realizations generation with actual field data.

Secondly, this research indicates that with the same porosity input, thousands of different geostatistical realizations can be generated based on Kriging estimation methods. Porosity distribution maps can be produced based on geostatistical analysis. From a statistics point of view, these realizations are equally-possible and all reflect data spatial correlation. However, most of them cannot hold when taking formation geological background and reservoir dynamic information into consideration.

Different realizations can predict different production performance. This was illustrated by comparing two porosity distribution realizations and their impact on production performance and economics. Updating the geological model using LWD data can result in reducing porosity or increasing it in areas not previously estimated in original Kriging efforts. Therefore, the geostatistical model is one of the critical part in reservoir characterization.

The variogram model of porosity in the Ile formation, Norne Field, is established in case study two. 100 geostatistical realizations are produced with the sequential Gaussian simulation method in this case study and a reliable porosity distribution map in the Ile formation is generated. Meanwhile a linear porosity-permeability relationship of the Ile formation is calculated in this research as well.

This research presents the methodology of how LWD can be incorporated into the geostatistical model in real time. In practice, the original well trajectory is rarely the optimal choice in most cases. That is the reason why it is necessary to incorporate information gathered while drilling to adjust well trajectory. One horizontal well in the field is selected as the drilling well and log data from this well is applied as LWD data. The porosity distribution map is updated every 50 m and the total drilling length is 400

m. The updated result show that, with new information continuously gathered from drilling, the porosity distribution along the well path can be updated and used to redesign a new well trajectory while drilling. Reservoir simulation results demonstrate that the updated model reveals better production rate and later water breakthrough time. The economic evaluation also proves the advantages of the updated model from an economic perspective.

Finally, numerous researchers have investigated updating models with logging while drilling data in recent years. Compared with the existing work, this research does present some different points. This geosteering workflow is built by open-source software and customized codes. It is totally free and flexibly adjusted. Data input in this study is point-set porosity data with coordinates format in ASCII. Data can be easily loaded and imported to most commercial software. Meanwhile Geostatistical realizations are updated directly with LWD data. The missing variables may increase the risk and uncertainty but this application is better for fast paced drilling in grain-dominated sandstone formations.

This study established a link between the porosity distribution map and the model updating process. The model is directly updated based on the porosity distribution generated from a geostatistical model. From the time efficiency point of view, it shows some advantages especially in reservoirs without minor structural effects. Meanwhile this study illustrates a dynamic updating process of estimating porosity distribution using geostatistical models. The well trajectory is guided by the latest data collected from logging while drilling, which can be flexibly adjusted.

5.1 Recommendations and Future Work

Geological structure is one of the dominating factors in geological modeling that may

affect the data spatial relationship and simulation results. The workflow presented in this research may encounter large uncertainty when applied in the formation with complex geological structures.

Well trajectories are mainly designed to chase high porosity distribution areas in this case study. However, the designed trajectories may be difficult to achieve in the actual drilling process due to the limitation of drilling techniques or costs. More feasible well trajectory plans with more parameters can be discussed in further research.

Seismic data in the Norne field were not available. The geostatistical model can be made even more robust if seismic data are integrated. Integrating seismic data into the geosteering process can provide additional insight to the reservoir structure and stratigraphy allowing for more accurate positioning of the well to improve operational efficiency and profitability.

References

Abdideh, M., & Mahmoudi N., (2013). UCS Prediction: A New Set of Concepts for Reservoir Geomechanical Modeling. *Petroleum Science and Technology*, *31*(24).

Agterberg, F. (2004). Georges Matheron Founder of Spatial Statistics. *Earth Sciences History*, *23*(2), 205-334.

Alberto,M., Ballard, A.,&Nicholas,B.(2002) Real-Time 3D Earth Model Updating While Drilling a Horizontal Well. *Society of Petroleum Engineering*. Paper presented at SPE Annual Technical Conference and Exhibition,29 September-2 October, San Antonio, Texas.

Alpay, O. A., (1972). A practical approach to defining reservoir heterogeneity. *Journal of Petroleum Technology*, *24*, 841–848.

Andre H., & Olivier D. (1994). Geostatistical inversion-a sequential method of stochastic reservoir modelling constrained by seismic data. *First Break*, *12*(11).

Chambers R. L., Yarus J. M., & Hird K. B. (2000). Petroleum Geostatistics for the Nongeostatistician—Part 2. *The Leading Edge, 19*(6), 592-599.

Chopra, A. K., Severson, C. D., & Carhart, S. R. (1990). Evaluation of Geostatistical Techniques for Reservoir Characterization. *Society of Petroleum Engineering*. Paper presented at SPE Annual Technical Conference and Exhibition, 23-26 September, New Orleans, Louisiana.

Chopra, S., & Marfurt, K. J. (2007). *Seismic attributes for prospect identification and reservoir characterization*. Tulsa, OK: Society of Exploration Geophysicists.

Clark, I. (2009). *Statistics or geostatistics? Sampling, error or nugget effect? The Southern African Institute of Mining and Metallurgy, 2010*. Paper presented at the SAIMM Conference, Fourth World Conference on Sampling & Blending.

Coburn, T. C. (1994). Reflections on the Proliferation of Geostatistics in Petroleum Exploration and Production. In J. M. Yarus & R. L. Chambers (Ed.), *Stochastic Modeling and Geostatistics: Principles, Methods, and Case Studies* (pp. 21-23). American Association of Petroleum Geologists.

Corvi, P. (1992). Reservoir Characterization Using Expert Knowledge, Data and Statistics. BP Research Sunbury-on-Thames, England

Krige, D. (1951). A statistical approach to some basic mine valuation problems on the Witwatersrand. *Journal of the Chemical, Metallurgical and Mining Society of*

South Africa. *52*(6), 119-139.

Darcy, H. (1856). *Les fontaines publiques de la ville de Dijon. Exposition et application des principes à suivre et des formules à employer dans les questions de distribution d'eau: ouvrage terminé par un appendice relatif aux fournitures d'eau de plusieurs villes au filtrage des eaux et à la fabrication des tuyaux de fonte, de plomb, de tole et de bitumen.* Nabu Press.

Dong, C., O'Keefe, M. D., Elshahawi, H., Hashem, M., Williams, S. M., Stensland, D., ... Donzier, E. (2007). New downhole fluid analyzer tool for improved reservoir characterization. *Society of Petroleum Engineers*.

Damsleth, E., & Omre, H. (1997). Geostatistical approaches in reservoir evaluation. *Journal of petroleum technology*, *49*(5), 498-501.

Glanville, C. R. (1970). Log Interpretations of Gas Sands from Multiple-Porosity and Resistivity Logging Programs. *The Log Analyst*, *11*(4), 3-11.

Goovaerts, P. (1997). *Geostatistics for Natural Resources Evaluation*. New York: Oxford University Press.

Kumang. (2012). Sperry Drilling Geosteering Solution Helps Reduce Costs and Increase Production with Precise Wellbore Placement. Halliburton. H09334

Henning, G. (1998). *Model Updating of Large Structural Dynamics Models Using Measured Response Functions*. Department of Mechanical Engineering. University of London, London, U.K.

Hewett, T. A. (1986, October 5-8). *Fractal Distributions of Reservoir Heterogeneity and Their influence on Fluid Transport*. Paper SPE 15386 presented at the 1986 SPE Annual Technical Conference and Exhibition, New Orleans.

Caers, J. (2001). Geostatistical reservoir modelling using statistical pattern recognition. *Journal of Petroleum Science and Engineering*, *29*(3), 177-188.

Kelkar, M. & Perez, G. (2002). *Applied Geostatistics for Reservoir Characterization*. Richardson, Tex: Society of Petroleum Engineers.

Khudiri, M. M. (2008). *Data Architecture of Real-time Drilling and Completions Information at Saudi Aramco*. doi: 10.2118/116848-RU

Kozeny, J. (1927). *Ueber Kapillare Leitung des Wasser sim Boden*. Sitzungsber Akad. Wiss., Wien, 136(2a):271-306.

Kroese, D. P. (2014). *Why the Monte Carlo method is so important today*. doi:10.1002/wics.1314

Lake, L. W. & Carroll H. B. (1986). *Reservoir Characterization.* Orlando, Florida: Academic Press.

Lake, L. W., Johnston, J. R., & Stegemeier, G. L. (1981). Simulation and performance prediction of a large-scale surfactant/polymer project. *Society of Petroleum Engineers Journal*, *21*(06), 731-739.

Liu, G. Li, B. J. (2012). Local upscaling and encrypt method in bottom water reservoir numerical simulation. *Science Technology and Engineering*, *12*(1).

Lantuejoul, C., (2002). *Geostatistical Simulation: Models and Algorithms*. Verlag, Berlin, Germany: Springer Science & Business Media.

Lucia, F. J. (1999). *Carbonate Reservoir Characterization.* New York: Springer.

Macleod,W. (2005). *Information sources in Engineering*. Walter De Gruyter: GmbH&Co KG.

Maharaja, A., (2008). Tigenerator: Object-based training image generator. *Computers & Geosciences, 34*(12), 1753-1761.

Marshall, G., Holt, J., Winters, W. (2000) Relevant time update of an Earth model with logging while drilling data[C]//SPE/AAPG Western Regional Meeting. *Society of Petroleum Engineers*.

Mottahedeh, R. (2005). *Horizontal Well Geo-Navigation: Planning, Monitoring and Geosteering*. Paper presented at Petroleum Society's 6th Canadian International Petroleum Conference.

Olea, R. E. (1991). *Geostatistical glossary and multilingual dictionary*. Oxford: Oxford University Press.

Oliver, D. S., Reynolds, A. C., & Liu, N. (2008). *Inverse theory for petroleum reservoir characterization and history matching*. Cambridge University Press.

Pardo, D (2012). Influence of borehole-eccentred tools on wireline and logging-while-drilling sonic logging measurements. *Geophysical Prospecting*, *61*(1), 268–283.

Partyka, G., Gridley, J., & Lopez, J. (1999). Interpretational applications of spectral decomposition in reservoir characterization. *The Leading Edge*, *18*(3), 353-360.

Peedersen, S. (2005). *Real Time Update of a Reservoir Property Model in Geosteering Applications*. Paper presented at 67th EAGE Conference & Exhibition.

Remy, N. (2011). *Applied Geostatistics with SGeMS, A User's Guide*. Cambridge University of Press.

Richardo, A. Olea. (1999). Geostatistics for Engineers and Earth Scientists. Kansas

Geological Survey, The University of Kansas Lawrence, USA

Rosman,A., Simon, R.J. (1977) Flow heterogeneity in reservoir rocks. International Journal of Rock Mechanics and Mining Sciences and Geomechanics. Vol.14(4), pp.60-60

Ross, S. A. (1995). Uses, abuses, and alternatives to the net-present-value rule. Financial management, 24(3), 96-102.

Sarma, P., Durlofsky, L. J. & Aziz, K. (2006). Efficient real-time reservoir management using adjoint-based optimal control and model updating[J]. *Computational Geosciences*, *10*(1), 3-36.

Scherbatskoy, S. A. (1982). *Systems, apparatus and methods for measuring while drilling*. Washington, DC: U.S. Patent and Trademark Office.

Schlumberger Modeling While Drilling Manual 2007

Segesman, F. F. (1995) Measurement while drilling. Reprint No 40, SPE Reprint,Series, SPE, Dallas, TX.

SES 5.x User Manual 2015

Sorenson, H. W. (1966). Kalman filtering techniques. *Advances in Control Systems Theory and Applications*, *3*, 219-292.

Statoil 2001 Annual Report.

Statoil 2006 Annual Report.

Toby. (2005). Well Logging and Formation Evaluation. Burlington. *Elsevier Science.*

Trina, S. (2010). *An Integrated Horizontal and Vertical Flow Simulation with Application to Wax Precipitation* (Unpublished master's thesis). Memorial University of Newfoundland, Newfoundland, Canada.

Wen, X. H. & Chen, W. H. (2006). Real-Time Reservoir Model Updating Using Ensemble Kalman Filter with Confirming Option. *Society of Petroleum Engineers*, *11*, 431-442.

Willcott, A. (2005). *Reducing the Risk in Drilling Production Wells: A Multidisciplinary Approach* (Unpublished master's thesis). Memorial University of Newfoundland, Newfoundland, Canada.

Zimino,A. (2015). Monte Carlo reservoir analysis combining seismic reflection data and informed priors. *Geophysics*, *80*(1), R31-R41.

Appendix A Tables and Data

Table A.1 Data used in figure 3.2: Relationships between Estimated Variogram and Covariance

Lag Distance	Estimated Variogram	Covariance
0	0	0.0039
1	0.0009	0.0034
3	0.0012	0.0032
5	0.0018	0.0027
6	0.0019	0.0026
7	0.0022	0.0023
8.5	0.0023	0.0021
9.5	0.0025	0.002
11	0.003	0.0017
12.5	0.0031	0.0015
13	0.0033	0.0013
14	0.00344	0.0012
15	0.0037	0.0007
17	0.004	0.00015
18	0.0041	0
19	0.00405	0.0001
21	0.00395	0.0003
23	0.0041	0
24	0.0041	0
25	0.00405	0.0001

Table A.2. Case Study Two: Well Report

Well	Sample Number	Valid Data Number	Measured Depth(m)	TVD(m)	Sample Interval
6608/10-E-1 H	8274	7381	3172.206-4349.953	2602.9-2623.663	0.125
6608/10-E-2 AH	5666	5410	3074.141-3750.391	2610.535-2611.97	0.125
6608/10-E-3H	8945	8719	2971.038-4060	2579.953-2625.26	0.125
6608/10-E-4 AH	8084	7798	3856.594-4831.344	2614.959-2634.64	0.125
6608/10-F-1H	8911	8692	2897.325-3983.825	2593.75-2621.409	0.125
6608/10-F-2H	7488	7081	4900.203-5785.581	2568.281-2574.463	0.125
6608/10-F-3H	10285	9883	4816.206-6051.587	2550.563-2572.871	0.125

Table A.3. Data Input for Case Study One

x	y	z	porosity
51	12	6	0.315
51	12	7	0.309
51	12	8	0.304
24	50	1	0.292
24	50	2	0.283
24	50	3	0.253779
24	50	4	0.259107
0	4	5	0.324
0	4	6	0.306
71	80	7	0.314581
71	80	8	0.312
40	11	3	0.281
40	11	4	0.301
40	11	7	0.304
40	11	8	0.317
40	11	9	0.272
84	6	2	0.269
84	6	3	0.319
19	35	1	0.278
19	35	2	0.286
69	114	0	0.291
69	114	2	0.315
69	114	3	0.2566
69	114	4	0.31
69	114	5	0.268
69	114	8	0.304
69	114	9	0.302
99	51	1	0.263
99	51	2	0.255
44	34	6	0.299
44	34	7	0.287
44	34	8	0.325
44	34	9	0.294

31	54	4	0.308
31	54	5	0.275
31	54	6	0.301
51	9	6	0.322
51	9	7	0.306
51	9	8	0.3258
94	115	1	0.245221
94	115	2	0.287
94	115	3	0.271
94	115	4	0.314
94	115	5	0.289
3	37	2	0.288554
3	37	3	0.285
3	37	4	0.297
3	37	5	0.353
3	37	6	0.31
32	101	5	0.284
32	101	6	0.3
32	101	7	0.291
32	101	8	0.265
32	101	9	0.317
46	50	0	0.309
46	50	2	0.249348
46	50	3	0.304
46	50	6	0.311
46	50	7	0.286
46	50	8	0.32
46	50	9	0.304
29	20	4	0.294
29	20	5	0.293
37	125	5	0.253
37	125	6	0.297
37	125	8	0.2196
53	9	6	0.303
53	9	7	0.309
53	9	8	0.302
35	93	4	0.299
35	93	8	0.302

35	93	9	0.302
56	73	7	0.273
56	73	8	0.3
89	111	3	0.311062
89	111	4	0.315
89	111	5	0.282
89	111	7	0.2689
89	111	8	0.219
72	39	8	0.281
60	19	8	0.247353
60	19	9	0.278498
72	21	7	0.301
48	116	0	0.31
48	116	1	0.29
48	116	7	0.281
48	116	8	0.238
36	36	0	0.299
36	36	3	0.33
36	36	4	0.245186
36	36	5	0.274
36	36	7	0.327
36	36	8	0.305
40	118	5	0.277
40	118	6	0.303
62	18	7	0.266696
62	18	8	0.279174
62	18	9	0.321009
83	58	2	0.27
83	58	3	0.256526
83	58	4	0.29
83	58	5	0.292
98	61	3	0.31
98	61	4	0.282
98	61	6	0.287
98	61	7	0.293
98	61	8	0.295
98	61	9	0.322
44	122	0	0.314

44	122	1	0.296
44	122	6	0.313
44	122	7	0.286
44	122	8	0.267
52	74	0	0.279
52	74	1	0.302
52	74	5	0.283
52	74	7	0.291
52	74	8	0.266
62	32	0	0.31
62	32	1	0.274
45	115	0	0.298
45	115	1	0.277
45	115	7	0.289
45	115	8	0.271
38	65	0	0.319319
38	65	1	0.252035
38	65	2	0.27
38	65	3	0.304
38	65	6	0.295
43	64	0	0.212
43	64	1	0.29318
92	22	1	0.265
92	22	2	0.271
92	22	3	0.293
64	63	0	0.29
51	79	0	0.271
51	79	1	0.313
51	79	2	0.267
51	79	3	0.281
62	87	5	0.264
62	87	7	0.263
62	87	8	0.324
69	99	0	0.303
69	99	1	0.299
69	99	2	0.303
69	99	7	0.267
69	99	8	0.306

37	87	4	0.304
37	87	6	0.2567
37	87	7	0.295
37	87	8	0.287108
37	87	9	0.2026
80	108	4	0.314
80	108	5	0.255
80	108	6	0.223
80	108	7	0.269
80	108	8	0.281
88	34	6	0.279
88	34	7	0.23
92	129	1	0.27
92	129	2	0.28
76	101	0	0.325
76	101	4	0.327
76	101	5	0.278
76	101	7	0.272
76	101	8	0.295
54	127	8	0.304
54	127	9	0.295
55	11	7	0.323
55	11	8	0.281
20	111	5	0.287
20	111	6	0.255
20	111	7	0.291
45	58	0	0.297
45	58	1	0.272
45	58	7	0.301
45	58	8	0.305
98	3	6	0.292
98	3	7	0.315
31	90	4	0.307
31	90	5	0.2876
31	90	6	0.282
31	90	7	0.275
31	90	8	0.274
31	90	9	0.304

16	16	3	0.272
16	16	4	0.303
16	16	6	0.294
16	16	7	0.263
16	16	8	0.293
16	16	9	0.253
39	87	6	0.285
39	87	7	0.288
39	87	8	0.263216
39	87	9	0.2026
9	25	1	0.248
9	25	2	0.203
9	25	3	0.261
9	25	4	0.285
9	25	6	0.3148
9	25	7	0.240445
68	116	0	0.298
68	116	2	0.305
68	116	3	0.286
68	116	4	0.304
68	116	5	0.268
68	116	8	0.292
68	116	9	0.29
20	27	0	0.322
20	27	6	0.280293
20	27	7	0.287
20	27	8	0.297
20	27	9	0.285
79	60	4	0.283
79	60	5	0.297
81	67	1	0.28
81	67	2	0.286
81	67	3	0.277
84	81	1	0.264
84	81	2	0.289
84	81	3	0.252
84	81	4	0.292
84	81	6	0.266

84	81	7	0.244
84	81	9	0.315
59	0	7	0.303
59	0	8	0.297
59	0	9	0.275
52	68	0	0.282
52	68	1	0.287
52	68	6	0.272
52	68	7	0.282
52	68	8	0.271
75	20	8	0.291
68	3	8	0.283
41	120	5	0.28
41	120	6	0.299
41	120	7	0.274
41	120	8	0.287
68	80	4	0.29
68	80	5	0.298
68	80	7	0.286739
68	80	8	0.316
84	109	4	0.317
84	109	5	0.286
84	109	7	0.268
84	109	8	0.315416
30	1	0	0.321
30	1	1	0.261
30	1	5	0.303
30	1	7	0.294
30	1	8	0.287
30	1	9	0.309
86	34	4	0.296
86	34	5	0.28
86	34	8	0.307
86	34	9	0.305
90	55	3	0.292
90	55	4	0.286
90	55	7	0.272
90	55	8	0.281

60	122	4	0.326
60	122	5	0.291
60	122	8	0.297
60	122	9	0.307
78	122	7	0.29
78	122	8	0.283
67	28	2	0.3
67	28	3	0.266
67	28	4	0.302
10	31	1	0.291
10	31	2	0.234014
10	31	3	0.295
10	31	4	0.269
74	32	2	0.278
74	32	3	0.282
74	32	4	0.317
74	32	7	0.298
74	32	9	0.285
0	96	1	0.265
0	96	2	0.223
0	96	5	0.313
0	96	6	0.301
74	115	0	0.345
5	41	3	0.274
5	41	4	0.277
5	41	5	0.345
5	41	6	0.307
51	95	2	0.279
51	95	3	0.312
64	25	3	0.279
64	25	4	0.287
41	83	2	0.266
41	83	3	0.276
41	83	6	0.276
41	83	7	0.285
41	83	8	0.240802
41	83	9	0.29394
24	77	4	0.303
24	77	7	0.29
24	77	8	0.291
24	77	9	0.305
53	22	3	0.33
53	22	4	0.281
70	49	7	0.272
70	49	8	0.29
80	33	4	0.296
80	33	5	0.305
80	33	8	0.29
80	33	9	0.281
33	19	0	0.279
33	19	1	0.288
42	97	1	0.271
42	97	3	0.297
42	97	4	0.278
42	97	6	0.3
42	97	7	0.223
42	97	8	0.305
42	97	9	0.28
70	85	7	0.231311
70	85	8	0.311
64	69	0	0.297
80	89	1	0.297
80	89	2	0.296
80	89	3	0.262
80	89	4	0.316
80	89	8	0.288
80	89	9	0.315
61	37	0	0.307
61	37	1	0.271
36	28	3	0.302018
36	28	4	0.240181
36	28	5	0.278
36	28	6	0.275
36	28	7	0.287
36	28	8	0.314
3	124	1	0.269

3	124	2	0.28
3	124	3	0.324
3	124	4	0.305
18	28	0	0.308
18	28	6	0.296
18	28	7	0.296
18	28	8	0.291
18	28	9	0.277
50	33	8	0.335
50	33	9	0.295
62	120	3	0.29
62	120	4	0.314
62	120	5	0.294
62	120	8	0.285
62	120	9	0.296
20	19	0	0.311
20	19	7	0.285
62	35	0	0.311
62	35	1	0.269
32	118	6	0.284
32	118	7	0.268
35	110	5	0.2362
35	110	6	0.295
38	72	2	0.276
38	72	3	0.302
38	72	4	0.285
38	72	5	0.272
38	72	6	0.287
38	72	8	0.267
38	72	9	0.306
98	59	1	0.278295
98	59	2	0.263
98	59	6	0.308
98	59	7	0.287
98	59	8	0.29
98	59	9	0.329
90	5	1	0.264
90	5	2	0.255

62	118	3	0.277
62	118	4	0.294
62	118	8	0.282
62	118	9	0.288
45	27	3	0.307
45	27	4	0.296
45	27	6	0.314
45	27	7	0.304
45	27	8	0.307
45	27	9	0.28
66	129	0	0.255436
66	129	2	0.29
66	129	3	0.272
28	31	0	0.322
28	31	7	0.31
28	31	8	0.294
28	31	9	0.273
56	109	4	0.317
56	109	8	0.299
56	109	9	0.272
51	101	0	0.294
51	101	1	0.3
51	101	8	0.233
51	101	9	0.277
60	19	8	0.29767
60	19	9	0.319678
28	121	5	0.28
28	121	6	0.269
28	121	7	0.279
96	73	3	0.305
96	73	4	0.273
37	22	3	0.30599
37	22	4	0.302029
37	22	8	0.292
37	22	9	0.298
67	84	7	0.2522
67	84	8	0.328
23	47	1	0.262

23	47	2	0.29
23	47	7	0.29
23	47	8	0.3
23	47	9	0.279
11	22	3	0.29
11	22	4	0.271
11	22	8	0.320762
11	22	9	0.254
28	44	1	0.322861
28	44	2	0.2882
28	44	5	0.268
28	44	6	0.282
28	44	7	0.3
28	44	8	0.335
28	44	9	0.299
25	111	8	0.267766
25	111	9	0.287
11	86	6	0.303
11	86	7	0.291
64	61	0	0.273
25	124	7	0.3
99	118	1	0.26
99	118	2	0.279
99	118	3	0.276
99	118	5	0.295
99	118	6	0.319976
99	118	7	0.262
99	118	8	0.29
99	118	9	0.3
44	71	0	0.307888
44	71	1	0.262425
44	71	5	0.249423
44	71	8	0.268
44	71	9	0.316
18	81	6	0.284
18	81	7	0.3215
30	120	4	0.308
30	120	5	0.269
30	120	6	0.282
21	47	2	0.297
21	47	8	0.307
21	47	9	0.277
87	22	2	0.233
87	22	3	0.3
40	106	7	0.27
7	44	3	0.283
7	44	4	0.285
7	44	5	0.348
7	44	6	0.301
6	8	1	0.238
6	8	3	0.255
6	8	5	0.343
6	8	6	0.286
72	37	8	0.273
69	74	4	0.283
69	74	5	0.292
88	37	4	0.2173
88	37	5	0.265
38	7	3	0.268
38	7	4	0.326
7	33	2	0.329555
7	33	3	0.271
7	33	4	0.29
7	33	5	0.3537
7	33	6	0.302
52	110	0	0.281
52	110	1	0.297
52	110	3	0.312
52	110	4	0.309
52	110	7	0.265
52	110	8	0.257
63	121	3	0.279
63	121	4	0.284
63	121	5	0.294
63	121	7	0.292
63	121	8	0.3

63	121	9	0.284
83	10	2	0.271
83	10	3	0.304
47	50	1	0.301
47	50	2	0.277
47	50	3	0.303
47	50	7	0.287
47	50	8	0.308
47	50	9	0.303
40	56	2	0.24613
40	56	3	0.313
40	56	4	0.269
25	82	3	0.29
25	82	4	0.295
50	129	6	0.306
50	129	7	0.267
77	4	5	0.287
77	4	7	0.300803
77	4	8	0.264
32	118	6	0.284
32	118	7	0.268
69	60	0	0.294
87	49	2	0.294
87	49	3	0.278
87	49	4	0.274
87	49	5	0.2436
87	49	7	0.273
87	49	8	0.313
85	95	6	0.269
85	95	7	0.266
99	22	2	0.268
99	22	3	0.29
99	22	8	0.303
65	3	7	0.296
65	3	8	0.286
64	54	8	0.298
42	56	2	0.206
42	56	3	0.295
42	56	4	0.27
74	43	7	0.274
74	43	8	0.266
59	128	0	0.280152
59	128	3	0.277
59	128	4	0.304
59	128	5	0.277

Table A.4. Log Data for Case study Two

Measure Depth(m)	X-Offset	Y-Offset	Porosity
3111.27	-557.68	-1110.38	0.26
3112.52	-558.62	-1111.15	0.21
3113.77	-559.56	-1111.93	0.22
3115.02	-560.50	-1112.70	0.28
3116.27	-561.44	-1113.47	0.28
3117.52	-562.39	-1114.25	0.28
3118.77	-563.33	-1115.02	0.28
3120.02	-564.27	-1115.79	0.28
3121.27	-565.21	-1116.58	0.27
3122.52	-566.15	-1117.38	0
3123.77	-567.08	-1118.17	0.22
3125.02	-568.02	-1118.96	0.25
3126.27	-568.96	-1119.76	0.26
3127.52	-569.90	-1120.55	0.18
3128.77	-570.84	-1121.34	0.25
3130.02	-571.78	-1122.13	0.25
3131.27	-572.72	-1122.93	0.24
3132.52	-573.66	-1123.72	0.26

3133.77	-574.60	-1124.51	0.27
3135.02	-575.54	-1125.30	0.26
3136.27	-576.48	-1126.10	0.26
3137.52	-577.42	-1126.89	0.26
3138.77	-578.36	-1127.68	0.28
3140.02	-579.30	-1128.47	0.28
3141.27	-580.23	-1129.29	0.27
3142.52	-581.17	-1130.10	0.26
3143.77	-582.10	-1130.91	0.25
3145.02	-583.04	-1131.72	0.26
3146.27	-583.98	-1132.54	0.27
3147.52	-584.91	-1133.35	0.26
3148.77	-585.85	-1134.16	0.26
3150.02	-586.78	-1134.98	0.28
3151.27	-587.72	-1135.79	0.28
3152.52	-588.65	-1136.60	0.27
3153.77	-589.59	-1137.41	0.28
3155.02	-590.52	-1138.23	0.26
3156.27	-591.46	-1139.04	0.26
3157.52	-592.40	-1139.85	0.27
3158.77	-593.33	-1140.66	0.26
3160.02	-594.27	-1141.48	0.25
3161.27	-595.20	-1142.31	0
3162.52	-596.12	-1143.14	0
3163.77	-597.05	-1143.97	0.18
3165.02	-597.98	-1144.80	0.27
3166.27	-598.91	-1145.63	0.31
3167.52	-599.84	-1146.46	0.32
3168.77	-600.77	-1147.29	0.32
3170.02	-601.70	-1148.12	0.32
3171.27	-602.63	-1148.95	0.31
3172.52	-603.56	-1149.78	0.31
3173.77	-604.49	-1150.61	0.32
3175.02	-605.41	-1151.44	0.33
3176.27	-606.34	-1152.27	0.32
3177.52	-607.27	-1153.10	0.32
3178.77	-608.20	-1153.94	0.33
3180.02	-609.13	-1154.77	0.32

3181.27	-610.05	-1155.61	0.33
3182.52	-610.97	-1156.46	0.32
3183.77	-611.89	-1157.30	0.33
3185.02	-612.81	-1158.15	0.32
3186.27	-613.73	-1158.99	0.32
3187.52	-614.65	-1159.84	0.33
3188.77	-615.57	-1160.68	0.33
3190.02	-616.49	-1161.53	0.32
3191.27	-617.41	-1162.38	0.33
3192.52	-618.33	-1163.22	0.32
3193.77	-619.25	-1164.07	0.33
3195.02	-620.17	-1164.91	0.32
3196.27	-621.09	-1165.76	0.31
3197.52	-622.01	-1166.60	0.31
3198.77	-622.93	-1167.45	0.3
3200.02	-623.84	-1168.31	0.32
3201.27	-624.74	-1169.17	0.3
3202.52	-625.65	-1170.03	0.3
3203.77	-626.55	-1170.89	0.31
3205.02	-627.46	-1171.75	0.3
3206.27	-628.36	-1172.61	0.31
3207.52	-629.27	-1173.47	0.31
3208.77	-630.17	-1174.33	0.3
3210.02	-631.07	-1175.19	0.31
3211.27	-631.98	-1176.06	0.29
3212.52	-632.88	-1176.92	0.31
3213.77	-633.79	-1177.78	0.31
3215.02	-634.69	-1178.64	0.32
3216.27	-635.60	-1179.50	0.32
3217.52	-636.50	-1180.36	0.32
3218.77	-637.41	-1181.22	0.32
3220.02	-638.31	-1182.08	0.33
3221.27	-639.22	-1182.95	0.33
3222.52	-640.12	-1183.81	0.32
3223.77	-641.03	-1184.67	0.32
3225.02	-641.93	-1185.53	0.33
3226.27	-642.83	-1186.39	0.32
3227.52	-643.72	-1187.26	0.32

3228.77	-644.61	-1188.13	0.33
3230.02	-645.49	-1189.00	0.32
3231.27	-646.38	-1189.88	0.33
3232.52	-647.26	-1190.75	0.33
3233.77	-648.15	-1191.62	0.34
3235.02	-649.04	-1192.49	0.34
3236.27	-649.92	-1193.37	0.33
3237.52	-650.81	-1194.24	0.34
3238.77	-651.69	-1195.11	0.33
3240.02	-652.58	-1195.98	0.34
3241.27	-653.46	-1196.85	0.33
3242.52	-654.35	-1197.73	0.32
3243.77	-655.23	-1198.60	0.32
3245.02	-656.12	-1199.47	0.32
3246.27	-657.00	-1200.34	0.33
3247.52	-657.89	-1201.22	0.32
3248.77	-658.78	-1202.09	0.32
3250.02	-659.66	-1202.96	0.31
3251.27	-660.55	-1203.83	0.31
3252.52	-661.43	-1204.70	0.3
3253.77	-662.32	-1205.58	0.27
3255.02	-663.20	-1206.45	0.24
3256.27	-664.06	-1207.35	0
3257.52	-664.89	-1208.26	0
3258.77	-665.72	-1209.18	0
3260.02	-666.56	-1210.09	0.26
3261.27	-667.39	-1211.01	0.27
3262.52	-668.22	-1211.93	0.29
3263.77	-669.05	-1212.84	0.3
3265.02	-669.88	-1213.76	0.3
3266.27	-670.71	-1214.68	0.3
3267.52	-671.55	-1215.59	0.29
3268.77	-672.38	-1216.51	0.3
3270.02	-673.21	-1217.42	0.3
3271.27	-674.04	-1218.34	0.29
3272.52	-674.87	-1219.26	0.3
3273.77	-675.71	-1220.17	0.31
3275.02	-676.54	-1221.09	0.28
3276.27	-677.37	-1222.01	0.27
3277.52	-678.20	-1222.92	0.29
3278.77	-679.03	-1223.84	0.29
3280.02	-679.87	-1224.75	0.29
3281.27	-680.70	-1225.67	0.29
3282.52	-681.53	-1226.59	0.29
3283.77	-682.36	-1227.50	0.28
3285.02	-683.13	-1228.47	0.27
3286.27	-683.89	-1229.45	0.28
3287.52	-684.66	-1230.43	0.3
3288.77	-685.42	-1231.40	0.31
3290.02	-686.18	-1232.38	0.29
3291.27	-686.95	-1233.36	0.28
3292.52	-687.71	-1234.33	0.27
3293.77	-688.47	-1235.31	0.25
3295.02	-689.24	-1236.29	0.16
3296.27	-690.00	-1237.26	0
3297.52	-690.76	-1238.24	0.24
3298.77	-691.52	-1239.22	0.27
3300.02	-692.29	-1240.19	0.27
3301.27	-693.05	-1241.17	0.26
3302.52	-693.81	-1242.15	0.25
3303.77	-694.58	-1243.12	0.26
3305.02	-695.34	-1244.10	0.28
3306.27	-696.10	-1245.08	0.27
3307.52	-696.87	-1246.05	0.25
3308.77	-697.63	-1247.03	0.24
3310.02	-698.39	-1248.01	0.25
3311.27	-699.14	-1249.00	0.25
3312.52	-699.87	-1250.00	0.26
3313.77	-700.61	-1251.00	0.25
3315.02	-701.35	-1252.00	0.25
3316.27	-702.09	-1253.00	0.25
3317.52	-702.82	-1254.00	0.24
3318.77	-703.56	-1255.00	0.25
3320.02	-704.30	-1256.00	0.25
3321.27	-705.03	-1257.00	0.27
3322.52	-705.77	-1258.00	0.27

3323.77	-706.51	-1259.00	0.28
3325.02	-707.25	-1260.00	0.28
3326.27	-707.98	-1261.00	0.28
3327.52	-708.72	-1262.00	0.28
3328.77	-709.46	-1263.00	0.27
3330.02	-710.19	-1264.00	0.27
3331.27	-710.93	-1265.00	0.24
3332.52	-711.67	-1266.01	0.24
3333.77	-712.41	-1267.01	0.24
3335.02	-713.14	-1268.01	0.23
3336.27	-713.88	-1269.01	0.23
3337.52	-714.62	-1270.01	0.24
3338.77	-715.35	-1271.02	0.25
3340.02	-716.08	-1272.03	0.24
3341.27	-716.81	-1273.04	0.25
3342.52	-717.54	-1274.05	0.25
3343.77	-718.27	-1275.06	0.25
3345.02	-719.00	-1276.07	0.25
3346.27	-719.73	-1277.08	0.25
3347.52	-720.46	-1278.09	0.25
3348.77	-721.19	-1279.10	0.25
3350.02	-721.92	-1280.11	0.25
3351.27	-722.65	-1281.13	0.24
3352.52	-723.38	-1282.14	0.25
3353.77	-724.11	-1283.15	0.25
3355.02	-724.84	-1284.16	0.25
3356.27	-725.57	-1285.17	0.24
3357.52	-726.30	-1286.18	0.25
3358.77	-727.03	-1287.19	0.25
3360.02	-727.76	-1288.20	0.26
3361.27	-728.49	-1289.21	0.25
3362.52	-729.22	-1290.22	0.25
3363.77	-729.95	-1291.24	0.25
3365.02	-730.68	-1292.25	0.26
3366.27	-731.39	-1293.27	0.25
3367.52	-732.06	-1294.33	0.25
3368.77	-732.72	-1295.38	0.26
3370.02	-733.39	-1296.44	0.26

3371.27	-734.05	-1297.50	0.25
3372.52	-734.72	-1298.55	0.26
3373.77	-735.38	-1299.61	0.26
3375.02	-736.05	-1300.67	0.25
3376.27	-736.72	-1301.72	0.25
3377.52	-737.38	-1302.78	0.25
3378.77	-738.05	-1303.84	0.25
3380.02	-738.71	-1304.89	0.25
3381.27	-739.38	-1305.95	0.26
3382.52	-740.04	-1307.01	0.26
3383.77	-740.71	-1308.06	0.25
3385.02	-741.38	-1309.12	0.25
3386.27	-742.04	-1310.18	0.25
3387.52	-742.71	-1311.23	0.25
3388.77	-743.37	-1312.29	0.24
3390.02	-744.04	-1313.35	0.25
3391.27	-744.70	-1314.40	0.25
3392.52	-745.37	-1315.46	0.24
3393.77	-746.03	-1316.52	0.25
3395.02	-746.70	-1317.57	0.24
3396.27	-747.37	-1318.63	0.25
3397.52	-748.03	-1319.69	0.25
3398.77	-748.70	-1320.74	0.25
3400.02	-749.36	-1321.80	0.25
3401.27	-750.03	-1322.86	0.25
3402.52	-750.69	-1323.91	0.25
3403.77	-751.36	-1324.97	0.24
3405.02	-752.03	-1326.03	0.24
3406.27	-752.69	-1327.08	0.25
3407.52	-753.36	-1328.14	0.24
3408.77	-754.02	-1329.20	0.24
3410.02	-754.69	-1330.25	0.24
3411.27	-755.35	-1331.31	0.23
3412.52	-756.02	-1332.37	0.24
3413.77	-756.68	-1333.42	0.24
3415.02	-757.35	-1334.48	0.22
3416.27	-758.02	-1335.54	0.22
3417.52	-758.68	-1336.59	0.24

3418.77	-759.35	-1337.65	0.24
3420.02	-760.01	-1338.71	0.24
3421.27	-760.68	-1339.76	0.25
3422.52	-761.34	-1340.82	0.25
3423.77	-762.01	-1341.88	0.26
3425.02	-762.68	-1342.93	0.23
3426.27	-763.34	-1343.99	0.23
3427.52	-764.01	-1345.05	0.24
3428.77	-764.67	-1346.10	0.25
3430.02	-765.34	-1347.16	0.24
3431.27	-766.00	-1348.22	0.25
3432.52	-766.67	-1349.27	0.24
3433.77	-767.34	-1350.33	0.25
3435.02	-768.00	-1351.39	0.24
3436.27	-768.67	-1352.44	0.25
3437.52	-769.33	-1353.50	0.25
3438.77	-770.00	-1354.56	0.25
3440.02	-770.66	-1355.61	0.24
3441.27	-771.33	-1356.67	0.25
3442.52	-771.99	-1357.73	0.25
3443.77	-772.66	-1358.78	0.24
3445.02	-773.33	-1359.84	0.25
3446.27	-773.99	-1360.90	0.25
3447.52	-774.66	-1361.95	0.25
3448.77	-775.32	-1363.01	0.24
3450.02	-775.99	-1364.07	0.25
3451.27	-776.66	-1365.12	0.25
3452.52	-777.34	-1366.17	0.25
3453.77	-778.02	-1367.22	0.25
3455.02	-778.70	-1368.26	0.23
3456.27	-779.38	-1369.31	0.23
3457.52	-780.05	-1370.36	0.24
3458.77	-780.73	-1371.41	0.25
3460.02	-781.41	-1372.46	0.25
3461.27	-782.09	-1373.51	0.23
3462.52	-782.77	-1374.56	0.24
3463.77	-783.44	-1375.61	0.25
3465.02	-784.12	-1376.66	0.24
3466.27	-784.80	-1377.70	0.24
3467.52	-785.48	-1378.75	0.24
3468.77	-786.16	-1379.80	0.24
3470.02	-786.83	-1380.85	0.23
3471.27	-787.51	-1381.90	0.23
3472.52	-788.19	-1382.95	0.23
3473.77	-788.87	-1384.00	0.24
3475.02	-789.55	-1385.05	0.23
3476.27	-790.22	-1386.09	0.24
3477.52	-790.90	-1387.14	0.23
3478.77	-791.58	-1388.19	0.2
3480.02	-792.26	-1389.24	0.24
3481.27	-792.94	-1390.29	0.24
3482.52	-793.61	-1391.34	0.24
3483.77	-794.29	-1392.39	0.23
3485.02	-794.97	-1393.44	0.23
3486.27	-795.65	-1394.49	0.24
3487.52	-796.33	-1395.53	0.24
3488.77	-797.00	-1396.58	0.24
3490.02	-797.68	-1397.63	0.24
3491.27	-798.36	-1398.68	0.24
3492.52	-799.04	-1399.73	0.23
3493.77	-799.72	-1400.78	0.23
3495.02	-800.39	-1401.83	0.24
3496.27	-801.07	-1402.88	0.24
3497.52	-801.75	-1403.93	0.24
3498.77	-802.43	-1404.97	0.25
3500.02	-803.11	-1406.02	0.22
3501.27	-803.78	-1407.07	0.22
3502.52	-804.46	-1408.12	0.23
3503.77	-805.14	-1409.17	0.22
3505.02	-805.82	-1410.22	0.24
3506.27	-806.50	-1411.27	0.24
3507.52	-807.17	-1412.32	0.24
3508.77	-807.85	-1413.36	0.25
3510.02	-808.60	-1414.36	0.25
3511.27	-809.35	-1415.36	0.25
3512.52	-810.10	-1416.36	0.24

3513.77	-810.85	-1417.36	0.25
3515.02	-811.60	-1418.36	0.25
3516.27	-812.35	-1419.36	0.25
3517.52	-813.10	-1420.36	0.25
3518.77	-813.85	-1421.36	0.25
3520.02	-814.60	-1422.36	0.25
3521.27	-815.35	-1423.36	0.25
3522.52	-816.10	-1424.36	0.25
3523.77	-816.85	-1425.36	0.25
3525.02	-817.60	-1426.36	0.25
3526.27	-818.35	-1427.36	0.25
3527.52	-819.10	-1428.36	0.25
3528.77	-819.85	-1429.36	0.25
3530.02	-820.60	-1430.36	0.25
3531.27	-821.35	-1431.36	0.25
3532.52	-822.10	-1432.36	0.24
3533.77	-822.85	-1433.36	0.25
3535.02	-823.60	-1434.36	0.25
3536.27	-824.35	-1435.36	0.25
3537.52	-825.12	-1436.35	0.25
3538.77	-825.91	-1437.32	0.26
3540.02	-826.70	-1438.29	0.24
3541.27	-827.49	-1439.26	0.24
3542.52	-828.28	-1440.23	0.23
3543.77	-829.07	-1441.20	0.23
3545.02	-829.85	-1442.16	0.23
3546.27	-830.64	-1443.13	0.24
3547.52	-831.43	-1444.10	0.23
3548.77	-832.22	-1445.07	0.23
3550.02	-833.01	-1446.04	0.23
3551.27	-833.80	-1447.01	0.23
3552.52	-834.59	-1447.98	0.24
3553.77	-835.38	-1448.95	0.23
3555.02	-836.17	-1449.92	0.23
3556.27	-836.96	-1450.88	0.23
3557.52	-837.75	-1451.85	0.23
3558.77	-838.54	-1452.82	0.24
3560.02	-839.33	-1453.79	0.24
3561.27	-840.11	-1454.76	0.24
3562.52	-840.90	-1455.73	0.24
3563.77	-841.69	-1456.70	0.23
3565.02	-842.48	-1457.67	0.24
3566.27	-843.33	-1458.59	0.24
3567.52	-844.18	-1459.51	0.23
3568.77	-845.02	-1460.42	0.24
3570.02	-845.87	-1461.34	0.24
3571.27	-846.72	-1462.26	0.24
3572.52	-847.56	-1463.18	0.24
3573.77	-848.41	-1464.10	0.23
3575.02	-849.26	-1465.02	0.23
3576.27	-850.10	-1465.94	0.24
3577.52	-850.95	-1466.86	0.23
3578.77	-851.80	-1467.78	0.24
3580.02	-852.64	-1468.70	0.24
3581.27	-853.49	-1469.62	0.23
3582.52	-854.34	-1470.54	0.23
3583.77	-855.18	-1471.46	0.23
3585.02	-856.03	-1472.38	0.24
3586.27	-856.87	-1473.30	0.24
3587.52	-857.72	-1474.22	0.24
3588.77	-858.57	-1475.14	0.24
3590.02	-859.41	-1476.06	0.23
3591.27	-860.26	-1476.98	0.24
3592.52	-861.12	-1477.89	0.24
3593.77	-862.00	-1478.77	0.24
3595.02	-862.89	-1479.65	0.23
3596.27	-863.77	-1480.53	0.24
3597.52	-864.66	-1481.41	0.23
3598.77	-865.55	-1482.30	0.26
3600.02	-866.43	-1483.18	0.25
3601.27	-867.32	-1484.06	0.25
3602.52	-868.20	-1484.94	0.25
3603.77	-869.09	-1485.82	0.25
3605.02	-869.98	-1486.70	0.24
3606.27	-870.86	-1487.59	0.24
3607.52	-871.75	-1488.47	0.24

3608.77	-872.63	-1489.35	0.24
3610.02	-873.52	-1490.23	0.26
3611.27	-874.41	-1491.11	0.25
3612.52	-875.29	-1491.99	0.24
3613.77	-876.18	-1492.87	0.23
3615.02	-877.06	-1493.76	0.24
3616.27	-877.95	-1494.64	0.24
3617.52	-878.84	-1495.52	0.25
3618.77	-879.72	-1496.40	0.26
3620.02	-880.61	-1497.28	0.25
3621.27	-881.49	-1498.16	0.25
3622.52	-882.38	-1499.04	0.25
3623.77	-883.30	-1499.89	0.24
3625.02	-884.22	-1500.73	0.24
3626.27	-885.14	-1501.58	0.23
3627.52	-886.06	-1502.43	0.24
3628.77	-886.98	-1503.27	0.24
3630.02	-887.90	-1504.12	0.23
3631.27	-888.82	-1504.97	0.23
3632.52	-889.74	-1505.81	0.23
3633.77	-890.66	-1506.66	0.23
3635.02	-891.58	-1507.51	0.21
3636.27	-892.50	-1508.35	0.22
3637.52	-893.42	-1509.20	0.25
3638.77	-894.34	-1510.05	0.25
3640.02	-895.25	-1510.89	0.25
3641.27	-896.17	-1511.74	0.25
3642.52	-897.09	-1512.59	0.25
3643.77	-898.01	-1513.43	0.25
3645.02	-898.93	-1514.28	0.26
3646.27	-899.85	-1515.13	0.25
3647.52	-900.77	-1515.98	0.26
3648.77	-901.69	-1516.82	0.26
3650.02	-902.61	-1517.67	0.26
3651.27	-903.54	-1518.50	0.26
3652.52	-904.51	-1519.29	0.26
3653.77	-905.48	-1520.08	0.26
3655.02	-906.44	-1520.88	0.26
3656.27	-907.41	-1521.67	0.25
3657.52	-908.37	-1522.46	0.26
3658.77	-909.34	-1523.25	0.25
3660.02	-910.31	-1524.05	0.27
3661.27	-911.27	-1524.84	0.26
3662.52	-912.24	-1525.63	0.26
3663.77	-913.20	-1526.42	0.26
3665.02	-914.17	-1527.22	0.26
3666.27	-915.14	-1528.01	0.25
3667.52	-916.10	-1528.80	0.25
3668.77	-917.07	-1529.60	0.25
3670.02	-918.03	-1530.39	0.25
3671.27	-919.00	-1531.18	0.25
3672.52	-919.97	-1531.97	0.24
3673.77	-920.93	-1532.77	0.25
3675.02	-921.90	-1533.56	0.25
3676.27	-922.86	-1534.35	0.25
3677.52	-923.83	-1535.14	0.25
3678.77	-924.80	-1535.94	0.25
3680.02	-925.81	-1536.67	0.25
3681.27	-926.82	-1537.40	0.26
3682.52	-927.83	-1538.13	0.25
3683.77	-928.85	-1538.87	0.25
3685.02	-929.86	-1539.60	0.26
3686.27	-930.88	-1540.33	0.26
3687.52	-931.89	-1541.06	0.26
3688.77	-932.90	-1541.79	0.26
3690.02	-933.92	-1542.52	0.27
3691.27	-934.93	-1543.25	0.23
3692.52	-935.94	-1543.99	0.25
3693.77	-936.96	-1544.72	0.25
3695.02	-937.97	-1545.45	0.26
3696.27	-938.98	-1546.18	0.26
3697.52	-940.00	-1546.91	0.26
3698.77	-941.01	-1547.64	0.26
3700.02	-942.02	-1548.37	0.26
3701.27	-943.04	-1549.11	0.25
3702.52	-944.05	-1549.84	0.26

3703.77	-945.06	-1550.57	0.25
3705.02	-946.08	-1551.30	0.25
3706.27	-947.10	-1552.02	0.25
3707.52	-948.14	-1552.71	0.28
3708.77	-949.18	-1553.41	0.28
3710.02	-950.22	-1554.11	0.27
3711.27	-951.25	-1554.80	0.27
3712.52	-952.29	-1555.50	0.27
3713.77	-953.33	-1556.19	0.27
3715.02	-954.37	-1556.89	0.28
3716.27	-955.40	-1557.59	0.28
3717.52	-956.44	-1558.28	0.27
3718.77	-957.48	-1558.98	0.27
3720.02	-958.52	-1559.68	0.28
3721.27	-959.55	-1560.37	0.28
3722.52	-960.59	-1561.07	0.28
3723.77	-961.63	-1561.77	0.29
3725.02	-962.67	-1562.46	0.28
3726.27	-963.71	-1563.16	0.29

3727.52	-964.74	-1563.86	0.28
3728.77	-965.78	-1564.55	0.28
3730.02	-966.82	-1565.25	0.28
3731.27	-967.86	-1565.94	0.27
3732.52	-968.89	-1566.64	0.27
3733.77	-969.93	-1567.34	0.27
3735.02	-970.98	-1568.02	0.28
3736.27	-972.05	-1568.67	0.26
3737.52	-973.11	-1569.32	0.27
3738.77	-974.18	-1569.97	0.26
3740.02	-975.24	-1570.62	0.26
3741.27	-976.31	-1571.27	0.26
3742.52	-977.37	-1571.92	0.25
3743.77	-978.44	-1572.57	0.25
3745.02	-979.50	-1573.23	0.26
3746.27	-980.57	-1573.88	0.25
3747.52	-981.64	-1574.53	0.26
3748.77	-982.70	-1575.18	0.25
3750.02	-983.77	-1575.83	0.27

Appendix B Geostatistics

Variogram Plot with different directions in Case study one.

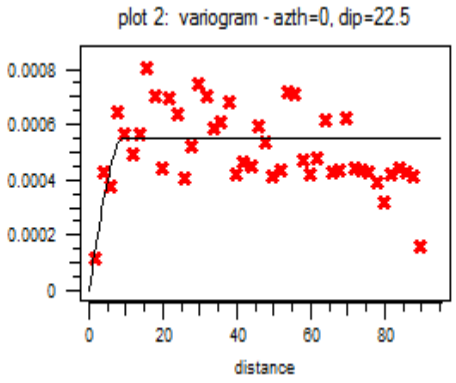

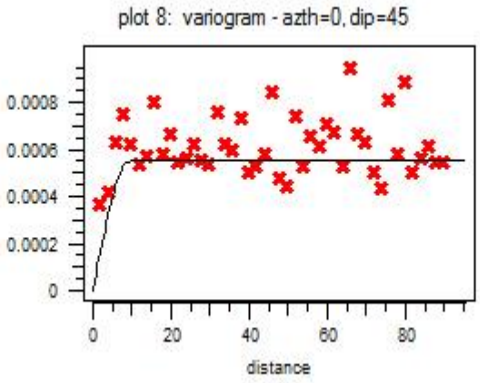

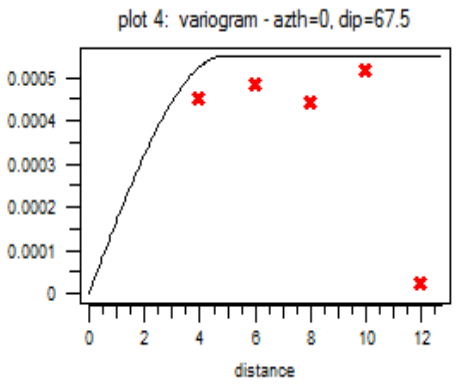

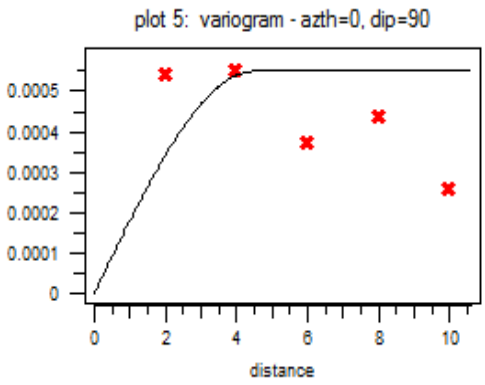

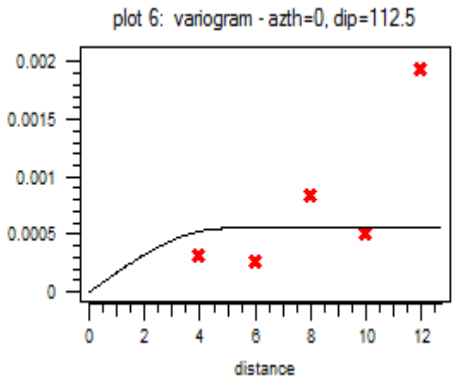

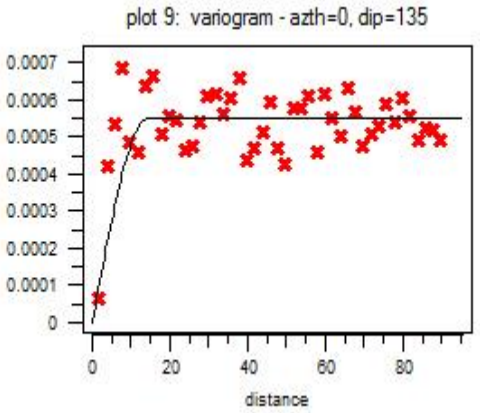

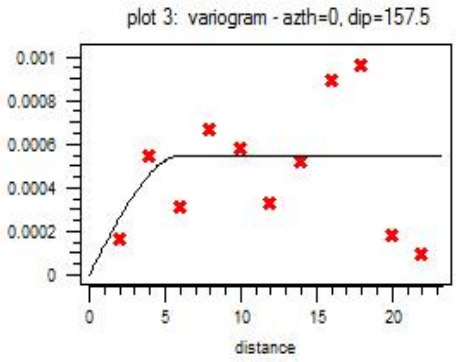
plot 3: variogram - azth=0, dip=157.5
0.001
0.0008
0.0006
0.0004
0.0002
0
0
5
10
15
20
distance

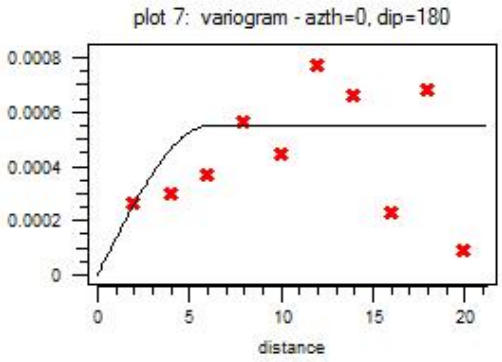
plot 7: variogram - azth=0, dip=180
0.0008
0.0006
0.0004
0.0002
0
0
5
10
15
20
distance

Appendix C Codes

SGeMS Code

%Case Study One

%Simple Kriging Estimation

```
<parameters>  <algorithm name="Kriging" />
  <Grid_Name value="Kriging" region=""  />
  <Property_Name  value="estimated porosity" />
  <Kriging_Type  type="Simple Kriging (SK)" >
  <parameters mean="0.2875" />
</Kriging_Type>
  <do_block_Kriging  value="0"  />
  <npoints_x  value="5" />
  <npoints_y  value="5" />
  <npoints_z  value="5" />
  <Hard_Data  grid="sample" region="" property="porosity"  />
  <Min_Conditioning_Data  value="0" />
  <Max_Conditioning_Data  value="80" />
  <Search_Ellipsoid  value="80 80 20
0 0 0" />
  <AdvancedSearch  use_advanced_search="0"></AdvancedSearch>
  <Variogram  nugget="0.0001" structures_count="1"  >
  <structure_1  contribution="0.00055"  type="Spherical"  >
    <ranges max="80"  medium="45"  min="20"  />
    <angles x="0"  y="0"  z="0"  />
  </structure_1>
</Variogram>
</parameters>
```

Eclipse Input File: Case Study One Base Model

```
RUNSPEC
Case Study One
RESERVOIR Base MODEL


DIMENS
   100    130    10  /



OIL

WATER

METRIC

EQLDIMS
    1 2000/

TABDIMS
    1    1   20   20    1   20 /

WELLDIMS
    1   20   1    1 /

START
   1 'APR' 2011  /


GRID
ECHO

GRIDFILE
    1    /

BOX
1 100 1 130 1 10/

DXV
   100*10
/

DYV
   130*10
/
DZ
  130000*10
/

-- Detpth to top layer must be specified


TOPS
 13000*2000
/
```

```
EQUALS
   'PERMX'   100     /
   'PERMY'   100     /
   'PERMZ'   100     /
/
INCLUDE

'POROSITY.PROP'/
/

INIT

RPTGRID
  -- Report Levels for Grid Section Data
  --
  'DX' 'DY' 'DZ'
 /

PROPS

--PVDO
--  150 1.4 20
--  200 1.35 21
-- /

--Dead oil constant properties
PVCDO

--200 1.12  1.65e-5 0.88 0.0 /
200 1.12  1.65e-5 0.88 0.0 /

PVTW
--Pref  Bw              Cw      viscosity  viscosibility
--150   1.0    4.0E-05   1.0    0.00E+00 /
  150   1.0    4E-5       1.0/

DENSITY
 850  1000  /

ROCK
--Pref     Crock            Cr_rock matrix
-- 150       0.40E-05 /
  150       0.40E-5 /


SWOF
   0.1000 0.0000 0.7   0
   0.1600 0.0005 0.610 0
   0.2200 0.0040 0.526 0
   0.2800 0.0135 0.448 0
   0.3400 0.0320 0.376 0
   0.4000 0.0625 0.311 0
   0.4600 0.1080 0.252 0
   0.5200 0.1720 0.199 0
   0.5800 0.2560 0.152 0
```

```
   0.6400 0.3650 0.112 0
   0.7000 0.5000 0.078 0
   0.8000 0.6670 0.035 0
   0.9000 0.8330 0.009 0
   1.0000 1.0000 0     0
/

RPTPROPS
   -- PROPS Reporting Options
   --
   'PVDO' 'PVTW'
/


SOLUTION


EQUIL
--depth P     owc
 2060   120   2200 /

DATUM
--reference depth
  2060.0 /

RPTSOL
  -- Initialisation Print Output
  --
'SWAT' 'RESTART=2' 'FIP=1' /

SUMMARY

FOPR
FWCT
FOE
FOPT
FWPR
FWCT
WBHP
/
BPR
1 1 1/
/
WBHP
/

SCHEDULE


--
--  WELSPECS and COMPDAT define well information in both
--  standard and LGC models.
--
WELSPECS
'OP','GROUP',  25,  25,  2060,'OIL'/
```

```
COMPDAT
'OP'   25   25   1   2 'OPEN'  1*    1*    0.1   1*      1*
1*     'Z' /
/

WCONPROD
'OP','OPEN','ORAT' 200 1* 1* 1* 1* 10/
/


RPTSCHED
   'RESTART=2' 'FIP=1' 'WELLS=1' 'SUMMARY=1' 'CPU=2' 'WELSPECS' 'NEWTON=1'
/

TSTEP
    100*5
/

END
```

Eclipse Input File: Case Study Two Base Model

```
RUNSPEC
CASE STUDY TWO
BASE MODEL

DIMENS
   200    400    10  /

OIL

WATER

METRIC

EQLDIMS
    1 20000/

TABDIMS
    1    1   20   20    1   20 /

WELLDIMS
    5   40    2    5 /

START
   1 'JAN' 2001  /


GRID
ECHO

GRIDFILE
    1    /


DXV
   200*1
/

DYV
   400*1
/

-- Depth to top layer must be specified
TOPS
80000*2650
/

DZ
  800000*5
/
```

```
INCLUDE
'POROSITY.PROP'
'PERM.PROP'
/


INIT

RPTGRID
  -- Report Levels for Grid Section Data
  --
  'DX' 'DY' 'DZ'
 /

PROPS

PVDO
  150 1.4 20
  200 1.35 21
 /



PVTW
 150   1.0    4.0E-05   1.0    0.00E+00 /


DENSITY
 859  1000  /

ROCK
 150       0.40E-05 /


SWOF
   0.1000 0.0000 0.7   0
   0.1600 0.0005 0.610 0
   0.2200 0.0040 0.526 0
   0.2800 0.0135 0.448 0
   0.3400 0.0320 0.376 0
   0.4000 0.0625 0.311 0
   0.4600 0.1080 0.252 0
   0.5200 0.1720 0.199 0
   0.5800 0.2560 0.152 0
   0.6400 0.3650 0.112 0
   0.7000 0.5000 0.078 0
   0.8000 0.6670 0.035 0
   0.9000 0.8330 0.009 0
   1.0000 1.0000 0     0
/

RPTPROPS
   -- PROPS Reporting Options
   --
   'PVDO' 'PVTW'
```

```
/


SOLUTION


EQUIL
 2650 238 2700 /

DATUM
  2700.0 /

RPTSOL
  -- Initialisation Print Output
  --
'SWAT' 'RESTART=2' 'FIP=1' /



SUMMARY

FOPR
FWCT
FPR
FOPT
FWPR
FWCT
WBHP
/

SCHEDULE


--
--  WELSPECS and COMPDAT define well information in both
--  standard and LGC models.
--
WELSPECS
'OP','GROUP',  100, 200, 2700,'OIL'/
'WI','GROUP',  10, 10, 2700, 'WAT'/
'WI','GROUP',  190, 10, 2700, 'WAT'/
'WI','GROUP',  10, 380, 2700, 'WAT'/
'WI','GROUP',  190, 380, 2700, 'WAT'/
/

COMPDAT
'OP'   108    200   4   4 'OPEN'  1*    1*    0.2   1*      1*      1*     'x' /
'OP'   109    201   4   4 'OPEN'  1*    1*    0.2   1*      1*      1*     'x' /
'OP'   110    202   4   4 'OPEN'  1*    1*    0.2   1*      1*      1*     'x' /
'OP'   103    203   4   4 'OPEN'  1*    1*    0.2   1*      1*      1*     'x' /
'OP'   104    204   4   4 'OPEN'  1*    1*    0.2   1*      1*      1*     'x' /
'OP'   105    205   4   4 'OPEN'  1*    1*    0.2   1*      1*      1*     'x' /
'OP'   106    206   4   4 'OPEN'  1*    1*    0.2   1*      1*      1*     'x' /
'OP'   107    207   4   4 'OPEN'  1*    1*    0.2   1*      1*      1*     'x' /
'OP'   108    208   4   4 'OPEN'  1*    1*    0.2   1*      1*      1*     'x' /
```

```
'OP'   109    209   4   4 'OPEN'  1*    1*    0.2   1*      1*      1*      'x' /
'OP'   110    210   4   4 'OPEN'  1*    1*    0.2   1*      1*      1*      'x' /
'OP'   111    211   4   4 'OPEN'  1*    1*    0.2   1*      1*      1*      'x' /
'OP'   112    212   4   4 'OPEN'  1*    1*    0.2   1*      1*      1*      'x' /
'OP'   113    213   4   4 'OPEN'  1*    1*    0.2   1*      1*      1*      'x' /
'OP'   114    214   4   4 'OPEN'  1*    1*    0.2   1*      1*      1*      'x' /
'OP'   115    215   4   4 'OPEN'  1*    1*    0.2   1*      1*      1*      'x' /
'OP'   116    216   4   4 'OPEN'  1*    1*    0.2   1*      1*      1*      'x' /
'OP'   117    217   4   4 'OPEN'  1*    1*    0.2   1*      1*      1*      'x' /
'OP'   118    218   4   4 'OPEN'  1*    1*    0.2   1*      1*      1*      'x' /
'OP'   119    219   4   4 'OPEN'  1*    1*    0.2   1*      1*      1*      'x' /
'OP'   120    220   4   4 'OPEN'  1*    1*    0.2   1*      1*      1*      'x' /
'OP'   121    221   4   4 'OPEN'  1*    1*    0.2   1*      1*      1*      'x' /
'OP'   122    222   4   4 'OPEN'  1*    1*    0.2   1*      1*      1*      'x' /
'OP'   123    223   4   4 'OPEN'  1*    1*    0.2   1*      1*      1*      'x' /
'OP'   124    224   4   4 'OPEN'  1*    1*    0.2   1*      1*      1*      'x' /
'OP'   125    225   4   4 'OPEN'  1*    1*    0.2   1*      1*      1*      'x' /
'OP'   126    226   4   4 'OPEN'  1*    1*    0.2   1*      1*      1*      'x' /
'OP'   127    227   4   4 'OPEN'  1*    1*    0.2   1*      1*      1*      'x' /
'OP'   128    228   4   4 'OPEN'  1*    1*    0.2   1*      1*      1*      'x' /

/

COMPDAT
'WI'   10   10   6   6 'OPEN'  1*    1*    0.2   1*      1*      1*      'x' /
'WI'   190  380   6   6 'OPEN'  1*    1*    0.2   1*      1*      1*      'x' /
'WI'   190   10   6   6 'OPEN'  1*    1*    0.2   1*      1*      1*      'x' /
'WI'   10   380   6   6 'OPEN'  1*    1*    0.2   1*      1*      1*      'x' /

/

WCONPROD
'OP','OPEN','ORAT' 150 1* 1* 1*  1* 10  /
/

WCONINJE
'WI' 'WAT' 'OPEN' 'RESV' 1*   200  1* 1* 1* 1* 1*  1* 1* /
/

RPTSCHED
   'RESTART=2' 'FIP=1' 'WELLS=1' 'SUMMARY=1' 'CPU=2' 'WELSPECS' 'NEWTON=1'
/

TSTEP
    200*5
/

END
```

Matlab File: Case study Two: Split Geostatistical Realizations in 10 Layers

```
%Split Geostatistical Realizations in Layers

Data =load ('realbasebase1.data');
NumReal = length(data)/100;
Numsplit=10;
b=0;
c=0;
for j=1:round(NumReal/NumSplit)
    a=0;
    c=0;
    for i=1:NumSplit
        c=c+1;
        While a<c*1820*2
        a=a+1;
        b=b+1;
        if b<length(data)
            file(a,1,j)=data(b,1);
            a=a+1;
            file(a,1,j)=data(b,2);
        end
    end
end
```

Appendix D Porosity Histogram for each step during Model Updaing Process in Case Study Two.

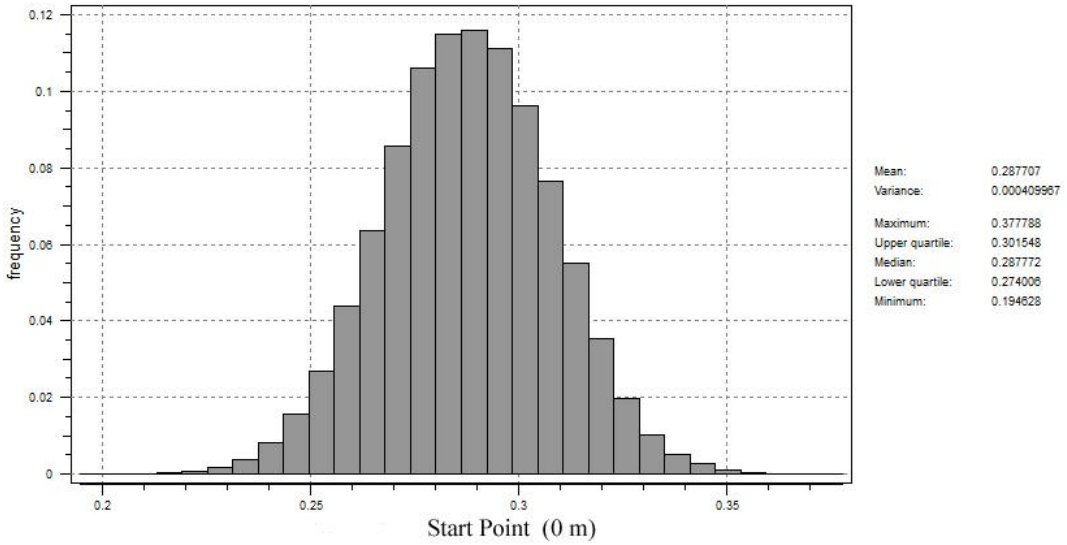

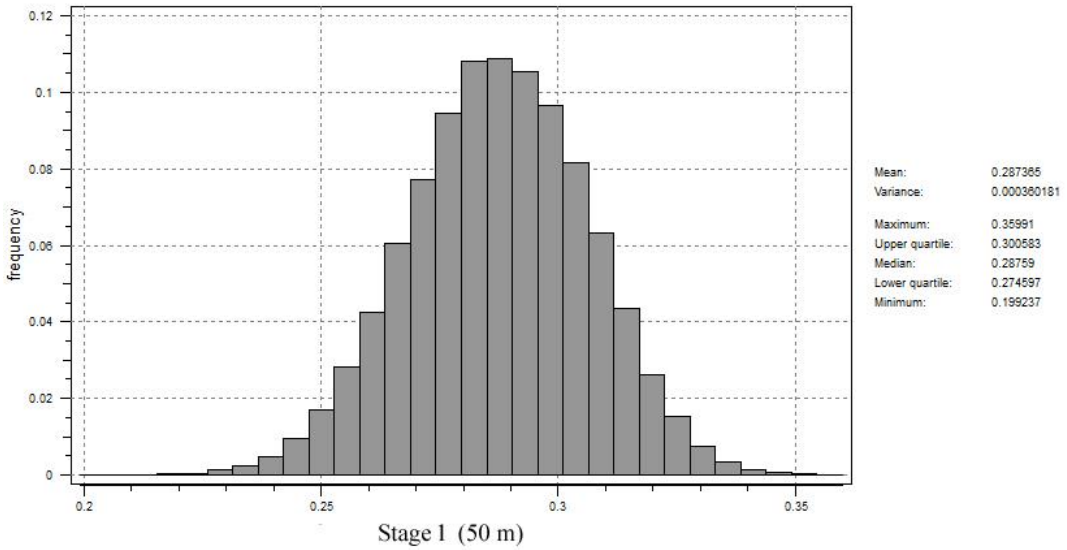

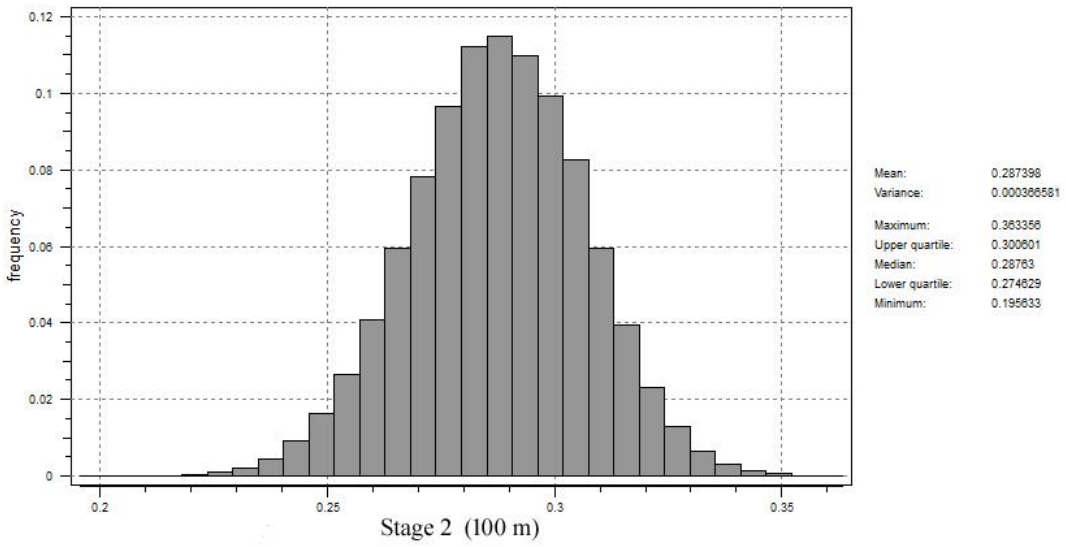

Stage 2 (100 m)

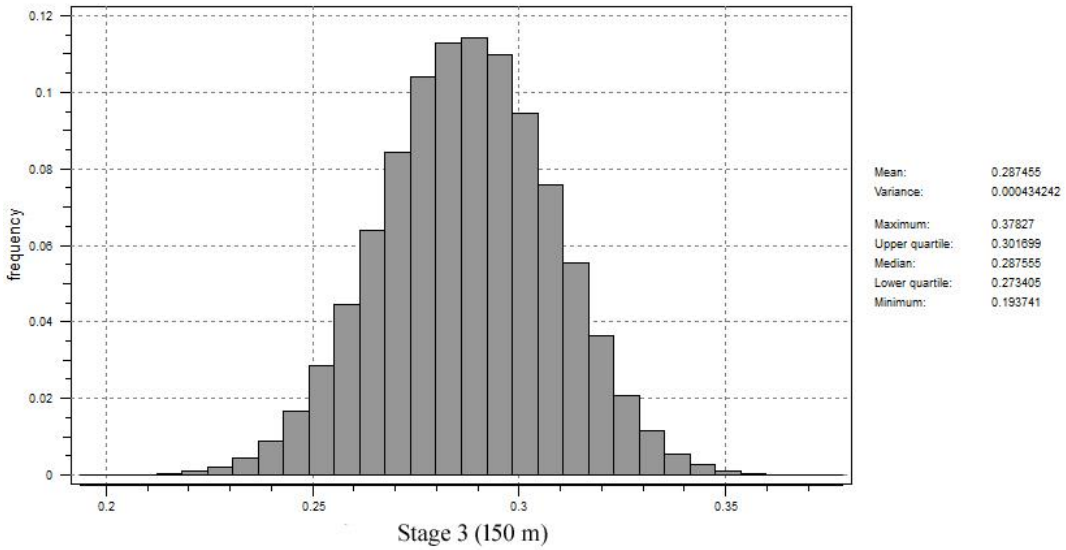

Stage 3 (150 m)

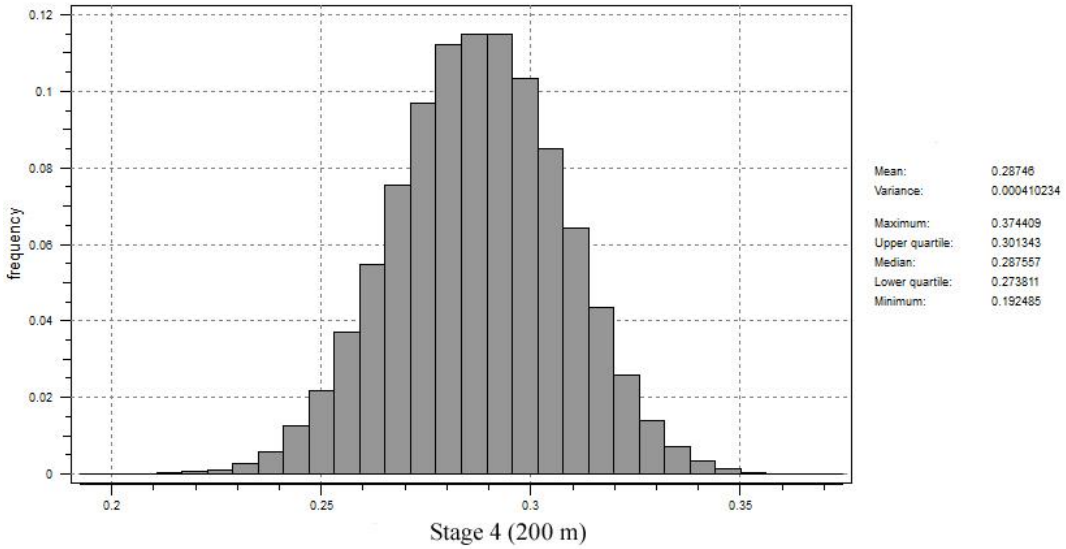

Stage 4 (200 m)

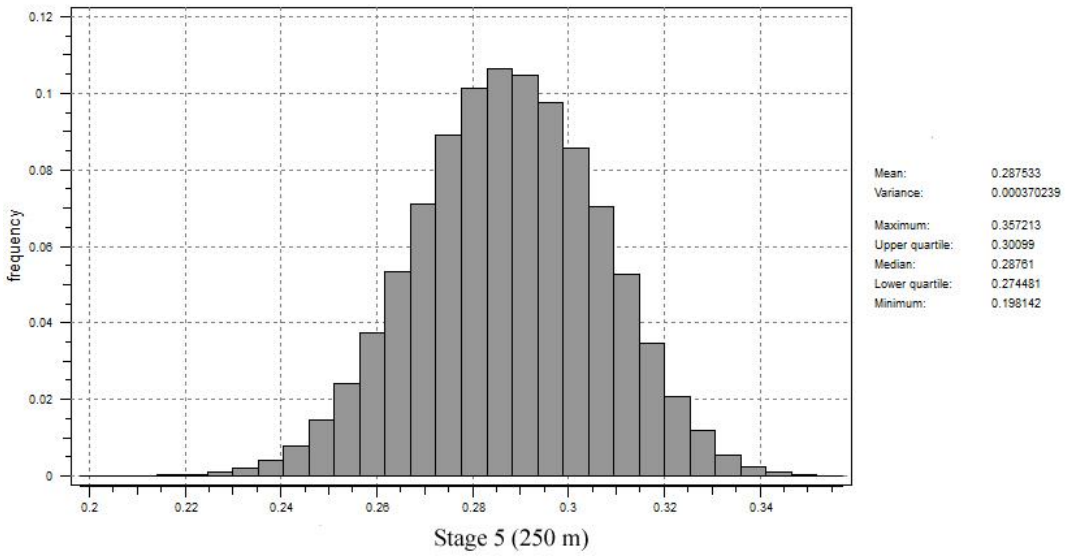

Stage 5 (250 m)

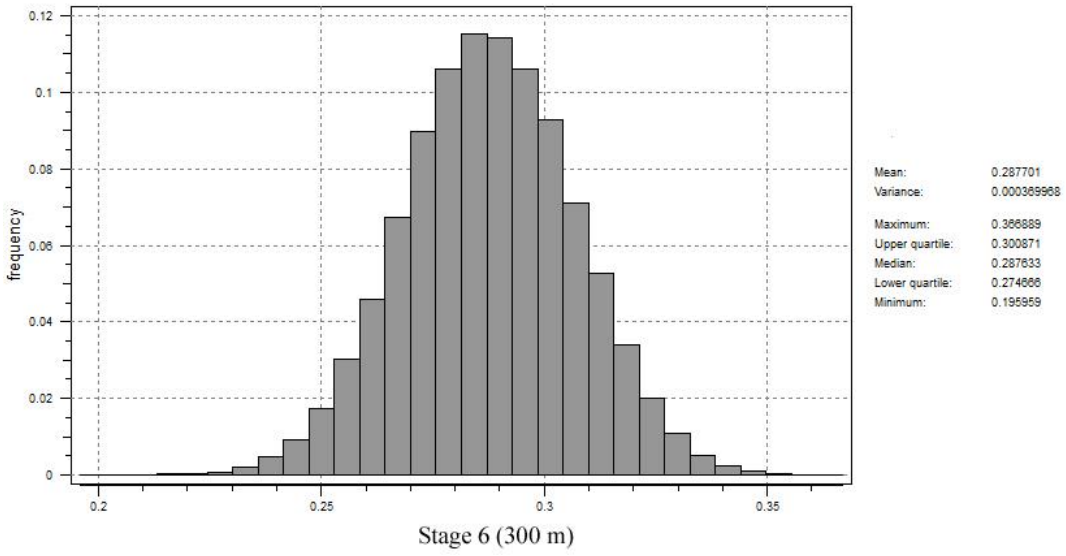

Stage 6 (300 m)

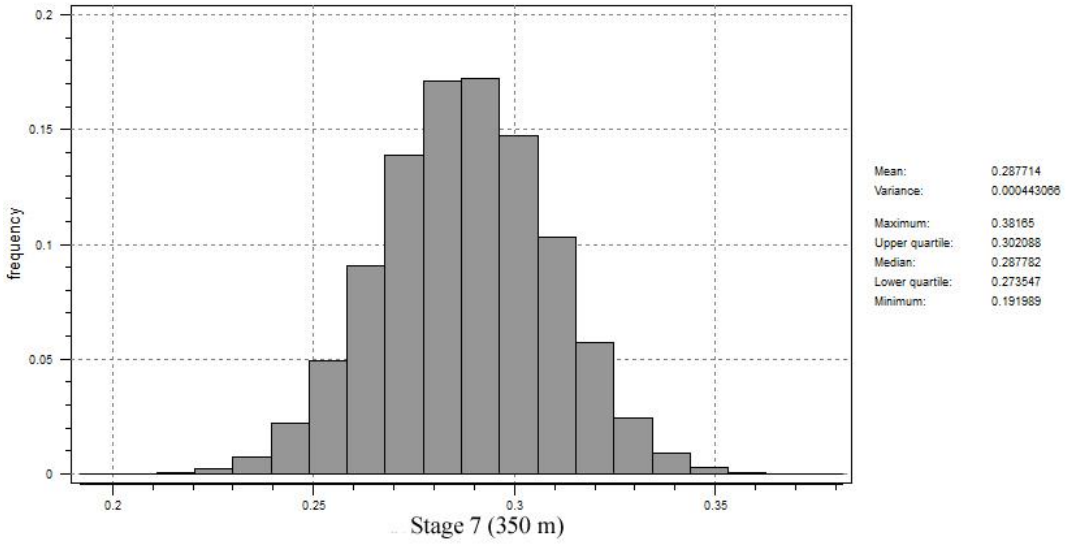

Stage 7 (350 m)

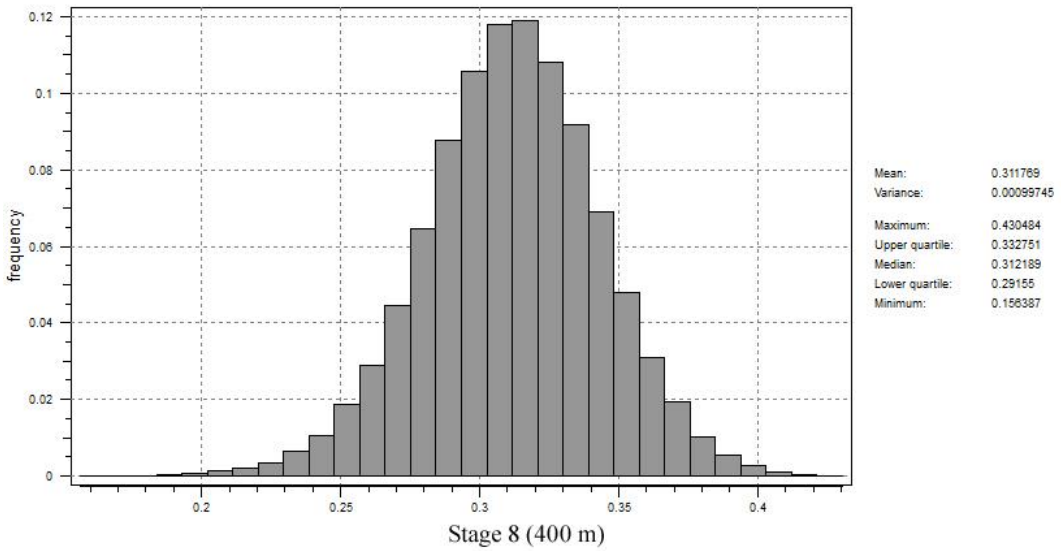
0.12
0.1
0.08
0.06
0.04
0.02
0
frequency
0.2
0.25
0.3
0.35
0.4
Mean: 0.311769
Variance: 0.00099745
Maximum: 0.430484
Upper quartile: 0.332751
Median: 0.312189
Lower quartile: 0.29155
Minimum: 0.156387

Stage 8 (400 m)